

Pattern formation in excitable media

Ehud MERON*

Department of Chemical Physics, Weizmann Institute of Science, Rehovot 76100, Israel

Received February 1992; editor: I. Procaccia

Contents:

1. Introduction	3	3.3. Experimental studies	27
2. Excitable systems	5	4. Patterns in two space dimensions	28
2.1. A simple model	5	4.1. Curved solitary wave-fronts	28
2.2. Examples	7	4.2. Plane waves and target patterns	33
3. Patterns in one space dimension	8	4.3. Spiral waves	34
3.1. Solitary waves	8	5. Discussion	60
3.2. Extended patterns	16	References	62

Abstract:

Excitable media are extended nonequilibrium systems having uniform rest states that are linearly stable but susceptible to finite perturbations. Depending on the forms of these perturbations, a variety of wave patterns can be triggered; solitary waves, target like patterns, and spiral waves are a few examples. These media are naturally encountered in biological systems and are also generated by a class of chemical systems, the most familiar of which is the Belousov–Zhabotinsky reaction. The recent progress that has been made in understanding patterns in one and two space dimensions is reviewed. Special attention is given to theoretical aspects, but experiments and numerical simulations are described as well. On the theoretical side two basic approaches are described, singular perturbation theories and kinematical theories. The two approaches have different ranges of validity and address different questions, but also have an overlap range that allows for comparison. The availability of large fast computers made extensive explorations of parameter spaces possible. New regimes of dynamical behavior found in that way are described. Finally, an account is given of the significant experimental progress that has been made recently by exploiting spectrophotometric and digital imaging techniques and by using new reactor designs.

* Present address: Department of Mathematics, University of Arizona, Tucson, AZ 85721, USA.

PATTERN FORMATION IN EXCITABLE MEDIA

Ehud MERON

Department of Chemical Physics, Weizmann Institute of Science, Rehovot 76100, Israel



NORTH-HOLLAND

1. Introduction

A variety of pattern formation phenomena in nonequilibrium systems result from the interplay between local dynamical processes and diffusive transport. Autocatalytic chemical reactions provide some of the most studied examples [FIB]. The possible appearance of stationary concentration patterns in chemical reactions has already been predicted by Turing [TUR] (in 1952). Stationary patterns, however, have not been observed in experiments until very recently [CDB]. What has been observed, instead, was traveling wave patterns [ZAZ1,WIN1] whose properties bear striking similarities to electric pulse (action potential) propagation along excitable membranes. The relation between the two phenomena [WIN2,TRO] was realized after the works of Hodgkin and Huxley [HOH] on nerve conduction and of Field et al. [FKN] on the mechanism of the Belousov–Zhabotinsky reaction [BEL,ZHA]. The fact that both phenomena belong to the same class of reaction–diffusion systems opened the way for an intensive interdisciplinary study of wave patterns in systems that have become known under the name “excitable media”.

The simplest patterns that appear in excitable media are solitary waves that propagate at constant speeds. These waves preserve their forms during propagation but, unlike solitons, annihilate each other upon face-to-face collisions. Excitable media also support continuous families of periodic wavetrains. The speeds of these wavetrains are related to their periods (or wavelengths) through dispersion relations, which at short periods become monotonic, the shorter the period the smaller the propagation speed. In two dimensions, expanding concentric circular waves (“target” patterns) and rotating spiral waves are commonly observed (fig. 1). Target patterns are generated by small oscillatory domains (“pacemakers”) whose periods determine their asymptotic wavelengths. This leads to patterns with varying wavelength as seen in the upper part of fig. 1. The asymptotic wavelength, or rotation frequency of spiral waves, on the other hand, cannot assume any value; in a medium that gives rise to a monotonic dispersion relation a unique frequency value is selected (lower part of fig. 1). Target and spiral waves generalize in three dimensions to expanding spherical waves and rotating scroll waves, respectively. The axis of the scroll wave (or vortex line) can terminate at the boundaries or close upon itself in a variety of ways to form vortex rings.

A review of traveling-wave phenomena in excitable media appeared a few years ago, emphasizing singular perturbation aspects [TYK1]. Numerous studies have appeared since then and one purpose of the present review is to describe the theoretical, numerical and experimental progress that has been made in these works. Another goal is to describe analytical approaches other than singular perturbation theory (in the sense of [TYK1]). These include extensive studies by Russian colleagues that have been described in the Western literature only recently. Part of the recent progress pertains to three-dimensional patterns. These are beyond the scope of the present review, however. For recent developments in three dimensions we refer the reader to refs. [KET1].

We begin in section 2 with a brief explanation of what excitable systems are and where such systems are encountered. We will avoid a detailed exposition of the numerous mathematical models that have been proposed to describe excitable systems and will focus, instead, on generic features captured by all such models. We will also describe in detail only one physical example of an excitable system, namely, the Belousov–Zhabotinsky reaction, as most experimental studies were carried out on that system. In

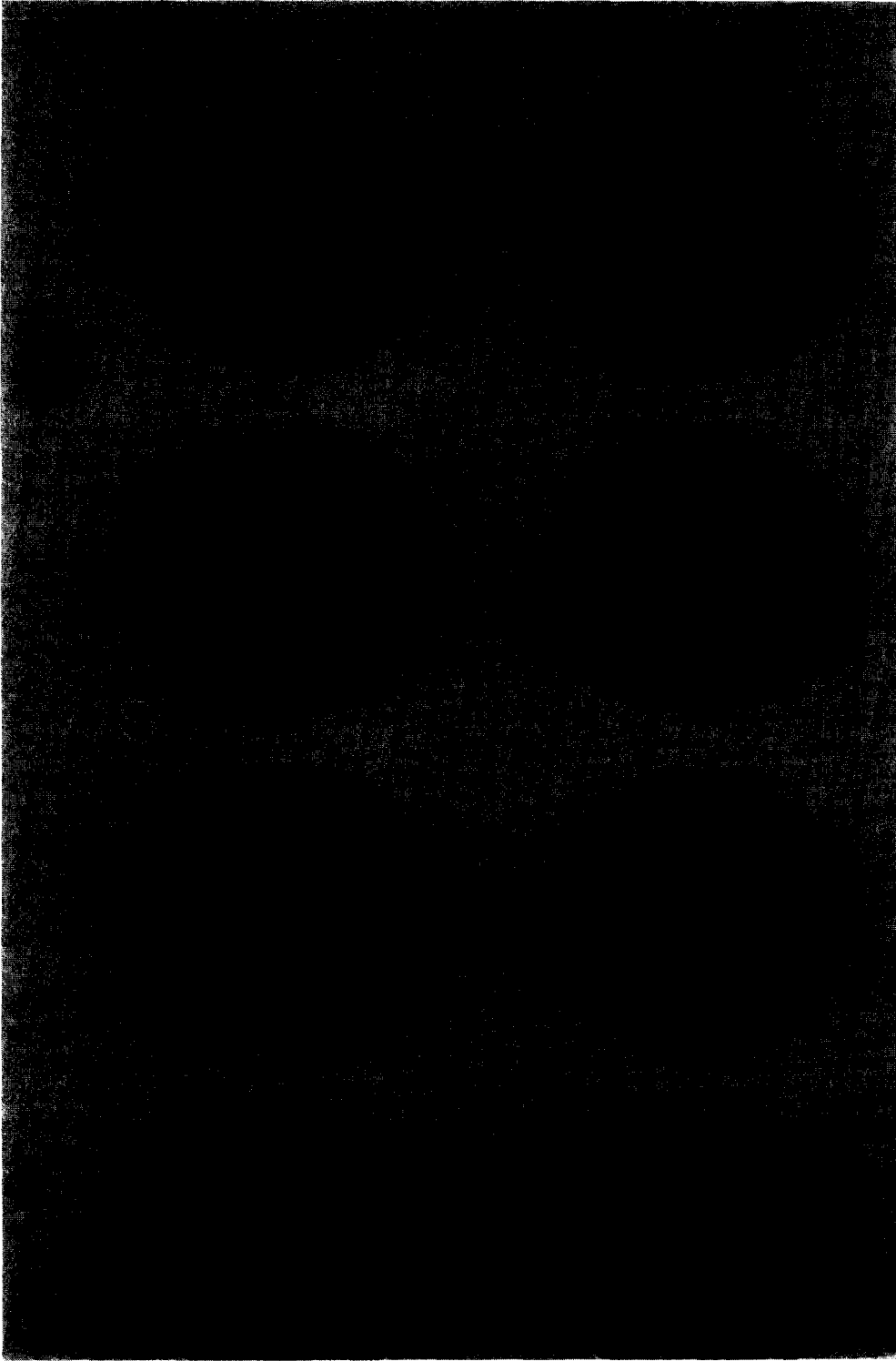


Fig. 1. Target and spiral patterns in the Belousov-Zhabotinsky reaction. Shown are four successive snapshots of each type of pattern taken about 1 min apart. Time proceeds from left to right. The field view is 66 mm in diameter. (From Winfree [WIN10], reproduced with permission.)

section 3 we consider one-dimensional patterns and address first pulse-like solitary waves (section 3.1). We then proceed to extended patterns (section 3.2). We describe the derivation of dispersion relations for periodic traveling waves using singular perturbation theory (section 3.2.1), and present a different, kinematical approach to traveling waves in excitable systems (section 3.2.2), which allows the consideration of relaxational aspects and the emergence of spatial complexity (section 3.2.2). An account of experimental studies is given in section 3.3.

Two-dimensional patterns are considered in section 4. We discuss first the role of curvature in two-dimensional patterning, present derivations of curvature–speed relations and describe an experimental test of such relations (section 4.1). Instabilities of planar traveling waves to transverse structure are considered in section 4.2 whereas the rest of section 4 is devoted to spiral waves. We focus on two outstanding problems, the selection of a unique frequency of rotation and the onset of nonsteady rotation, and describe experimental, numerical and theoretical progress that has been made on these problems. Many additional aspects of pattern formation in two dimensions are not covered in this review. These include spiral-wave interactions, the onset of turbulence, cellular-automaton models etc. We briefly discuss these topics in section 5.

2. Excitable systems

2.1. A simple model

In order to understand what we mean by “excitable” systems, it is instructive to consider first a simple model of a bistable system,

$$\dot{u} = -u(u - a)(u - 1) - v, \quad (2.1a)$$

where the dot denotes differentiation with respect to a dimensionless time and a and v are constant parameters. Equation (2.1a) is derivable from a potential,

$$\dot{u} = -\delta\mathcal{F}/\delta u. \quad (2.2)$$

In a range of parameter values, $v_{\min}(a) < v < v_{\max}(a)$, \mathcal{F} is a double-well potential. In general the two wells will be of different depths. The deeper the well the more stable the attractor and the larger the basin of attraction. We will refer to the shallower well as describing a *metastable* state. The forms of \mathcal{F} for increasing values of v and a fixed value of $a \in (0, \frac{1}{2})$, are illustrated in fig. 2a. For $v = 0$ the well on the left, centered at $u = 0$, describes a metastable state. If we prepare the system in this state and perturb it by increasing the value of u beyond the potential barrier at $u = a$, the system will evolve toward the stable state $u = 1$. As v increases (a held constant), the original metastable state, $u = 0$, becomes more stable and drifts toward negative u values. The well on the right becomes shallower and eventually disappears.

Imagine now that v is not a constant parameter but, instead, a dynamical variable that evolves on a time scale much longer than that of u .*) It is important that v will respond to variations in u in a certain way, and the simple differential equation

$$\dot{v} = \varepsilon u, \quad 0 < \varepsilon \ll 1, \quad (2.1b)$$

*) The view of dynamical systems as slowly deforming potential systems has proved useful in other contexts as well [MSP].

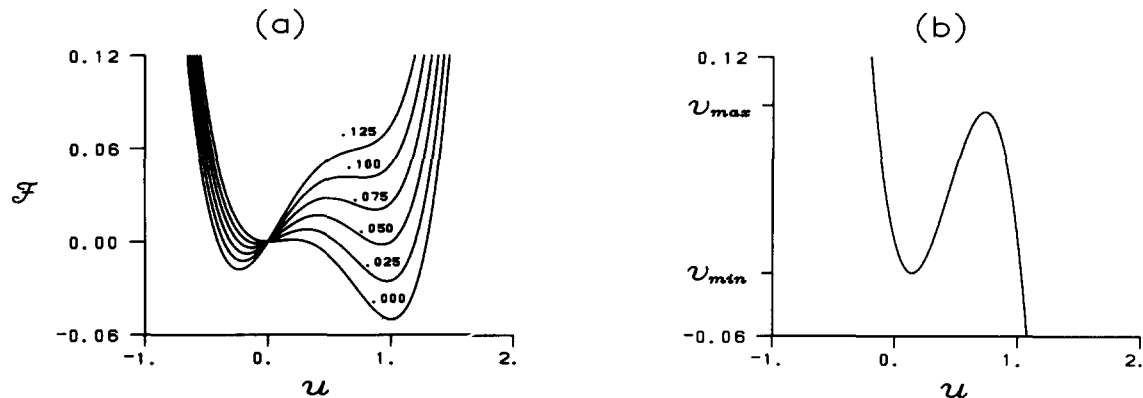


Fig. 2. a. The potential $\mathcal{F}(u)$ of eq. (2.1a) at increasing constant values of v (denoted on the right side of the potential). b. The locus of extremal potential values, $\delta\mathcal{F}/\delta u$, in the (u, v) plane.

is sufficient for that purpose (for generalizations see section 3.1.1). The new dynamical system (2.1a, b) is no longer potential, but it is still useful to keep in mind the form of \mathcal{F} as time evolves. It is easy to check that $u = v = 0$ is a stationary stable state of the new system. Suppose that we prepare the system in this state and perturb u beyond the *threshold* value $u = a$ (the location of the potential barrier of \mathcal{F}). On a short time scale [of $O(1)$] the system converges toward the deep well on the right as if ε were zero. On a longer time scale [of $O(\varepsilon^{-1})$], however, v starts increasing (since u is now positive) and, as a result, the right well becomes shallower and shallower (see fig. 2a). The fast variable u follows this change adiabatically and the system remains “inside the well” until the well disappears. At this moment the system “falls” down into the deep well that has developed on the left. This well is located now at a negative u value and, consequently, v starts decreasing while u adiabatically adjusts itself to the varying well position. This process continues until complete convergence to the original stable state $u = v = 0$ is achieved. Thus, perturbations larger than a threshold value do not immediately decay but, instead, drive the system to long excursions in the (u, v) plane before relaxation back to the stationary state occurs. We say that such perturbations “excite” the system.

A convenient way to follow the dynamics in the (u, v) plane is to look at the locus of extremal potential values, $\delta\mathcal{F}/\delta u = 0$, shown in fig. 2b.*¹ The right and left branches correspond to the two potential wells, while the middle branch describes the location of the potential barrier. Figure 3 shows the rapid decay of a subthreshold perturbation (trajectory A) and the long excursion initiated by a superthreshold perturbation (trajectory B). The final stage of this excursion involves the relaxation of the system back to the stationary state along the left branch (or well). During the early stages of this relaxation process the system is *refractory* to perturbations, despite the fact that it has already returned to the branch of the stationary state. The reason for that becomes evident when we look at figs. 2 and 3. At high v values the threshold is too large, or the left well too wide, for small perturbations to induce a transition to the right branch. The refractory phase in the relaxation process is extremely significant for pattern formation in excitable media.

The double-well-potential picture drawn above applies in the limit of small ε . In this limit the potential barrier dictates a sharp threshold of excitation. When ε is not too small the threshold of excitation is no longer sharp [FIT1,CGB] and one may speak of a *threshold zone* [MNS]. The response of the system to perturbations that lie within that zone varies continuously from immediate decay to fast

*¹ This locus is often referred to in the literature as the “slow manifold” or the nullcline associated with the variable u .

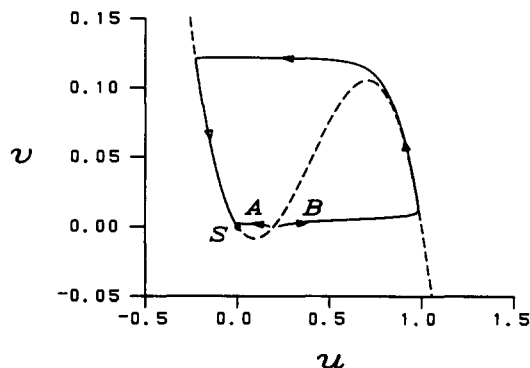


Fig. 3. Phase portraits of eqs. (2.1) showing the response of the system to subthreshold (A) and super-threshold (B) perturbations of the rest state S .

growth. A sharp threshold can also be obtained in systems that undergo saddle-node bifurcations. The threshold is then dictated by the stable manifold of the saddle point [RIE,MNS].

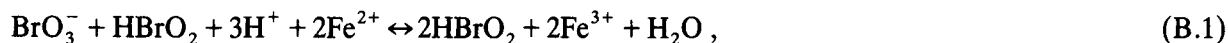
2.2. Examples

The most studied example of an excitable system, at least as far as pattern formation aspects are concerned, is the Belousov–Zhabotinsky (BZ) reaction [BEL,ZHA]. The overall effect of this reaction is a catalytic oxidation of malonic acid in an acidic bromate solution. The catalyst in this reaction is a metal ion, usually ferroin (Fe^{2+}) or cerium (Ce^{3+}). The fact that the two oxidation states of the catalyst have different colors makes the reaction clearly visible (see fig. 1). According to a mechanism proposed by Field et al. [FKN], the reaction involves three main processes.

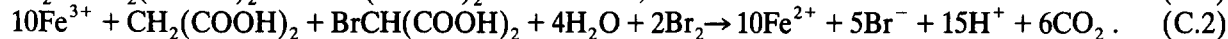
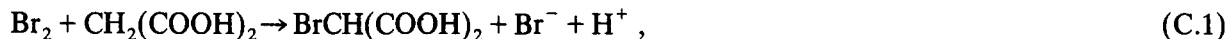
Process A



Process B



Process C



We note that not all of the reaction steps displayed above represent elementary reactions. For example, the single-electron oxidation reaction (B.1) involves a free radical intermediate, BrO_2 . A detailed consideration of these reaction steps is given in refs. [FKN,FIE,TYS1].

The key steps in the FKN mechanism are the autocatalytic production of bromous acid (HBrO_2) in reaction (B.1), and the elimination of bromous acid by bromide ions (Br^-) in reaction (A.2). When the initial concentration of Br^- is sufficiently large, reaction (A.2) removes HBrO_2 before it can enter the autocatalytic step (B.1), and a steady state results (concentrations of intermediate species are

independent of time). When the concentration of Br^- drops below a critical value there are not enough bromide ions to suppress the autocatalytic reaction (B.1) and the concentration of bromous acid starts to accumulate exponentially. The rapid increase in bromous-acid concentration eventually saturates because of reaction (B.2). The bromine (Br_2) and the oxidized form of the metal catalyst (Fe^{3+}), that are produced in processes A and B, respectively, can now trigger process C whose effect is to reduce Fe^{3+} back to Fe^{2+} and to produce bromide ions. The latter react with bromous acid [step (A.2)] to bring back the concentrations of both reactants to their initial values and a new cycle can now start.

Thus, depending on the initial level of bromide ions, the reaction can be either in a *steady* or in an *oscillatory* state. Excitability is achieved when the bromide-ion concentration is only slightly above the critical level below which spontaneous oscillations set in. Decreasing the concentration of bromide ions below the critical level will free the way for step (B.1) and a whole cycle of oxidation–reduction will take place before the steady state is re-established.

The mass–action equations for the full FKN mechanism yield a complicated dynamical system. A reduced mechanism, consisting of only five essential steps, has been proposed in [FIN1]. It leads to a three-variable dynamical system, known as the Oregonator, which in appropriate parameter regimes has solutions describing both oscillatory [FIN1,HAM] and excitable states [TRF]. The three-variable model has been further reduced to a two-variable model that has the gross structure of (2.1) with the concentrations of HBrO_2 and Fe^{3+} playing the roles of u and v , respectively [TYF]. Other reduced versions of the FKN mechanism have been proposed. These models are reviewed in [TYS1].

Another well studied example of an excitable system is the axon of a nerve cell [AID,KAS]. Here, the fast variable is the transmembrane potential difference. At the non-firing rest state it assumes a constant value that reflects a balance between electrical and ion-concentration gradients across the membrane. The excitation process in this system amounts to a change of about 100 mV in the transmembrane potential difference. The potential change and the subsequent recovery of the system to the rest state are due to nonlinear responses of the various ionic conductances to potential variations. In their seminal work Hodgkin and Huxley proposed a phenomenological four-variable model to describe the process of membrane excitation. They studied their model numerically and demonstrated quantitative agreement with experimental observations [HOH]. The complexity of the model, however, motivated the formulation of simpler models which still capture the key qualitative features of the original system [RIN1]. The most familiar one is the FitzHugh–Nagumo model [FIT2, NAY] of which (2.1) is a special case.

Much effort has been devoted to the study of excitable *cardiac* cells as well. We will return to this example when we discuss wave-propagation phenomena in two space dimensions as these bear on the important problem of ventricular fibrillation [KRI,WIN3]. Others examples of excitable systems include biochemical reactions such as cyclic AMP production in the slime mold *dictyostelium discoideum* [GER,MGO,LER] and predator–prey models of population dynamics [MUR].

3. Patterns in one space dimension

3.1. Solitary waves

3.1.1. General

So far we have considered homogeneous states whose temporal evolutions are described by excitable systems such as (2.1). When spatial gradients develop, dissipative transport processes take place in the

form of molecular diffusion (chemical systems) or ion conduction (biological membranes). The coupling of excitability and diffusion can lead to wave propagation phenomena. One may imagine an extended chemical system at rest that is locally perturbed beyond the threshold of excitation. The fast growth of the autocatalytic species creates a steep concentration gradient. Diffusion to the adjacent area then provides the superthreshold perturbation needed to trigger the autocatalytic reaction in that area, thus spreading the excitation. Eventually, any excited region relaxes back to the rest state. The outcome, therefore, is two counter-propagating solitary waves propagating invariably at constant speeds. Typical propagation speeds are of the order of $10^{-3} \text{ cm s}^{-1}$ for chemical waves in the BZ medium, and 10^3 cm s^{-1} for action potentials in squid axons. Propagating waves in excitable media are sometimes referred to as “trigger waves” because of the triggering effect of diffusion.

To account for transport processes, diffusion terms should be added to the right hand side (rhs) of (2.1). More generally, we will consider dimensionless reaction–diffusion equations of the form

$$\partial_t u = f(u, v) + \nabla^2 u, \quad \partial_t v = \varepsilon g(u, v) + \delta \nabla^2 v, \quad (3.1a, b)$$

$$\varepsilon = \tau_u / \tau_v, \quad \delta = D_v / D_u, \quad (3.1c)$$

where τ_u and τ_v are the time scales associated with the fast u variable and the slow v variable, respectively, and D_u and D_v are the corresponding transport coefficients. The variables u and v are sometimes referred to as the *propagator* and *controller* variables, respectively [FIF1, FIF3]. To resume dimensions the transformations $t \rightarrow t/\tau_u$ and $x \rightarrow x/(\tau_u D_u)^{1/2}$ should be made. The time-scale ratio ε is usually much smaller than unity. The value of the transport-coefficient ratio, δ , depends on the context; in chemical systems normally $\delta \sim O(1)$, whereas in the context of excitable membranes $\delta = 0$, as v represents ion-channel openness, a property that does not diffuse. The other extremity, $\delta \gg 1$, has been used in activator–inhibitor type models to account for stationary biological patterns [MEI]. We will consider the latter case only briefly (see section 3.1.5). The qualitative forms of the functions $f(u, v)$ and $g(u, v)$ are illustrated by the dashed curves in fig. 4b. The u -nullcline, $f(u, v) = 0$ is N-shaped while the v -nullcline, $g(u, v) = 0$ is monotone. They intersect each other on the left branch of the u -nullcline at a point $S = (u_s, v_s)$ which describes the rest state of the medium. To guarantee excitable dynamics as described in section 2.1., the function f is chosen to be negative (positive) above (below) the u -nullcline, whereas g is chosen to be positive (negative) on the right (left) of the v -nullcline.

Another form of excitable reaction–diffusion equations, commonly used in the literature, is obtained from (3.1a–c) by rescaling space and time according to $t' = \varepsilon t$ and $x' = \varepsilon x$. It reads

$$\varepsilon \partial_{t'} u = f(u, v) + \varepsilon^2 \nabla'^2 u, \quad \partial_{t'} v = g(u, v) + \varepsilon \delta \nabla'^2 v, \quad (3.1d, e)$$

where ∇'^2 is the Laplacian operator in terms of the rescaled spatial coordinates. Throughout this paper we will be using the original form (3.1a–c) unless we mention otherwise.

The structure of a solitary wave solution of (3.1a, b), for ε values sufficiently small, is illustrated in fig. 4. It consists of a *wave-front* which drives the system from the rest state on the left branch of $f(u, v) = 0$ to the right branch ($S \rightarrow a$), an excited domain ($a \rightarrow b$), a *wave-back* which brings the system back to the left branch ($b \rightarrow c$), and a refractory tail ($c \rightarrow S$) which terminates at the rest state S .*) Notice that the slow variable v hardly changes in the transition zones, $S \rightarrow a$ and $b \rightarrow c$. For higher ε

*) The refractory tail amounts to a phase in the local dynamics during which the system is recovering from excitation. It is sometimes referred to as a “recovery region” and we will use both terms interchangeably.

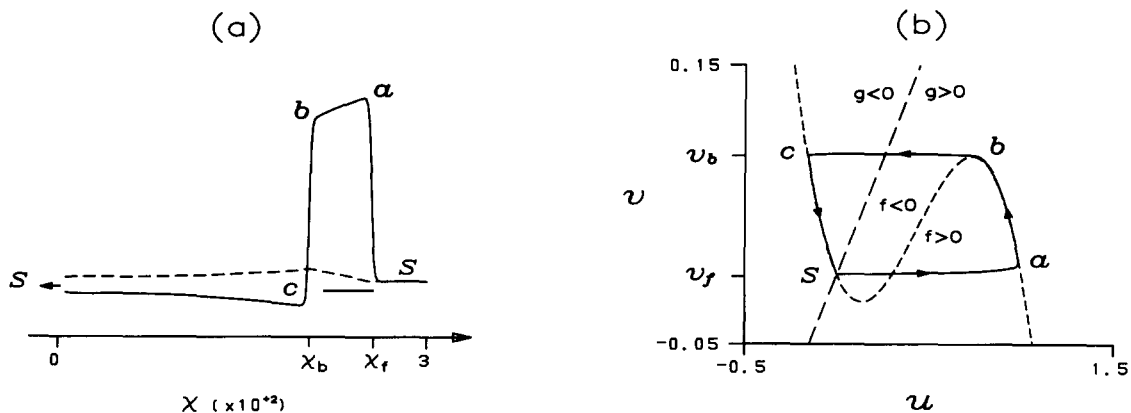


Fig. 4a. $u(\chi)$ (solid curve) and $v(\chi)$ (dashed curve) for a solitary wave solution of (3.1) with $f(u, v)$ as in (2.1) and $g = u - bv$. The abscissa represents $\chi = x - ct$. Parameters used: $\varepsilon = 3 \times 10^{-4}$, $a = 0.3$, $b = 3.0$. The singular structure is clearly seen; narrow front ($S \rightarrow a$) and back ($b \rightarrow c$) regions separate excited ($a \rightarrow b$) and refractory ($c \rightarrow S$) domains. b. Phase portrait of the solitary wave solution (homoclinic orbit) in the (u, v) plane.

values the variation of v in the transition zones may not be negligible. For yet higher values the decomposition of a solitary wave into a wave-front, an excited domain and a wave-back may no longer apply. The three regions rather merge together to form a single pulse-like structure followed by a refractory tail as fig. 5 demonstrates.

3.1.2. Singular perturbation theory

An approximate solitary wave solution, valid for ε small enough, can be obtained using a singular perturbation approach [CCL, ORR, FIF2, KEE1, DKT, KEL1]. In this approach a distinction is made between an outer region in which u varies smoothly in space and time, and an inner region where u varies abruptly. The former includes the excited and the refractory regions, while the latter consists of the narrow wave-front and wave-back zones. In the outer region u follows adiabatically the slow

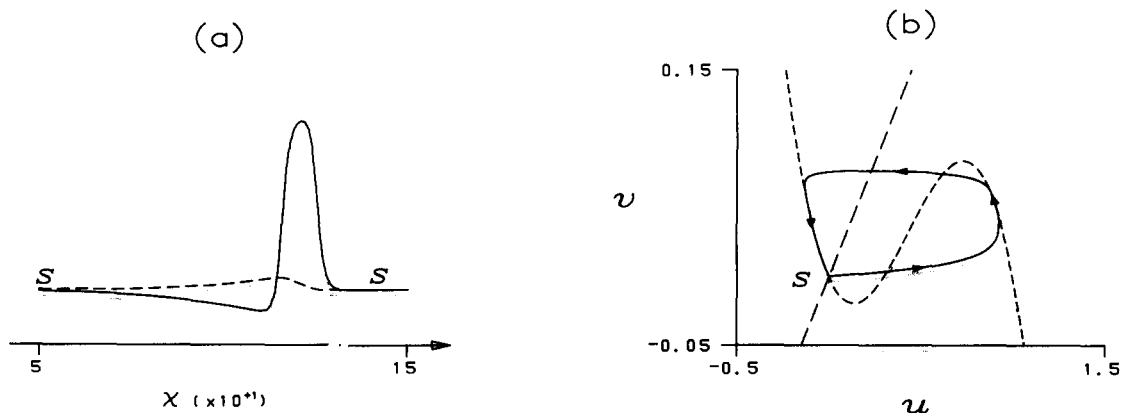


Fig. 5. Same as figs. 4 except that $\varepsilon = 1.5 \times 10^{-3}$ is now five-fold larger. The singular structure of the solitary wave solution is lost; it consists of a pulse structure followed by a refractory tail. Note the change of the χ scale.

evolution of v . The temporal and spatial derivatives of u are small and (3.1a) becomes to leading order an algebraic equation, $f(u, v) = 0$, that can be solved for u . This amounts to setting $\varepsilon = 0$ in the rescaled system (3.1d, e). The left and right solution branches of this equation correspond to the refractory and excited regions and are denoted by $u_-(v)$ and $u_+(v)$, respectively. For a solitary wave that propagates at speed c_∞ through a medium at rest we have

$$u = u_-(v), \quad -\infty < \chi < \chi_b; \quad u = u_+(v), \quad \chi_b < \chi < \chi_f; \quad (3.2)$$

$$u = u_-(v_s) = u_s, \quad \chi_f < \chi < \infty, \quad \chi = x - c_\infty t,$$

where χ_f and χ_b are the wave-front and wave-back positions in a frame moving with speed c_∞ , respectively. Using these solution branches in (3.1b) and assuming that v is a function of the single variable χ , we obtain

$$\delta v'' + c_\infty v' + \varepsilon G_-(v) = 0, \quad -\infty < \chi < \chi_b; \quad (3.3a)$$

$$\delta v'' + c_\infty v' + \varepsilon G_+(v) = 0, \quad \chi_b < \chi < \chi_f; \quad G_\pm(v) = g(u_\pm(v), v) \quad (3.3b)$$

where the prime denotes differentiation with respect to χ . Equations (3.3) should be supplemented by the following continuity and boundary conditions [DKT]:

$$v(\chi \rightarrow \chi_b^+) = v(\chi \rightarrow \chi_b^-) = v_b, \quad v'(\chi \rightarrow \chi_b^+) = v'(\chi \rightarrow \chi_b^-), \quad (3.4)$$

$$v(\chi \rightarrow \chi_f^-) = v(-\infty) = v_s, \quad v'(\chi \rightarrow \chi_f^-) = v'(-\infty),$$

where v_b is the wave-back value of v , and the superscripts $+$ and $-$ denote the approach to the designated value from above and below, respectively.

The solutions of (3.3) and (3.4) together with (3.2) give the large length scale form of the solitary wave solution. The wave-front and wave-back appear on this length scale as discontinuities in the fast variable u . On a smaller scale these discontinuities constitute boundary layers whose analysis allows the determination of the two unknown parameters c_∞ and v_b . In these layers temporal and spatial derivatives of u cannot be neglected but, on the other hand, v can be assumed to be constant. We therefore obtain from (3.1a)

$$u_f'' + c_\infty u_f' + f(u_f, v_s) = 0, \quad u_b'' + c_\infty u_b' + f(u_b, v_b) = 0, \quad (3.5a, b)$$

where u_f and u_b are the wave-front and wave-back solutions, respectively. Since the solitary wave propagates without change in shape the same propagation speed, c_∞ , has been assumed for u_f and u_b . The wave-front and wave-back solutions should match the outer solution (3.2). This can be achieved by demanding

$$u_f(\chi - \chi_f) = \begin{cases} u_-(v_s), & \chi \rightarrow \infty, \\ u_+(v_s), & \chi \rightarrow -\infty, \end{cases} \quad u_b(\chi - \chi_b) = \begin{cases} u_+(v_b), & \chi \rightarrow \infty, \\ u_-(v_b), & \chi \rightarrow -\infty, \end{cases} \quad (3.6a, b)$$

in the limit $\varepsilon \rightarrow 0$.

Equations (3.5a) and (3.6a) constitute an eigenvalue problem for c_∞ . Once c_∞ is known, eqs. (3.5b) and (3.6b) can be used to determine v_b . Alternatively, multiplying (3.5a) and (3.5b) by u'_i and u'_b , respectively and integrating from $\chi = -\infty$ to $\chi = \infty$ we obtain

$$c_\infty = \mu(v_s) = -\mu(v_b), \quad (3.7)$$

$$\mu(v) = \frac{\int_{u_-(v)}^{u_+(v)} f(u, v) du}{\int_{-\infty}^{\infty} u'(v)^2 d\chi}. \quad (3.8)$$

In (3.8) $u(v)$ is an interface solution of (3.5) at a constant v value. We thus have two equations for the two unknowns c_∞ and v_b . In general, $c_\infty = \mu(v_s)$ is a monotone decreasing function of v_s crossing the zero at a value $v = v^*$ determined by

$$\int_{u_-(v^*)}^{u_+(v^*)} f(u, v^*) du = 0.$$

For the system (2.1) one finds [CCL,MUR]

$$c_\infty = (1 - 2a)/\sqrt{2}, \quad (3.9)$$

or in dimensional terms

$$c_\infty = (D_u/2\tau_u)^{1/2}(1 - 2a).$$

Thus, the speed c_∞ decreases from a magnitude of order unity at low thresholds, $a \ll 1/2$, toward a zero value at threshold values approaching $1/2$. We will see in the next section that deviations from the singular limit $\varepsilon = 0$ may have significant effects on the speed of propagation. For the general system (3.1) we find it useful to define the quantity $\Delta \equiv v^* - v_s$. High threshold values then amount to Δ values approaching zero, or to v_s values approaching v^* , the value at which $c_\infty = \mu(v_s) = 0$.

The value of v_b obtained from (3.7) is smaller than v_{\max} . In the language of section 2.1, a wave-back at $v_b < v_{\max}$ amounts to a transition from the right well *before* it disappears. The perturbation that makes the transition possible is provided by diffusion of u from the excited region to the refractory region behind it, thus reducing the value of u below the potential barrier, or beyond the *threshold of de-excitation*. We can therefore refer to a wave-back occurring at $v_b < v_{\max}$ as to a trigger wave in as much as we do so for the wave-front. The speed of the trigger wave-back increases as the threshold of de-excitation decreases, or as v_b increases. When the wave-back speed is still smaller than the wave-front speed, c_∞ , as v_b approaches v_{\max} , the wave-back becomes a ‘‘phase’’ wave; the transition to the left branch (well) is forced by the local dynamics at (approximately) $v_b = v_{\max}$, rather than being triggered by diffusion [TYS2,FIF1,FIF4].

The analysis presented in this section illuminates a general property of nonequilibrium systems, namely, that localized structures such as solitary waves often arise because of the nonvariational character of these systems (or the absence of a free energy to minimize) [FAT]. When $\varepsilon = 0$,

$v = \text{constant}$ is a stable solution of (3.1b), and (3.1a) becomes variational. In that case only two solutions exist that connect the $u_+(v)$ and $u_-(v)$ branches. They are related by the symmetry transformation $\chi \rightarrow -\chi$ and $c_\infty \rightarrow -c_\infty$, and, consequently, propagate in opposite directions. A local perturbation will thus lead to a growing “excited” domain, in as much as a “droplet” of a stable phase grows at the expense of a metastable phase in thermodynamic phase transitions. When $\varepsilon > 0$ v evolves in time and eqs. (3.1a, b) are no longer variational. For an excited domain to retain its size, the wave-front and wave-back should propagate in the *same* direction. This is exactly the effect of the time evolution of v ; the wave-front and wave-back occur at values, $v_f < v^*$ and $v_b > v^*$, respectively, where v^* is the value at which the speed of an interface solution of (3.5) changes sign.

3.1.3. Deviations from the singular limit

The solitary wave speed c_∞ given by (3.7) has been obtained in the singular limit $\varepsilon = 0$. When the time scale separation of u and v is not sharp enough, it is no longer justified to assume constant values for v in the wave-front and wave-back zones. Equations (3.1a, b) do not decouple then from (3.3) and (3.5) and we must analyze the full system. Such an analysis has been carried out in [CCL] (see also [ZYK1]) for a nondiffusive v variable. It leads to an ε dependent propagation speed as we now show.

A wave-front solution propagating invariably with speed c_∞ satisfies

$$u'' + c_\infty u' + f(u, v) = 0, \quad c_\infty v' + \varepsilon g(u, v) = 0, \quad (3.10)$$

where it has been assumed that $\delta = 0$. We now expand u , v and c_∞ in powers of ε ,

$$u = u_f + \varepsilon u_1 + \dots, \quad v = v_s + \varepsilon v_1 + \dots, \quad c_\infty = \mu(v_s) + \varepsilon c_1 + \dots, \quad (3.11)$$

where u_f satisfies (3.5a) and v_s is the constant rest value of v . Substituting these expansions in (3.10) and equating terms to first order in ε we obtain

$$\mathcal{M}u_1 = -c_1 u_f' - v_1 \partial_v f(u, v)|_{u_f, v_s}, \quad \mu(v_s) v_1' = -g(u_f, v_s), \quad (3.12a, b)$$

$$\mathcal{M} = \partial_\chi^2 + \mu(v_s) \partial_\chi + \partial_u f(u, v)|_{u_f, v_s}. \quad (3.13)$$

The operator \mathcal{M} is singular as can be verified by deriving (3.5a) with respect to χ ,

$$\mathcal{M}\xi = 0, \quad \xi = u_f'. \quad (3.14)$$

Solvability of (3.12a) requires then

$$\int_{-\infty}^{\infty} d\chi \xi^\dagger (c_1 u_f' + v_1 \partial_v f(u, v)|_{u_f, v_s}) = 0, \quad (3.15)$$

where ξ^\dagger is a null vector or zero eigenmode of the adjoint operator \mathcal{M}^\dagger . The latter has the same form as \mathcal{M} except that the sign of the $\mu(v_s) \partial_\chi$ term in (3.13) is reversed. The solution of $\mathcal{M}^\dagger \xi^\dagger = 0$ is

$$\xi^\dagger = u_f' \exp[\mu(v_s)\chi]. \quad (3.16)$$

Equation (3.15) gives the first-order correction to the speed

$$c_1 = - \frac{\int_{-\infty}^{\infty} d\chi \xi^\dagger v_1 \partial_v f(u, v)|_{u_f, v_s}}{\int_{-\infty}^{\infty} d\chi \xi^\dagger \xi}, \quad (3.17a)$$

where v_1 can be obtained by integrating (3.12b),

$$v_1(\chi; v_s) = \frac{1}{\mu(v_s)} \int_{\chi}^{\infty} d\chi' g(u_f(\chi'), v_s). \quad (3.17b)$$

Notice that $v_1 \rightarrow 0$ as $\chi \rightarrow \infty$ because ahead of the wave-front the medium is at rest and $v = v_s$. The explicit form of the correction c_1 can be evaluated for particular model systems. It is generally a negative quantity, implying that as ε is increased the speed decreases.

We can write now the speed of a wave-front propagating through a medium at rest as

$$c_\infty = \mu(v_s) + c_1(v_s)\varepsilon + O(\varepsilon^2), \quad (3.18)$$

where $\mu(v_s)$ and $c_1(v_s)$ are given by (3.8) and (3.17). In general, the speed can be reduced by increasing either v_s or ε . The speed of propagation can be used as a measure for the *excitability* of the medium; the higher the speed at which excitation spreads, the more excitable the medium. Thus, sharper time scale separations (smaller ε values) and smaller thresholds (larger $\Delta = v^* - v_s$ values) pertain to higher excitability.

In the singular limit ($\varepsilon = 0$) the wave-front speed goes to zero as v_s approaches v^* . When $\varepsilon > 0$, a stationary solitary wave solution may not exist, for the slow local increase of v may eventually induce de-excitation and recovery to the rest state (diffusion of v , however, may stabilize a stationary wave. See section 3.1.5). In that case there will be a critical value $v_s = v_c(\varepsilon) < v^*$ and a minimal speed, $c_{\min}(\varepsilon, v_c) > 0$ (for ε fixed), at which forward propagation fails [RIK]. For a nondiffusive v variable the minimal propagation speed has been found to scale with ε like [RIK, KHR, ZYK1]

$$c_{\min} \sim \varepsilon^{1/2}. \quad (3.19)$$

This scaling form follows straightforwardly from the requirement that the size of the excited domain, $\lambda_+ = \chi_f - \chi_b$, is of the order of the wave-front width, $w_f \sim O(1)$ [KAR3]. To see this we integrate (3.10) between χ_b and χ_f ,

$$\lambda_+ = c_\infty T_+, \quad T_+ = \frac{1}{\varepsilon} \int_{v_s}^{v_b} \frac{dv}{G_+(v)}, \quad (3.20)$$

where T_+ is the duration of excitation. Expanding $c_\infty(v_s)$ and $T_+(v_s)$ around $v_s = v^*$ we find $T_+ \sim c_\infty/\varepsilon + O(1)$. Using (3.20) and demanding $\lambda_+ \sim O(1)$ we obtain $c_\infty = c_{\min} \sim \varepsilon^{1/2}$.

Alternatively, one can hold v_s fixed and increase ε . Again, there will be a critical value, $\varepsilon_c(v_s)$ and a minimal speed, $c_{\min}(\varepsilon_c, v_s) > 0$, at which propagation fails [ZYK1]. Figures 6a, b show schematically c_∞ versus v_s and c_∞ versus ε curves for a nondiffusive v variable. There are two solution branches in each figure representing high amplitude, stable solitary waves (solid lines) and low amplitude, unstable

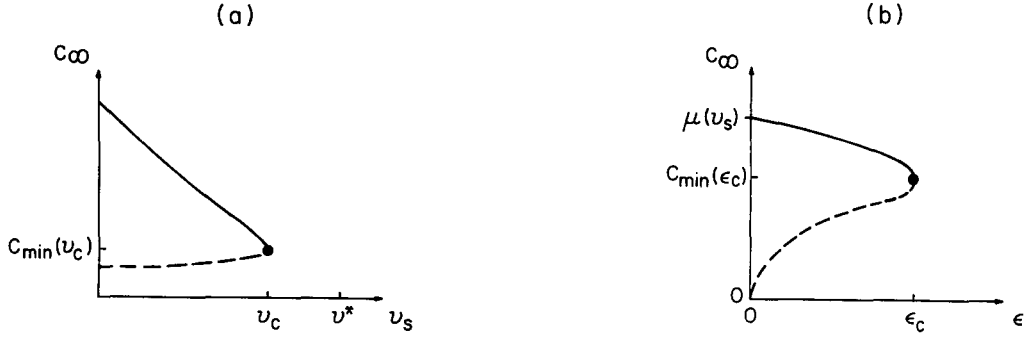


Fig. 6. Failure of propagation at finite minimal speed c_{\min} for a nondiffusive v variable may be obtained (a) by increasing the threshold or v_s to a critical value, $v_c(\epsilon)$, or (b) by increasing ϵ to a critical value $\epsilon(v_s)$.

solitary waves (dashed lines). The knees at which the stable and unstable branches merge define the critical points (c_{\min}, v_c) and (c_{\min}, ϵ_c) [RIK,ZYK1].

3.1.4. The solitary wave as a homoclinic orbit

From the point of view of dynamical-systems theory [GUH] the solitary wave solution is a homoclinic orbit of the system

$$u'' + c_{\infty}u' + f(u, v) = 0, \quad \delta v'' + c_{\infty}v' + \epsilon g(u, v) = 0, \quad (3.21)$$

obtained from (3.1) when u and v are assumed to be functions of $\chi = x - c_{\infty}t$ alone. That is,

$$u(\chi) \rightarrow u_s, \quad v(\chi) \rightarrow v_s, \quad \text{as } \chi \rightarrow \pm\infty. \quad (3.22)$$

Notice that (u_s, v_s) , the linearly stable rest state of (3.1), becomes a saddle node of (3.21). Existence proofs of homoclinic solutions of particular model systems were obtained by several authors [CAR, CON,HAS,JKL].

The asymptotic forms of the solitary wave solution can be obtained from a linear analysis of (3.21) around the rest state $S = (u_s, v_s)$. In this analysis only those eigenvectors pertaining to slowest growth from $\chi = -\infty$ and slowest decay as $\chi \rightarrow \infty$ can be considered. All other eigenvectors will contribute exponentially smaller terms. The growth and decay rates are determined by the real parts of the corresponding eigenvalues. We denote these real parts by η_{ℓ} and η_r , where the subscripts stand for left ($\chi \rightarrow -\infty$) and right ($\chi \rightarrow \infty$) asymptotic forms. The imaginary parts, if they exist, represent oscillations superposed on the exponential growth or decay. The tails of solitary waves in excitable media are sometimes accompanied by such oscillations [SKW,AID]. They are expected to be found at ϵ values sufficiently large and threshold values [a in model (2.1a)] sufficiently small as fig. 7 illustrates. We thus assume the following asymptotic forms:

$$H(\chi) \sim A_{\ell} \exp(\eta_{\ell}\chi) \cos(\nu_{\ell}\chi + \phi_{\ell}), \quad \chi \rightarrow -\infty; \quad H(\chi) \sim A_r \exp(-\eta_r\chi), \quad \chi \rightarrow \infty, \quad (3.23)$$

where $H \equiv (h_u, h_v)$ is the homoclinic solution of (3.21), A_{ℓ} and A_r are constant vectors and η_{ℓ} and η_r are positive.

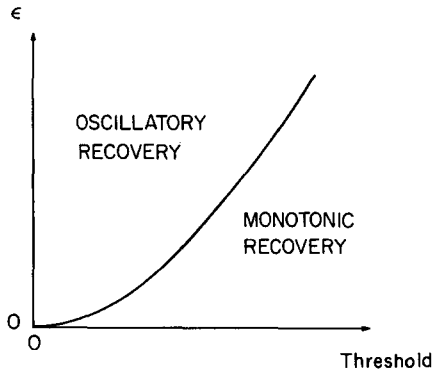


Fig. 7. Schematic illustration of parameter regimes where monotonic and oscillatory recoveries (tails) are expected to be found.

The discussion in section 3.1.2 suggests that for excitable media η_r is normally much larger than η_ℓ . The reason is that the head of the solitary wave is described by the wave-front solution, u_f , while the tail (refractory region) is given by the much smoother solution, v (see also fig. 4a). This property has an important consequence when the tail is oscillatory, that is, when $v_\ell \neq 0$. A theorem due to Shil'nikov implies then the existence of a strange set of recurrent trajectories near the homoclinic orbit [SHI,TRE,GUH]. We will return to this issue in section 3.2.3.

3.1.5. Nonpropagating solitary waves

We have seen in the previous sections that wave propagation results from the coupling of excitability and diffusion of the *fast* variable u [see (3.9)]. The diffusion of the slow variable v did not appear to play a crucial role. Indeed, propagating solitary waves have been observed both in chemical systems [$\delta \sim O(1)$] and in electrophysiological systems ($\delta = 0$). The situation might be different, however, when the diffusion length of the slow field, $l_v = (D_v \tau_v)^{1/2}$, becomes sufficiently large with respect to the corresponding length, l_u , of the fast field, as a comparison of the two terms on the right-hand side of (3.1b) suggests [$(\delta/\varepsilon) = (l_v/l_u)^2$]. For in that case, the diffusion of v ahead of the excited domain can inhibit further excitation and, at the same time, balance the local production of v , thus preventing the recovery to the rest state. The outcome is a nonpropagating excited region [KOK,EHT,SUO]. This region need not be stationary; when the timescale separation is sufficiently sharp a Hopf bifurcation may occur, leading to a nonpropagating “breathing” domain that expands and shrinks periodically in time [KOK,NIM]. Lateral inhibition of an autocatalytic process by diffusion of a slow field has been suggested as a basic principle that underlies a variety of stationary (Turing type) patterns in biological systems [MEI].

3.2. Extended patterns

3.2.1. Periodic traveling waves

In addition to the solitary wave solution, eqs. (3.1) admit a continuous family of stable, periodic traveling-wave solutions. The target and spiral-wave patterns of fig. 1 (away from their centers where curvature effects are negligible) are two-dimensional physical realizations of these solutions. A considerable amount of information about wave patterns in excitable media can be extracted from the dispersion relation of periodic traveling waves, namely, the relation between the speed of propagation

and the traveling-wave period [RIK]. The singular perturbation approach of section 3.1.2 can be used to derive an approximate form of this relation. We sketch this derivation, following primarily ref. [DKT] (see also refs. [ZYK1,DOK,KEL1]).

The repeated structure in a periodic traveling wave consists of a wave-front centered at χ_f , excited region, a wave-back centered at χ_b , and a refractory region that terminates at the location of the successive wave-front, χ_s . The outer equations are

$$\delta v'' + cv' + \varepsilon G_-(v) = 0, \quad \chi_s < \chi < \chi_b; \quad \delta v'' + cv' + \varepsilon G_+(v) = 0, \quad \chi_b < \chi < \chi_f, \quad (3.24a, b)$$

where c is the speed of a periodic traveling wave, $\chi = x - ct$ and $G_{\pm}(v) = g(u_{\pm}(v), v)$. These equations should be supplemented by the continuity and periodicity conditions

$$\begin{aligned} v(\chi \rightarrow \chi_b^+) &= v(\chi \rightarrow \chi_b^-) = v_b, & v'(\chi \rightarrow \chi_b^+) &= v'(\chi \rightarrow \chi_b^-), \\ v(\chi \rightarrow \chi_f^-) &= v(\chi \rightarrow \chi_s^+) = v_f, & v'(\chi \rightarrow \chi_f^-) &= v'(\chi \rightarrow \chi_s^+), \end{aligned} \quad (3.25)$$

where v_f is the value of v at the wave-front position. The inner equations and the matching conditions are the same as (3.5) and (3.6) except that the solitary-wave speed, c_{∞} , is replaced by c , and v_s by v_f . In analogy to (3.7) we obtain (in the singular limit)

$$c = \mu(v_f) = -\mu(v_b). \quad (3.26)$$

Equations (3.25) provide six constraints for two second-order equations. One should therefore view the sizes of the excited and refractory regions, $\lambda_+ = \chi_f - \chi_b$ and $\lambda_- = \chi_b - \chi_s$, respectively, as unknowns. A parametric form of the dispersion curve in terms of v_f can then be obtained by solving (3.24), (3.25) and (3.26) to yield the wavelength $\lambda = \lambda_+(v_f) + \lambda_-(v_f)$, and by evaluating $c = \mu(v_f)$ in (3.26).

The nonlinear nature of (3.24) makes these equations difficult to solve, in general. The case of a nondiffusive v variable ($\delta = 0$) is obviously simpler. Even when $\delta \neq 0$ (but not too large) there are circumstances which allow the neglect of the diffusion term: large wavelengths or speeds c close to the solitary-wave speed, c_{∞} . To see this one can linearize (3.24a, b) around some fixed value of v , solve the linearized equations and use the solutions to estimate the sizes of the diffusion terms. Assuming that $c \sim c_{\infty} \sim O(1)$ and that δ is at most of order unity, one finds that the diffusion terms are of $O(\varepsilon^2)$ whereas the other terms are of $O(\varepsilon)$. Without the diffusion term (3.24) can be integrated directly to yield

$$\lambda_+(v_f) = \chi_f - \chi_b = \mu(v_f) T_+(v_f), \quad T_+ = \frac{1}{\varepsilon} \int_{v_f}^{v_b} \frac{dv}{G_+(v)}, \quad (3.27a)$$

$$\lambda_-(v_f) = \chi_b - \chi_s = -\mu(v_f) T_-(v_f), \quad T_- = \frac{1}{\varepsilon} \int_{v_f}^{v_b} \frac{dv}{G_-(v)}, \quad (3.27b)$$

where v_b is related to v_f through (3.26). Equations (3.26) and (3.27) give a parametric form of the

dispersion relation, $c = c(\lambda)$, valid for a nondiffusive v variable, or for large wavelengths [speeds $c \sim O(1)$] in the diffusive case ($\delta \neq 0$). The limit $v_f \rightarrow v_s$ corresponds to the solitary-wave solution (see section 3.1.2). Indeed, in this limit $\mu(v_f) = c_\infty$ and $\lambda_-(v_f) \rightarrow \infty$ since $G_-(v_s) = 0$. Notice that the excited region, $\lambda_+(v_s)$, remains finite, so that

$$\lambda_+/\lambda_- \rightarrow 0 \quad \text{as} \quad c \rightarrow c_\infty \sim O(1). \quad (3.28a)$$

When $c \ll 1$ the diffusion of v cannot be neglected in general. Indeed, assuming the scaling form $c \sim \varepsilon^{1/2}$ [DKT] and transforming $x \rightarrow \varepsilon^{1/2}x$ we find for $\delta \sim O(1)$ that the diffusive terms in (3.24) have the same orders of magnitude as the other terms. In this case, one may try to simplify (3.24) by linearizing the nonlinear terms in (3.24) around the value $v = v^*$ at which the speed $c = \mu(v)$ is zero,

$$G_\pm(v) \approx \pm a_\pm - b_\pm(v - v^*). \quad (3.29)$$

Equations (3.24) can be solved then exactly,

$$v(\chi) - v^* = \begin{cases} a_+/b_+ + \alpha_+ \exp[\eta_+^{(1)}(\chi - \chi_b)] + \beta_+ \exp[\eta_+^{(2)}(\chi - \chi_b)] & \chi_b < \chi < \chi_f \\ -a_-/b_- + \alpha_- \exp[\eta_-^{(1)}(\chi - \chi_b)] + \beta_- \exp[\eta_-^{(2)}(\chi - \chi_b)] & \chi_s < \chi < \chi_b \end{cases}, \quad (3.30a)$$

$$\eta_\pm^{(1)} = [-c + (c^2 + 4\varepsilon\delta b_\pm)^{1/2}]/2\delta, \quad \eta_\pm^{(2)} = [-c - (c^2 + 4\varepsilon\delta b_\pm)^{1/2}]/2\delta. \quad (3.30b)$$

The coefficients α_\pm and β_\pm in (3.30a) are determined in terms of λ_\pm and c using the continuity and periodicity conditions (3.25). Linearizing the speed relation $c = \mu(v)$ as well, and using (3.26) one obtains

$$v(\chi_b) = v_b = v^* - c/\mu'(v^*), \quad v(\chi_f) = v_f = v^* + c/\mu'(v^*), \quad (3.31)$$

or using (3.30a)

$$J_1(\lambda_+, \lambda_-, c) = a_+/b_+ + \alpha_+ \exp(\eta_+^{(1)}\lambda_+) + \beta_+ \exp(\eta_+^{(2)}\lambda_+) - c/\mu'(v^*) = 0, \quad (3.32)$$

$$J_2(\lambda_+, \lambda_-, c) = -a_-/b_- + \alpha_- + \beta_- + c/\mu'(v^*) = 0.$$

Solutions of (3.32) give λ_+ and λ_- as functions of c , or the dispersion relation [DKT,DOK].

A different scaling form for the speed, $c \sim \varepsilon^{1/3}$, has been suggested in refs. [FIF1,FIF3] in the context of spiral waves, and later used in [KEL1] to study dispersion curves. This scaling allows further simplification of (3.24) but is more restrictive. Setting $x = \varepsilon^{-1/3}\tilde{x}$, $c = \varepsilon^{1/3}\tilde{c}$ and $v - v^* = \varepsilon^{1/3}\tilde{v}$, we find from (3.24) and (3.29) the leading-order form

$$\delta\tilde{v}'' + \tilde{c}\tilde{v}' \pm a_\pm = 0, \quad (3.33)$$

which amounts to setting $b_\pm = 0$ in (3.29). The range of v is restricted, however, to an $\varepsilon^{1/3}$ neighborhood of v^* .

In the large wavelength regime, $\lambda_+/\lambda_- \rightarrow 0$ as $c \rightarrow c_\infty$ [see (3.28a)]. Equation (3.33) can be used to obtain the corresponding relation for the short wavelengths or $c \ll 1$. Solving (3.33) instead of (3.24)

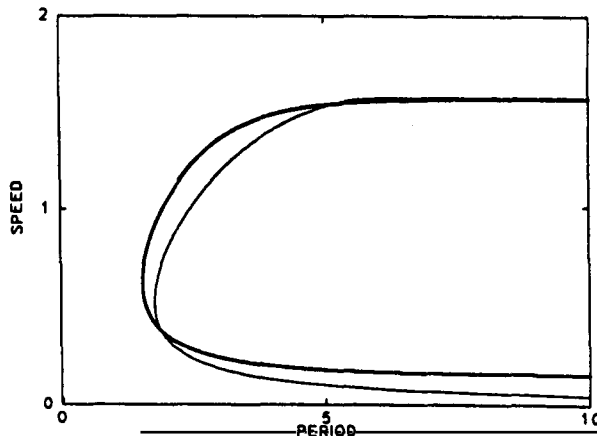


Fig. 8. Dispersion relations for the Oregonator model, calculated by numerical integration of the reaction diffusion equations (thin line) and by solving (3.32) (thick line). (Adapted from Dockery et al. [DKT] with permission.)

and applying the continuity and periodicity conditions one finds [DKT,KEL1]

$$\lambda_+/\lambda_- = a_-/a_+, \quad c \ll 1. \quad (3.28b)$$

Thus, wavelength variations at low speeds involve variations of both the recovery and the excited domains.

The extent to which dispersion relations derived from (3.32) fit direct numerical evaluations is shown in fig. 8 for the Oregonator model. Notice that the dispersion relation in this figure has two branches. They correspond to two families of traveling-wave solutions, high speed stable solutions and low speed unstable solutions [RIK,MAG1,MAG2]. The knee where the two branches meet defines a minimal wavelength, λ_{\min} , or period, T_{\min} , below which propagation fails, in as much as there exists a critical value v_c of v above which propagation becomes impossible (see section 3.1.3). The two branches do not always merge into each other; at sufficiently large δ values the two branches intersect the $c = 0$ axis at different points. These intersection points pertain to nonpropagating periodic solutions which are actually solutions in two one-parameter families of nonpropagating solutions from which the traveling waves bifurcate. At still higher δ values the traveling-wave solutions disappear and only nonpropagating solutions exist. A bifurcation diagram of traveling and nonpropagating wave solutions is given in [DOK]. The stability of nonpropagating waves to breathing type motion (see section 3.1.5) has been studied in [OIT]. The interactions between nearly excited domains were found to induce an in-phase synchronized oscillation.

3.2.2. Kinematical approach

So far we discussed periodic traveling waves that propagate invariably at constant speeds. It is known, however, that traveling waves may deform during propagation [RIN2]. In contrast to a few other physical contexts where such deformations are described in terms of large length-scale phase fields [HOK,KUR,CRN], here, a kinematical approach seems more appropriate (see however [BER]). We have already pointed out that in the large wavelength regime [$c \sim c_\infty \sim O(1)$] the excited region, λ_+ , does not vary significantly as the wavelength of the pattern changes. It is rather the refractory region between two successive excited domains that shrinks or expands as the pattern deforms. One can

therefore view extended sparse patterns as many-body systems of interacting excited domains that accelerate or decelerate during their motion but preserve their shapes. Each excited domain, or pulse, is then characterized by its instantaneous position $x_i(t)$ or, alternatively, by the passage time, $t_i(x)$, through a given point x (the particular point in the excited domain that x_i designates is immaterial as the pulse shape is preserved). The view of an excited domain as an integral entity is also useful when the deviations from the singular limit $\varepsilon = 0$ are relatively large, for in that case the decomposition of a pulse into a wave-front and a wave-back may not be valid (see fig. 5a).

A kinematical approach of this kind has been advanced in refs. [MIR,RIM]. The basic assumptions in these studies are that the velocity of a given pulse depends solely on the time elapsed since the passage of the preceding pulse, and that this dependence is given by the dispersion relation, $c = c(T)$, where T is the (temporal) period of a periodic traveling wave. In mathematical terms, $dx_i(t)/dt = c[t_i(x) - t_{i-1}(x)]$ or, using $dt_i(x)/dx = dt/dx_i(t)$,

$$dt_i/dx = c^{-1}[t_i(x) - t_{i-1}(x)]. \quad (3.34)$$

Equations (3.34) reproduce remarkably well trajectories, $x_i(t)$, obtained by direct numerical simulations [RIM].

More recently, a formal derivation of kinematic pulse equations has been presented [EMS1,EMS2,EMR]. We outline now the main steps of this derivation. To simplify notations we rewrite eqs. (3.1) in the general form

$$\partial_t U = LU + N(U) + D \partial_x^2 U, \quad U = (u, v), \quad D = \text{diag}(1, \delta), \quad (3.35)$$

where L and N are the linear and nonlinear reaction parts of (3.1), respectively. We confine ourselves to homogeneous media and thus assume that (3.35) is invariant under space translations. To describe a general wavetrain of pulses a solution in the form of a superposition of solitary wave solutions, H , is proposed,

$$U(x, t) \approx \sum_i H(\chi - \chi_i), \quad (3.36)$$

where χ_i is the position of the i th pulse in a frame moving with speed c_∞ , and $\chi_i > \chi_j$ if $i < j$. For such a form to be valid the pulses should be well separated. More specifically, if λ_0 is a typical spacing between successive pulses then $\gamma \equiv \exp(-\eta_\varepsilon \lambda_0)$ should be a small parameter. This condition guarantees that at each pulse position the fields of all other pulses are small. Despite the smallness of these fields, their effects on pulse positions can be significant because of the translational invariance of the system.

To derive equations of motion for pulse positions, an exact wavetrain solution is written in the form

$$U(x, t) = \sum_i H(\chi - \chi_i(t)) + R(\chi, t), \quad (3.37)$$

where R is a small correction term and the following orders of magnitude are assumed: $d\chi_i/dt \sim R \sim \partial_\chi R \sim O(\gamma)$, and $\partial_t R \sim O(\gamma^2)$. Inserting (3.37) into (3.35) one finds to leading order in γ

$$\mathcal{L}R = - \sum_i \dot{\chi}_i H'_i + I(\{H_i\}), \quad (3.38)$$

where \mathcal{L} is the linear operator

$$\mathcal{L} = c_\infty \partial_x + D \partial_x^2 + L + \nabla_U N \left(\sum_i H_i \right), \quad (3.39)$$

and I is a pulse interaction term given by

$$I = \sum_i N(H_i) - N \left(\sum_i H_i \right). \quad (3.40)$$

In these equations $H_i \equiv H(\chi - \chi_i)$, $\dot{\chi}_i \equiv d\chi_i/dt$ and $\nabla_U N$ is the Jacobian matrix of $N(U)$ with respect to U . Notice that I is of $O(\gamma)$. A consequence of the translational invariance of (3.35) is that the operator

$$\mathcal{L}_j = c_\infty \partial_x + D \partial_x^2 + L + \nabla_U N(H_j), \quad (3.41a)$$

has a null vector or zero eigenmode,

$$\mathcal{L}_j \Xi_j = 0, \quad \Xi_j \equiv H'_j. \quad (3.41b)$$

Comparing (3.39) with (3.41) we find

$$\mathcal{L} \Xi_j = O(\gamma), \quad (3.42)$$

where we used the fact that H is localized and therefore $\nabla_U N(\sum_i H_i) \cdot H'_j = \nabla_U N(H_j) H'_j + O(\gamma)$.

Equations (3.38) and (3.42) suggest that R may contain a ‘‘small denominator’’ component. The requirement that R remains of order γ leads to equations of motion for the χ_i . To see this let us define an inner product

$$(P, Q) = \int_{-\infty}^{\infty} dx P(x) \cdot Q(x), \quad (3.43)$$

where the dot denotes the usual scalar product in \mathcal{R}^n . The existence of a null vector of \mathcal{L}_j suggests that the null space of the adjoint operator, \mathcal{L}_j^\dagger , is nonempty as well. We assume that a null vector of \mathcal{L}_j^\dagger indeed exists and denote it by $\Xi_j^\dagger = \Xi^\dagger(\chi - \chi_j)$. Since H_j is localized around $\chi = \chi_j$ so should Ξ_j^\dagger . It therefore follows that

$$\mathcal{L}_j^\dagger \Xi_j^\dagger = O(\gamma). \quad (3.44)$$

Taking the inner product of (3.38) with Ξ_j^\dagger we find that the left-hand side is of $O(\gamma^2)$ [if R is indeed of $O(\gamma)$]. The right-hand side contains, on the other hand, terms of $O(\gamma)$. To leading order in γ these terms should cancel each other. Using the localized nature of H and Ξ^\dagger we obtain

$$\dot{\chi}_j = (\Xi_j^\dagger, I) / (\Xi_j^\dagger, \Xi_j). \quad (3.45)$$

The integral (Ξ_j^\dagger, I) in (3.45) can be evaluated by exploiting the fact that the pulses are well separated

and that next-nearest-neighbor interactions can be neglected [EMS2, EMR]. Using the asymptotic forms (3.23) we finally obtain

$$\dot{\chi}_j = q_r(\chi_j - \chi_{j+1}) + q_\ell(\chi_j - \chi_{j-1}), \quad (3.46a)$$

where q_r and q_ℓ are given by

$$q_r(\chi) = a_r \exp(-\eta_r \chi), \quad \chi > 0; \quad q_\ell(\chi) = a_\ell \exp(\eta_\ell \chi) \cos(\nu_\ell \chi + \psi_\ell), \quad \chi < 0. \quad (3.46b)$$

The quantities a_r , a_ℓ and ψ_ℓ are related to A_r , A_ℓ and ϕ_ℓ , respectively [EMR].

Equations (3.46) should be supplemented by initial conditions which specify the positions of all pulses, $\{x_i(t_0)\}$ at a given time t_0 . In biological applications wavetrains are often generated by local pacemakers. The temporal behavior imposed at the pacemaker location defines a boundary value problem which is not in gear with (3.46). A way out of this difficulty is to reformulate the problem in terms of the set of timings $\{t_i(x)\}$ [EMR]. This leads to kinematical equations of the form (3.34). A pacemaker located at x_0 then defines ‘‘initial’’ values, $\{t_i(x_0)\}$ for the functions $\{t_i(x)\}$.

The kinematical equations (3.46) can be used to derive the dispersion relation in the limit of large wavelength. Setting $\dot{\chi}_j = c - c_\infty$ and $\chi_{j-1} - \chi_j = \lambda$ for any i (recall that χ_j is the position of the j th pulse in a frame moving with speed c_∞) we obtain

$$c = c_\infty + q_\ell(-\lambda) + q_r(\lambda). \quad (3.47)$$

Let us compare this expression with the dispersion relation obtained in section 3.2.1 using the singular perturbation approach. We first simplify (3.47) by neglecting the last term on the right-hand side. This is justified since η_r is normally much larger than η_ℓ (see section 3.1.4). If we further restrict ourselves to monotonic recovery for which $\nu_\ell = 0$, we find (see also ref. [GLE])

$$c = c_\infty + a_\ell \exp(-\eta_\ell \lambda). \quad (3.48)$$

The exponent η_ℓ can be obtained from a linear analysis of (3.3a) around the rest state $v = v_s$. Such an analysis yields $\eta_\ell = \eta_- = -\varepsilon G'_-(v_s)/c_\infty$. Consider now eqs. (3.27). In the limit of large wavelength v_f approaches v_s . One consequence of this is that $\lambda_- \gg \lambda_+$ because $G_-(v_s) = 0$. For the same reason the main contribution to the integral in (3.27b) comes from v values close to v_f . For such values we can linearize G_- around v_s . We thus obtain

$$\lambda \approx \lambda_- \approx -[\mu(v_f)/\varepsilon G'_-(v_s)] \ln[(v_b - v_s)/(v_f - v_s)]. \quad (3.49)$$

Expanding $\mu(v_f)$ around $\mu(v_s)$ and using (3.7) and (3.26) we find $v_f - v_s = (c - c_\infty)/\mu'(v_s)$. Using this result in (3.49) we obtain

$$c = c_\infty + \mu'(v_s)(v_b - v_s) \exp(-\eta_\ell \lambda) + O(\exp(-2\eta_\ell \lambda)),$$

which coincides with (3.48) once we identify a_ℓ with $\mu'(v_s)(v_b - v_s)$.

The kinematical approach presented above is valid for $c \sim 1$. When $c \ll 1$ the excited domains do not preserve their sizes during propagation, for according to (3.28b) λ_+/λ_- is constant, and a description in

terms of a single position variable, $x_i(t)$, is no longer sufficient. In this case one should introduce two variables for each excited domain describing the instantaneous wave-front and wave-back positions, or alternatively, consider λ_+ and λ_- independently [KEE1].

3.2.3. Homoclinic chaos in space

The dispersion curve, $c = c(\lambda)$, provides a relation between the constant velocity of a periodic wavetrain and the *uniform* spacing, λ , between successive pulses. Constant speed wavetrains, however, need not necessarily be equally spaced. When the recovery to the rest state is oscillatory (i.e., when $\nu_1 \neq 0$) a multitude of nonuniformly spaced wavetrains exist [KAK,EFF,HAS,RIM,MAG3,FER]. For such wavetrains the usefulness of the dispersion relation is no longer apparent as there is no single spacing to relate the speed to. We will see at the end of this section that under certain simplifying assumptions significant information can still be extracted from the dispersion relation. Before resorting to such simplifications, however, we want to examine the kinematical equations (3.46) as they are, and for that purpose another relation proves useful. It is a *map* that relates successive spacings in a wavetrain of a given speed. To derive this map we simply set $\dot{\chi}_j = \Delta c = c - c_\infty$ for any j in (3.46). Using the definition $Z_j \equiv q_r(\chi_{j-1} - \chi_j)$ we obtain

$$Z_{j+1} = f(Z_j) \equiv \Delta c - bZ_j^\eta \cos(\nu \ln Z_j + \varphi); \quad \eta = \eta_e/\eta_r < 1, \quad \nu = \nu_e/\eta_r. \quad (3.50a, b)$$

We assume that a_r in (3.46b) is positive as this seems to be the case for excitable media; a given pulse facilitates (though very weakly) the propagation of its predecessor. Thus $Z_j > 0$ for all j . The reader should not confuse f in (3.50a) with the reaction part, f , of (3.1a).

One-dimensional maps of this form are well known [ACS,GLS,COE,FOW]. They are obtained as approximate first return maps of low-dimensional flows that admit homoclinic orbits at critical parameter values [GUH]. In the present context the low-dimensional flow is given by (3.21) with c_∞ replaced by the parameter c . The homoclinic orbit exists at the critical parameter value $c = c_\infty$ or $\Delta c = 0$, and pertains to the solitary wave solution. To see how (3.50) is related to this flow, consider the three-dimensional space spanned by the eigenvectors, X, Y, Z , that correspond to the three eigenvalues, $\eta_e \pm i\nu_e$ and η_r , respectively. Let the origin be at the rest state S (the saddle focus to which the homoclinic orbit is biasymptotic as $\chi \rightarrow \pm\infty$). A Poincaré section at constant Y near S yields (after proper rescaling of coordinates) a two-dimensional map of the form [ACS,GLS]

$$X_{j+1} = 1 - b_1 X_j Z_j^\eta \sin(\nu \ln Z_j + \varphi_1), \quad (3.51a)$$

$$Z_{j+1} = \Delta c - b_2 X_j Z_j^\eta \cos(\nu \ln Z_j + \varphi_2). \quad (3.51b)$$

The homoclinic orbit is given by the fixed point $X^* = 1, Z^* = 0$ at $\Delta c = 0$. If we restrict ourselves to trajectories that pass close enough to the homoclinic orbit we can set $X_j \approx 1$ in (3.51b) and thus obtain (3.50a). Evidently, this restriction amounts to considering large wavelengths, a presumption that indeed has been used in deriving (3.46) and consequently (3.50).

The relation between constant-speed wavetrain solutions of (3.1) and trajectories of (3.50) is readily seen. Wavetrains with equal spacings λ , correspond to fixed points, $Z^* = f(Z^*)$, where $Z^* = q_r(\lambda)$. This is just a different way of writing the dispersion relation (3.47). The solitary wave solution is obtained in the limit $\lambda \rightarrow \infty$ and pertains to the homoclinic fixed point $Z^* = 0$ at $\Delta c = 0$. Periodic wavetrains with

two alternating spacings correspond to period-2 orbits and so on. To find stable wavetrain solutions of (3.1) we can first look for periodic orbits of (3.50) and then linearize (3.46) about these orbits to evaluate the stability of the corresponding wavetrains. We will illustrate this strategy with fixed-point solutions of (3.50) [EMS1,EMS2].

When $\eta < 1$ and $\nu_\ell \neq 0$, a result due to Shil'nikov [SHI] states that any neighborhood of the homoclinic orbit contains infinitely many periodic orbits of the saddle type. When we allow for speeds $c \neq c_\infty$, infinitely many more homoclinic orbits appear [EFF,HAS,GLS,GAS,FER], describing multi-pulse solitary waves. The structure of possible solutions is in fact far richer as (3.51) contains (for $\Delta c = 0$) an infinite number of horseshoe maps, and trajectories of (3.51) can communicate between different horseshoes. We refer the reader to refs. [GUH,GLS] for more details concerning solutions of (3.51). Much of this picture carries over to the one-dimensional map (3.50). Figure 9 shows this map for $\Delta c = 0$ and $\eta < 1$ (note that only positive Z_j values have physical meaning). There are infinitely many intersections with the diagonal accumulating near $Z = 0$. The slopes of the map at these intersection points diverge in absolute value as $Z \rightarrow 0$, suggesting that complete cascades of period-doubling bifurcations have developed near these points. These cascades are closely related to the horseshoe maps of (3.51) [YOA]. We thus recover the result that in any neighborhood of the homoclinic orbit $Z = 0$ there are infinitely many unstable periodic orbits. To find n -pulse homoclinic orbits we look for Δc values for which orbits of the form $(Z_1 = 0, Z_2 = \Delta c, \dots, Z_{n+1} = 0)$ exist. Thus, double-pulse orbits ($n = 2$) occur at Δc values that satisfy

$$\Delta c = b \Delta c^\eta \cos(\nu \ln \Delta c + \varphi). \quad (3.52)$$

Evidently, there are infinitely many such values.

Let us consider now a fixed-point solution of (3.50), $Z^* = q_r(\lambda)$, and study the stability of the corresponding wavetrain, $\chi_j^0 = \Delta c t - (j-1)\lambda + \chi_1^0(0)$. To that end we write $\chi_j = \chi_j^0 + \theta_j(t)$ where θ_j is small, insert this form into (3.46a) and keep only terms linear in θ_j . We obtain

$$\dot{\theta}_j = \eta_r Z^* [\alpha \theta_{j-1} - (1 + \alpha) \theta_j + \theta_{j+1}], \quad (3.53)$$

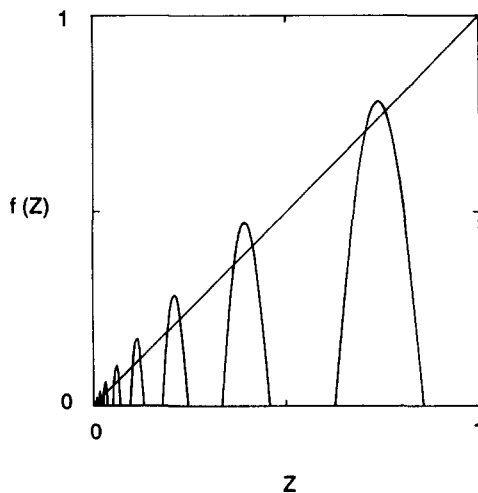


Fig. 9. The map (3.50) for $\Delta c = 0$ and $\eta < 1$. Intersection points of the map with the diagonal correspond to equally spaced wavetrains.

where $\alpha = f'(Z^*)$ is the slope of the map at Z^* . The solutions of (3.53) are of the form $\theta_j = \Theta_k \exp(s_k t + 2\pi i k j / N) + \text{c.c.}$, where c.c. means complex conjugate, N is the number of pulses in the wavetrain and k is an integer. Inserting this form into (3.53) we obtain

$$\text{Re}(s_k) = -\eta_r Z^* (1 + \alpha) [1 - \cos(2\pi k / N)]. \quad (3.54)$$

The condition for stability, $\text{Re}(s_k) < 0$, is $\alpha > -1$. Since $|\alpha| \rightarrow \infty$ as $Z \rightarrow 0$, each hump in fig. 9, sufficiently close to $Z = 0$, contributes one fixed point that corresponds to a *stable* wavetrain. We can therefore conclude that there are infinitely many stable, equally spaced wavetrains.

The stability analysis of higher-order periodic orbits of (3.50) is straightforward but tedious. Numerical studies suggest [EMS1,EMS2] that there exists a rich structure of stable non equally spaced wavetrains as well (see also below). This form of spatial complexity or “spatial chaos” is closely related to the low-dimensional chaos exhibited by (3.50). We wish to note, however, that while the irregular nature of low-dimensional chaos is primarily due to the existence of infinitely many *unstable* periodic orbits [CVI,PRO], spatial chaos, at least as revealed here and in a number of other examples [CER], results from the coexistence of infinitely many *stable* patterns.

The existence of stable constant speed wavetrains suggests relaxational wave propagation; given initial conditions for pulse positions, $\chi_j(0)$, convergence toward uniform propagation with a selected speed, $c = \dot{\chi}_j$, generally occurs. The relaxation process may involve multiple time scales. The basic reason for that lies in (3.54); the relaxation time associated with pulse interaction grows exponentially with the spacing. When nonuniform spacings develop different time scales appear. This may lead to sequential relaxation as fig. 10 illustrates. Shown in this figure are “world lines”, $\chi_j(t)$, for an initially unstable equally spaced wavetrain. According to fig. 9, this wavetrain lies between two stable equally spaced wavetrains with smaller and larger spacings. The initial relaxation stage therefore involves the appearance of the nearby “stable” spacings. The wavetrain consequently decomposes into groups of pulses within each of which dynamics occurs on a short time scale. The inter-group spacings, in general, will not be stable and dynamics on a longer time scale, involving groups of impulses, takes place. This process continues until all spacings are stable and pertain to the same propagation speed.

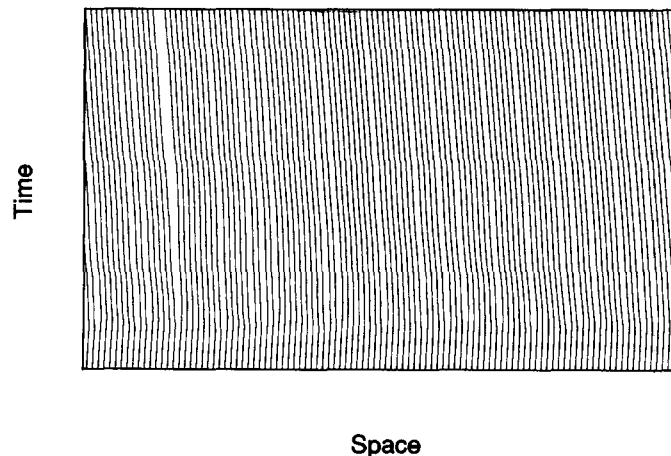


Fig. 10. Typical world lines, $\chi_j(t)$, of an initially unstable, equally spaced wavetrain, obtained by integrating the kinematical equations (3.46).

A more intuitive understanding of pulse dynamics can be obtained once certain simplifications of the kinematical equations (3.46) are made. Using the fact that in excitable media η_e is typically much smaller than η_r , we can neglect the first term on the right-hand side of (3.46) and thus obtain the simpler kinematical equation,

$$\dot{\chi}_j = q_e(\chi_j - \chi_{j-1}). \quad (3.55)$$

If we further confine ourselves to finite trains propagating along an infinite line, the kinematical equations decouple. The first pulse propagates with speed c_∞ as there is no pulse ahead of it to hinder its motion, and the effect of the successive pulse has been neglected. Thus, $\dot{\chi}_1 = 0$. The dynamics of any other pulse is determined by the known dynamics of its predecessor.

Consider now a pair of pulses and let $\lambda = \chi_1 - \chi_2$ be the spacing. We get $\dot{\lambda} = -q_e(-\lambda)$. For monotonic recovery where $q_e(\lambda) = a_e \exp(\eta_e \lambda)$ with $a_e = \mu'(v_s)(v_b - v_s) < 0$ we find that the spacing increases logarithmically with time. Thus pulses are *repelled* by their predecessors when the recovery to the rest state is monotonic. This repulsion is due to the refractory period imposed at the forefront of a propagating pulse by the tail of the preceding pulse. In the case of an oscillatory recovery, there are many zeros of $q_e(\lambda)$ [see (3.46b)], and consequently many stationary solutions, $\lambda = \lambda_k = \text{constant}$. The stability condition, $(dq_e/d\lambda)|_{\lambda_k} > 0$, implies that any second solution is stable. We therefore conclude that in media that give rise to oscillatory recovery pairs of pulses tend to lock at fixed distances or to form *bound* pairs. Physically, oscillatory recovery implies damped oscillations of the threshold of excitation about the threshold value of the rest state. Stationary states are obtained when pulses are located at points pertaining to rest threshold values. Perturbations about these locations decay when the threshold is locally a decreasing function of the spacing.

The decoupling of the kinematical equations simplifies tremendously the stability analysis of nonuniformly spaced finite trains. Denoting by $\{\lambda_k\}$ the nonequal spacings, a general finite train, propagating at uniform speed c_∞ can be written as $\chi_j^0 = \chi_1^0 - \sum_{k=1}^{j-1} \lambda_k$, $j \geq 2$ (notice that in this simplified analysis all finite trains assume the same uniform propagation speed c_∞). Perturbing the finite train by small displacements, θ_j , as before, and linearizing (3.55) we get $\dot{\theta}_j = (\theta_j - \theta_{j-1})q'_e(-\lambda_{j-1})$ or, using (3.47) (with q_r neglected), $\dot{\theta}_j = -(\theta_j - \theta_{j-1})c'(\lambda_{j-1})$. The characteristic equation is $\prod_{k=1}^{N-1} [c'(\lambda_k) + s] = 0$, and thus we conclude that a nonuniform finite train is stable if and only if $c'(\lambda_k) > 0$ for each k . This result makes the dispersion relation useful again, as illustrated in fig. 11. Consider the intersection

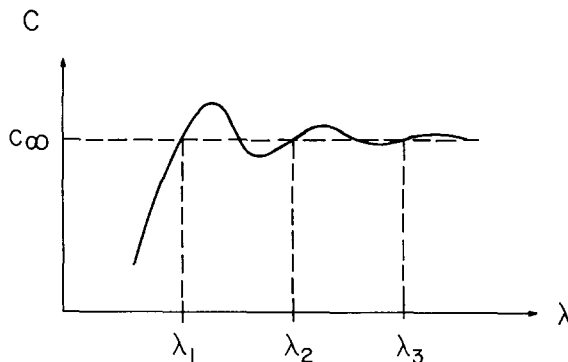


Fig. 11. A typical dispersion curve in the case of oscillatory recovery. Intersections with the line $c = c_\infty$ at positive slopes define stable spacings, $\lambda_1, \lambda_2, \dots$

points of the dispersion curve with the line $c = c_\infty$. All points, λ_k , at which the slope of the dispersion curve is positive define stable spacings. These spacings can be used to construct a great variety of stable nonuniform finite trains. Notice, however, that in this simplified picture the fine horseshoe structure of (3.51) has disappeared.

3.3. Experimental studies

Experimental measurements of propagation speeds of solitary waves in excitable BZ media have been reported in refs. [FIN2,SHO,SEM1,WOR,KKP,KUK,NTH]. The speed was found to be sensitive to the acidity of the solution, $[H^+]$, and to the bromate ion concentration, $[BrO_3^-]$. This is not surprising as both species participate in the autocatalytic step (reaction B.1 in process B). The actual dependence was found to be^{*)}

$$c_\infty \propto ([H^+][BrO_3^-])^{1/2}. \quad (3.56)$$

Using the speed of propagation as a measure for excitability (see section 3.1.3) we conclude that high acidity and/or high bromate-ion concentration pertain to high excitability.

Spatial profiles of solitary waves have been measured in refs. [WOR,NMT] using spectrophotometric detection methods. In this type of experiment, a sample of a BZ solution is placed in a closed cell (petri dish) and illuminated with a monochromatic light tuned at an absorption line of the catalyst, 488 nm for ferroin, 344 nm for cerium. The transmitted light is detected using photodiode array [WOR] or video camera [NMT], and the images are processed to yield spatial intensity (concentration) distributions of the catalyst (oxidized form thereof). In [WOR], the tail of a solitary wave profile could have been well fitted to an exponential function even for catalyst concentrations deviating significantly from the rest-state value. In [NMT] wave profiles have been measured for various initial concentrations of the BZ reagents. A comparison with calculated profiles using a modified Oregonator model has been presented as well.

No systematic studies of dispersion relations or relaxational dynamics of wavetrains have appeared so far. The lack of such studies can be attributed in part to the fact that most experiments have been conducted in closed systems. Such systems cannot be controlled over long time scales because of the ultimate approach toward thermodynamic equilibrium. A novel experimental setup that overcomes this problem has been proposed in ref. [NHM]. It consists of an annular reactor continuously fed with chemicals at the inner and outer rims so as to maintain steady conditions. To damp convective motion the reactor is filled with an inert gel. This set up has been used with the BZ reagent where potassium bromate and sulphuric acid are fed through the outer rim while malonic acid $[CH_2(COOH)_2]$ and the ferroin catalyst through the inner rim. Wavetrains of pulses were initiated by local perturbations of the chemical composition so as to induce a source of pulses (pacemaker) and a barrier which blocks propagation in one direction. After a desired number of pulses were created the composition perturbations were removed. An extensive quantitative study has not been done yet with that system. It is hoped, however, that experimental setups of this kind will soon be used for measuring dispersion relations, for studying instabilities that set in at low speeds [KEL2], and for demonstrating homoclinic chaos in space.

^{*)} The reader is referred to ref. [TYS1] for further discussion of (3.56).

4. Patterns in two space dimensions

4.1. Curved solitary wave-fronts

4.1.1. General

The dispersion relation reflects the manner in which the speed of a propagating wave-front is affected by previous activity. Another significant factor that affects wave propagation in two space dimensions is the wave-front curvature. The effect of positive curvature (center of curvature is behind the propagating front) is to reduce the speed of propagation; the convex geometry defocuses diffusion and thereby reduces the diffusion flux into the quiescent medium ahead of the propagating front. Negative curvature, on the other hand, speeds up the front. This effect of curvature acts to stabilize propagating wavefronts against short-wavelength perturbations as fig. 12 illustrates. The effect of curvature on wave-front speed has been studied for a variety of interfacial phenomena, including crystal growth [BCF,MBK] and flame propagation [MAR,FRS]. In the context of excitable media, curvature–speed relations were derived first in ref. [ZYK2] and later in refs. [ZYK1,KEE2,KET2,FIF4,TYK1,BDZ1,MER1,MIZ]. Following these works we derive here the curvature–speed relation in the singular limit (section 4.1.2) and for small and large deviations from that limit (section 4.1.3).

4.1.2. The curvature–speed relation in the singular limit

For ε sufficiently small we can consider the wave-front and wave-back independently and assume that in these boundary layers the slow field v is constant. Equation (3.1a) then simplifies to

$$\partial_t u = f(u, v_f) + \nabla^2 u, \quad \partial_t u = f(u, v_b) + \nabla^2 u, \quad (4.1a, b)$$

where v_f and v_b are the constant values of v in the front and back, respectively. Let $X(s, t)$ represent the instantaneous position vector of the wave-front in the (x, y) plane, where s is the arclength. It is convenient to define a coordinate system (r, s) that moves with the front

$$\mathbf{x} = X(s, t) + r\hat{\mathbf{r}}(s, t), \quad (4.2)$$

where $\hat{\mathbf{r}} = Y_s \hat{\mathbf{x}} - X_s \hat{\mathbf{y}}$ is a unit vector normal to the curve X and the subscript s denotes partial derivative with respect to s . The curved front solution is now written as

$$u(r, s, t) = u_f(r) + \delta u(r, s, t), \quad (4.3)$$

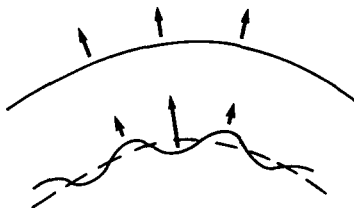


Fig. 12. Curvature acts to smooth out short-wavelength perturbations in the course of propagation, for normal velocity (indicated by arrows) decreases as curvature increases.

where u_f is a planar front solution propagating at speed $\mu(v_f)$ [see (3.26)] and satisfying

$$u_f'' + \mu(v_f)u_f' + f(u_f, v_f) = 0, \quad (4.4)$$

and δu is a correction term. We assume that the curvature, $\kappa = X_s Y_{ss} - Y_s X_{ss}$, is sufficiently small so that δu can be considered as a perturbation. We should bear in mind though that the main effect of curvature is to slow or speed the front rather than to deform its spatial profile. This stems from the translational symmetry of the system and the existence of a soft translational mode. We may therefore expect this perturbation theory approach to remain valid even for moderately small curvature values. In addition we assume that κ is a weak function of s and t so that $|\partial_s \delta u| \sim |\partial_t \delta u| \ll |\partial_r \delta u|$.

The curved front solution u satisfies (4.1a) which in the moving frame becomes

$$\partial_r^2 u + \left[c_r + \frac{\kappa}{(1+r\kappa)} \right] \partial_r u + f(u, v_f) = 0, \quad (4.5)$$

where $c_r = X_t \cdot \hat{r}$ is the normal velocity and we neglected partial derivatives of u with respect to s and t . Equation (4.5) can be written in the form

$$\partial_r^2 u + \mu(v_f) \partial_r u + f(u, v_f) = \delta p, \quad \delta p = [\mu(v_f) - c_r - \kappa/(1+r\kappa)] \partial_r u. \quad (4.6a, b)$$

Inserting (4.3) into (4.6) and using the smallness of δp we find to leading order

$$\mathcal{M} \delta u = \delta p(u_f), \quad (4.7)$$

where the operator \mathcal{M} is given by [cf. eq. (3.13)]

$$\mathcal{M} = \partial_r^2 + \mu(v_f) \partial_r + \partial_u f(u, v_f)|_{u_f, v_f}. \quad (4.8)$$

Since \mathcal{M} is singular,

$$\mathcal{M} \xi = 0, \quad \xi \equiv \partial_r u_f, \quad (4.9)$$

the right-hand side of (4.7) should be orthogonal to the null vector, ξ^\dagger , of the adjoint operator \mathcal{M}^\dagger . This leads to the relation

$$c_r = \mu(v_f) - \left(\frac{\int_{-\infty}^{\infty} dr \xi^\dagger \xi (1+r\kappa)^{-1}}{\int_{-\infty}^{\infty} dr \xi^\dagger \xi} \right) \kappa.$$

If we denote by w_f the (dimensionless) wave-front width and assume $\kappa \ll w_f^{-1}$ this relation simplifies to

$$c_r = c - \kappa, \quad (4.10)$$

or, in dimensional terms, to $c_r = c - D_u \kappa$, where $c = \mu(v_f)$. A similar analysis can be carried out for the back. Equation (4.10) clearly reflects the effect of curvature discussed in the previous section; positive (negative) curvature decreases (increases) the speed of propagation. The assumptions under which

(4.10) has been derived are small curvature and weak curvature dependence on arclength and time. When these assumptions do not hold arclength-derivative terms and nonlinear corrections will appear in the right-hand side of (4.10).

4.1.3. Deviations from the singular limit

When the time scale separation is not sufficiently sharp, it is no longer possible to consider v as constant in the front and back transition zones, and one has to resort back to the full system (3.1). In a frame moving with the front this system becomes

$$\partial_r^2 u + [c_r + \kappa/(1 + r\kappa)] \partial_r u + f(u, v) = 0, \quad (4.11a)$$

$$\delta \partial_r^2 v + [c_r + \delta\kappa/(1 + r\kappa)] \partial_r v + \varepsilon g(u, v) = 0, \quad (4.11b)$$

where we have neglected partial derivatives with respect to s and t . Following refs. [ZYK1,ZYK2,MIZ], we consider a nondiffusive v variable (i.e., $\delta = 0$), assume small curvature, $\kappa \ll w_f^{-1}$, and write (4.11) as

$$\partial_r^2 u + (c_r + \kappa) \partial_r u + f(u, v) = 0, \quad (c_r + \kappa) \partial_r v + \varepsilon^* g(u, v) = 0, \quad (4.12a, b)$$

$$\varepsilon^* = \varepsilon(1 + \kappa/c_r). \quad (4.13)$$

Equations (4.12) describe a planar front propagating at speed

$$c(\varepsilon^*) = c_r + \kappa, \quad c(\varepsilon^*) = \mu(v_f) + \varepsilon^* c_1, \quad (4.14)$$

where c_1 is given by (3.17) with v_s replaced by v_f . Inserting (4.13) into (4.14) we obtain

$$c_r = c(\varepsilon) - \kappa + \varepsilon c_1 \kappa / [\mu(v_f) - \kappa] + O(\varepsilon^2), \quad c(\varepsilon) = \mu(v_f) + \varepsilon c_1. \quad (4.15)$$

Thus the curvature–speed relation becomes *nonlinear* even when the condition $\kappa \ll w_f^{-1}$ is satisfied. It reduces to the linear relation (4.10) as $\varepsilon \rightarrow 0$. The validity of (4.15) has been tested in refs. [ZYK1,ZYK2] by comparison with direct numerical simulations. Good agreement has been obtained in a fairly broad ε range. The generalization to a diffusing v variable has not yet been accomplished (see ref. [MIZ]), but the special case $\delta = 1$ is easy to treat. Here, there is no need to renormalize ε and we obtain at once the linear relation $c_r = c(\varepsilon) - \kappa$.

We now rederive (4.15) using the approach of the previous section. Equations (4.11) can be written as

$$\partial_r^2 u + \mu(v_f) \partial_r u + f(u, v) = \delta p(u), \quad c_r \partial_r v = -\varepsilon g(u, v), \quad (4.16a, b)$$

where $\delta p(u)$ is given by (4.6b) and, as before, we consider the case $\delta = 0$. In analogy to (4.3) we write the curved front solution as

$$u(r, s, t) = u_f(r) + \delta u(r, s, t), \quad v(r, s, t) = v_f + \delta v(r, s, t), \quad (4.17)$$

and insert this form into (4.16). We obtain to leading order

$$\mathcal{M}\delta u = \delta p(u_f) - \partial_v f(u, v)|_{u_f, v_f} \delta v, \quad c_r \partial_r \delta v = -\varepsilon g(u_f, v_f), \quad (4.18a, b)$$

where \mathcal{M} is given by (4.8). Equation (4.18b) can be integrated at once to give [cf. eq. (3.17b)]

$$\delta v = \frac{\mu(v_f)}{c_r} \varepsilon v_1(r), \quad v_1(r) = \frac{1}{\mu(v_f)} \int_r^\infty dr' g(u_f(r'), v_f). \quad (4.19a, b)$$

The requirement that the right-hand side of (4.18) is orthogonal to ξ^\dagger , the zero eigenmode of \mathcal{M}^\dagger , yields

$$c_r = \mu(v_f) - \kappa + [\mu(v_f)/c_r] \varepsilon c_1(v_f), \quad (4.20)$$

where c_1 is given by (3.17a) and we have assumed that $\kappa \ll w_f^{-1}$. Equation (4.20) can be brought to the form (4.15) using the relation $c(\varepsilon) = \mu(v_f) + \varepsilon c_1$. Notice that for small curvature values, $\kappa \ll \mu(v_f)$, (4.15) assumes the linear form

$$c_r = c(\varepsilon) - \bar{D}\kappa, \quad \bar{D} = [1 - \varepsilon c_1/\mu(v_f)]. \quad (4.21)$$

The curvature–speed relation (4.15) generalizes (4.10) for small deviations from the singular limit, $\varepsilon = 0$, where it still makes sense to decompose a propagating wave into a front and back. When these deviations are sufficiently large the singular perturbation approach of section 3.1.2 may no longer apply; a propagating wave should rather be regarded as one integral entity. We derive now a formal curvature–speed relation applicable to that case. In this derivation we no longer restrict ourselves to a nondiffusive v variable.

We denote by U_p a planar wave that propagates at speed $c = c(\varepsilon)$, and write a curved wave as

$$U(r, s, t) = U_p(r) + \delta U(r, s, t). \quad (4.22)$$

In analogy to (4.6) we obtain

$$D \partial_r^2 U + c \partial_r U + LU + N(U) = \delta P, \quad (4.23)$$

where D , L and N are as in (3.35) and δP has the components

$$\delta p_u = [c - c_r - \kappa/(1 + r\kappa)] \partial_r u, \quad \delta p_v = [c - c_r - \delta\kappa/(1 + r\kappa)] \partial_r v. \quad (4.24)$$

Substituting (4.22) into (4.23) and using the fact that U_p solves the homogeneous problem we find to leading order

$$\mathcal{L}_p \delta U = \delta P(U_p), \quad (4.25)$$

where \mathcal{L}_p is given by (3.41a) with r , c and U_p replacing χ , c_∞ and H_j , respectively. From (3.41b) \mathcal{L}_p is singular, $\mathcal{L}_p \Xi = 0$, $\Xi = U_p'$. Solvability of (4.25) then implies

$$c_r = c - \bar{D}\kappa, \quad \bar{D} = (\Xi^\dagger, D\Xi) / (\Xi^\dagger, \Xi), \quad (4.26a, b)$$

where Ξ^\dagger denotes a null vector of the adjoint of \mathcal{L}_p . In deriving (4.26) we assumed a radius of curvature much larger than the wave width in order to neglect nonlinear contributions. The coefficient \bar{D} , or more precisely its dimensional form, is a weighted average of the two diffusion constants D_u and D_v . It reduces to (4.10) for $D_v = D_u$ or $\delta = 1$, and should reduce to (4.21) for ε sufficiently small. Analytical expressions of \bar{D} in terms of model parameters have not been evaluated yet.

4.1.4. The critical curvature

In first order phase transitions droplets of the stable phase whose size is smaller than a critical value shrink and disappear [LIP]. A similar phenomenon applies to excitable media; for an excited domain to grow and evolve into a concentric wave (i.e., an expanding ring) its initial size should be sufficiently large. In the singular limit, the critical radius below which propagation fails can be estimated from (4.10) by setting $c_r = 0$. This leads to a critical curvature, $\kappa_c = \mu(v_f)$. To obtain the critical curvature for small but finite ε values, assuming a nondiffusive v variable, we exploit (4.20). Setting $c_r = 0$, however, leads to a divergent critical curvature. This suggests that failure of propagation occurs at finite speed. Numerical simulations [ZYK1, MIZ] indeed indicate the existence of a critical speed, c_{rc} , below which propagation fails. It has been suggested in refs. [ZYK1, MIZ] that c_{rc} can be estimated as the value of c_r at which $d\kappa/dc_r = 0$. Applying this condition to (4.20) we find

$$c_{rc}^2 = -\mu(v_f)\varepsilon c_1, \quad (4.27)$$

where we recall that c_1 is a negative quantity. For the critical curvature we obtain

$$\kappa_c = \mu(v_f) - 2c_{rc}. \quad (4.28)$$

In the limit $\varepsilon = 0$, $\kappa_c = \mu(v_f)$, the value obtained from (4.10) by setting $c_r = 0$. It should be stressed that these considerations provide estimates rather than exact values, for it may well be that wave propagation becomes unstable already at curvature values smaller than the above value of κ_c [MIZ]. Nevertheless, a pretty good agreement with direct numerical simulations has been reported for a particular model [ZYK1, ZYK2]. Another point that deserves attention concerns the special case $\delta = 1$. In that case the curvature–speed relation is linear even for finite ε (assuming $\kappa \ll w_f^{-1}$). The estimated critical speed is therefore zero.

4.1.5. Experimental studies

An experimental evaluation of the curvature–speed relation for chemical waves in the BZ medium has been reported in [FMH]. To obtain a wide range of curvature values cusplike structures were produced by letting circular wave-fronts collide (such cusps are seen in fig. 1). These structures were followed in time using a spectrophotometric microscope video imaging technique similar to that described in section 3.3. The wave-front velocity was determined by recording images at fixed time intervals. The curvature was evaluated by fitting isoconcentration lines near the cusps to hyperbolas. The resulting data was fitted to a straight line yielding a value $\bar{D} = 2 \times 10^{-5} \text{ cm}^2 \text{ s}^{-1}$.

4.2. Plane waves and target patterns

In section 3.2 we studied traveling wave patterns in one space dimension. In two dimensions these patterns describe planar waves. We consider now the stability of such waves to transversal perturbations, following primarily ref. [KEL2]. Related results have been obtained in refs. [OMK,OHM].

It has been found in ref. [KEL2] that below a critical propagation speed and for δ values sufficiently large, planar waves become unstable with respect to a transverse structure. For small enough ε the instability disappears as the velocity is decreased below a second threshold. In refs. [OMK,OHM] a similar instability has been found for nonpropagating excited domains (see section 3.1.4). Planar domains become unstable to transverse structure when their widths are increased. A possible explanation of this type of instability is the following. Imagine an outward bulge in the front position. In the quasistatic regime [LAN], where front dynamics is slow in comparison with the diffusive relaxation of the bulk field v , diffusion of v from the bulge to the sides will slow down the front at the neighborhood and consequently the bulge will grow [OHM]. This destabilizing diffusive effect competes with two stabilizing factors. The first is that of curvature as fig. 12 illustrates. The other factor applies to extended patterns where a given front propagates into the refractory tail that follows the preceding front. As the bulge grows it penetrates into a highly refractory region which acts to damp the growth process (see section 3.2.3). The instability to transverse structure disappears when δ is decreased, for then front dynamics is not sufficiently slow. For such δ values, plane waves may become unstable to longitudinal oscillations [OMK,OHM,KEL2].

The stability analysis of periodic plane wave solutions is based on the curvature–speed relation (4.10) and on the outer equations

$$\partial_t v = c \partial_\chi v + \delta \nabla^2 v + \varepsilon G_-(v), \quad \chi_s < \chi < \chi_b, \quad (4.29a)$$

$$\partial_t v = c \partial_\chi v + \delta \nabla^2 v + \varepsilon G_+(v), \quad \chi_b < \chi < \chi_f, \quad (4.29b)$$

where $v = v(\chi, y, t)$ and $\chi = x - ct$. To simplify the analysis the G_\pm terms are linearized as in (3.29) and the scaling $c \rightarrow \varepsilon^{1/3} c$, $x \rightarrow \varepsilon^{-1/3} x$, $t \rightarrow \varepsilon^{-2/3} t$ and $v - v^* \rightarrow \varepsilon^{1/3} v$, is used to eliminate the b_\pm term in (3.29) (see section 3.2.1). The rescaled equations have the same form as (4.29) except that $\varepsilon G_\pm(v)$ are replaced by $\pm a_\pm$. These equations are supplemented by the continuity and periodicity conditions (3.2), where to leading order [see (3.31) and (4.10)]

$$v_f = -v_b = c/\mu'(v^*) = (c_r + \kappa)/\mu'(v^*). \quad (4.30)$$

A plane wave solution, periodic in x (or χ) and propagating at speed c , has the form

$$\begin{aligned} v(\chi) &= B_1 \{ \exp[-c\delta^{-1}(\chi - \chi_b)] - 1 \} - (a_+/c)(\chi - \chi_b) - c/\mu'(v^*), \quad \chi_b < \chi < \chi_f, \\ v(\chi) &= B_2 \{ \exp[-c\delta^{-1}(\chi - \chi_b)] - 1 \} + (a_-/c)(\chi - \chi_b) - c/\mu'(v^*), \quad \chi_s < \chi < \chi_b, \end{aligned} \quad (4.31)$$

where B_1, B_2 are determined using (3.25) [these conditions yield also (3.28b)]. To study the stability of this solution with respect to transversal perturbations, the front and back are deformed in the y direction according to

$$\chi = \chi_f + \delta_f e^{\omega t} \cos(py), \quad \chi = \chi_b + \delta_b e^{\omega t} \cos(py), \quad (4.32)$$

respectively. These deformations will induce new terms in the v field of the form

$$A_1 \cos(py) \exp[k_1(\chi - \chi_b) + \omega t] + A_2 \cos(py) \exp[k_2(\chi - \chi_b) + \omega t], \quad \chi_b < \chi < \chi_f, \quad (4.33)$$

$$A_3 \cos(py) \exp[k_1(\chi - \chi_b) + \omega t] + A_4 \cos(py) \exp[k_2(\chi - \chi_b) + \omega t], \quad \chi_b < \chi < \chi_f,$$

$$k_{1,2} = \{-c \pm [c^2 + 4\delta(\omega + \delta p^2)]^{1/2}\} / 2\delta. \quad (4.34)$$

Substitution of the full form of v into the boundary conditions (3.25) and (4.30) yields six linear equations for the coefficients A_1 to A_4 and for the growth rate ω and mode structure δ_f/δ_b . Since the instability is expected to occur in the quasistatic regime, one can simplify these equations by assuming temporal growth rates $\omega \ll \delta p^2$. Then, the spatial growth rates, k_i , become independent of ω . Solving the equation for ω one finds an instability occurring at finite wave vector as the speed c is decreased. As c is decreased further, a second critical value is reached where the instability disappears.

The stability analysis of plane wave solutions has been extended in ref. [KEL2] also to arbitrary c values where G_{\pm} in (4.29) is given by (3.29) with $b_{\pm} \neq 0$ and to ω values for which the quasistatic approximation does not hold. For large enough δ values the results of the previous analysis were recovered. When δ becomes sufficiently small a Hopf bifurcation, describing longitudinal oscillations or breathing motion, is found to precede the instability to transverse structure.

Plane wave patterns can be formed in an experiment by forcing the medium periodically along a line. The period of the forcing determines the wavelength of the pattern and thus the speed of propagation. Instabilities to transverse structure or to longitudinal oscillations have been observed in numerical simulations [OMK], but, so far, not in experiments.

Forcing the medium at a point instead of a line leads to target-like patterns. Such patterns are commonly observed in chemical systems (see fig. 1). The forcing at the center is many times due to an impurity (e.g. dust particle) which makes the local reaction self-oscillating [WIN5]. Target patterns have also been observed in dictyostelium aggregation [ALM,GPT]. Here, the centers are believed to consist of spontaneously oscillating cells. A similar mechanism operates in the heart where the sino-atrial node, a small core of oscillating cells, drives the surrounding excitable atrium [JFC].

Far away from the center of a target pattern curvature effects are negligible and the results obtained for planar waves are applicable. Near the center curvature effects become important. In fact, if the core radius is smaller than $\kappa_c^{-1} \approx \bar{D}/c(\varepsilon)$ target patterns will not form. For the BZ reaction $\bar{D} \sim 10^{-5} \text{ cm}^2 \text{ s}^{-1}$ and $c \sim 10^{-3} \text{ cm s}^{-1}$ giving a minimal core size of the order of 100 μm .

4.3. Spiral waves

4.3.1. General

Another common pattern in two-dimensional excitable media is the rotating spiral wave^{*)}. The interest in this type of pattern derives not only from its wide occurrence in chemical and biological media, but also because of its universal character; spiral waves appear in spontaneously oscillating media as well [HAG,KUR] and, from a topological point of view, are equivalent [YKP,LEG] to

^{*)} In the Russian literature spiral waves are sometimes referred to as “reverberators”.

dislocation type defects in striped patterns like convective rolls [SIZ]. There are important respects, however, in which spiral waves in excitable media differ from their counterparts in the other pattern forming systems and we will mention them as we proceed.

Spiral waves can be created by nonexcitable transient heterogeneities in the medium. Such “obstacles” break propagating wave-fronts and thus produce free ends. Any free end becomes the tip^{*)} of a rotating spiral wave. The process by which a broken wavefront evolves toward a rotating spiral wave has been addressed in refs. [FIF3,FIF4,ZYK1,MEP]. As pointed out in ref. [FIF4], along the interface separating the excited and the recovery regions, there exists a point where the normal velocity of the interface changes sign (see section 4.3.5). This induces a twisting action on the interface motion and, as a result, the interface starts wrapping around some center of rotation, to form a spiral structure. Eventually (and in an appropriate parameter range) a state of steady rotation is achieved during which the spiral tip rotates about a disk-like core region at constant angular velocity. The size of the core depends on the medium excitability: highly excitable media give rise to pointwise cores,^{**)} whereas less excitable media allow for a whole range of core sizes. In the latter case the core remains at rest at all times (or close to the rest state if diffusion of v is allowed) for the tip never penetrates into it [ZYK1]. The failure of the tip to penetrate into the core has been attributed to the high curvature of the front at the tip neighborhood; if that curvature value assumes the critical value, κ_c , propagation into the core becomes impossible [ZYK1].

While the initial stage of spiral wave formation is intuitively understood, no clear picture as to what factors affect the convergence to steady rotation, seems to exist. More specifically, assuming that it is indeed the critical curvature, κ_c , that prevents the tip from penetrating into the core region, one would like to understand why the curvature at the tip increases toward κ_c as the front curls. For spiral waves with large core sizes one may attempt the following explanation. The curvature at the tip, κ_{tip} , is roughly determined by the width of the excited domain at a distance of $O(\kappa_{tip}^{-1})$ from the tip. The latter is affected by the normal velocity of the front; the lower the front velocity the thinner is the excited domain. The normal velocity, in turn, is determined by the curvature of the front and by v_f , the front level of v [see for example (4.10)]. As the front curls, the curvature and the value of v_f at a distance of $O(\kappa_{tip}^{-1})$ from the tip, both increase. Consequently, the normal velocity decreases, the excited domain becomes thinner and the curvature at the tip higher.

Another way of creating spiral waves is by means of a spatially graded perturbation applied to a medium in the recovery phase after excitation [WIN3,WIN5]. Both means of creating spiral waves (i.e., by breaking a propagating wave or by applying appropriate perturbation) have been demonstrated and used in experiments and will be discussed in greater detail in section 4.3.2.

The discussion above suggests the existence of unique core size and frequency of rotation for spiral waves in a given medium. This is indeed the case for a medium that recovers monotonically from an excitation (see fig. 1). Oscillatory recovery, on the other hand, allows for a discrete family of core sizes and rotations frequencies [WIN6,WIN7]. Spiral waves do not always rotate rigidly or steadily. Nonsteady forms of rotation, known as “meander” [WIN3], have been observed both in experiments [APR,JSW,SKS,PMH] and in numerical simulations [ROK,VCD,ZYK1,ZYK3,LUG,JSW,BKT,KAR1,JAW]. Figure 13 shows steady and nonsteady spiral-wave rotations observed in the BZ medium.

^{*)} The tip of a spiral wave and its immediate neighborhood are sometimes referred to as “rotor” [WIN3].

^{**)} By a “pointwise core” we refer to a core whose size is of the order of the interface width, that is, of $O(1)$, or $O(\epsilon)$ for the rescaled systems (3.1d, e).

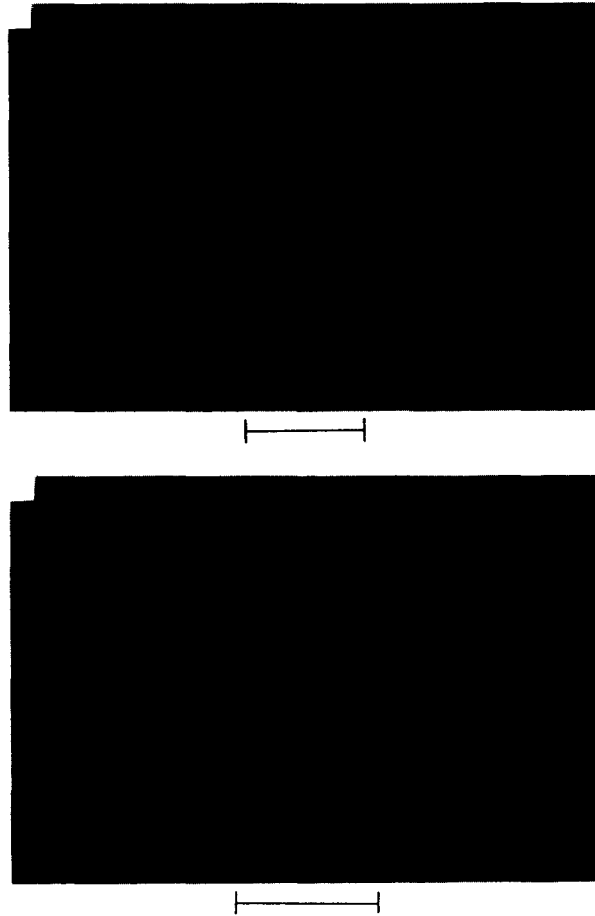


Fig. 13. Superposed snapshots of a spiral front in the BZ medium during steady rotation (top) and compound rotation (bottom). The transition to compound rotation has been obtained by increasing the bromate-ion concentration (increasing excitability). The bars represent 1 mm. (From Skinner and Swinney [SKS], reproduced with permission.)

The selection of a unique frequency of rotation (in the case of monotonic recovery) and the onset of nonsteady rotation are two outstanding problems that have attracted much attention recently. In the following we will describe the different theoretical approaches that have been proposed to attack these problems and the progress that has been made so far. These works divide into two main categories: kinematical theories in which evolution equations for the spiral arm are sought while keeping the analysis of the spiral tip at a phenomenological level (section 4.3.4), and free boundary formulations which attempt a fuller consideration of the tip but address mainly static aspects such as the shape of steadily rotating spiral waves and the frequency selection problem (section 4.3.5). Other theories [GRE,PMT,MKR,ZYK1,KEE2,KET2,TYK2,TAM] have been reviewed in ref. [TYK1] and will be described only in so far as we need them for presenting the above theoretical approaches. Before embarking on the theory of spiral waves, however, we describe first experimental (section 4.3.2) and numerical (section 4.3.3) studies.

4.3.2. Experimental studies

Most experimental studies of spiral waves in excitable media have used the BZ reaction (see section 2.2). We will therefore focus our attention on this chemical medium and refer only briefly to other excitable systems. Experimental observations of spiral waves in BZ media have been reported for the first time in refs. [ZAZ2,WIN1]. In their simplest forms spiral waves rotate rigidly or steadily about fixed centers. The spiral tip traces a circular trajectory and the curvature of the spiral wave-front remains constant in time (see fig. 13). Quantitative studies of steadily rotating spiral waves are described in refs. [MPH1,MPH2]. They confirmed an earlier suggestion [WIN1] that spiral waves have the geometries of involutes of circles (we will see later on that deviations from an involute may become significant near the tip), and exploited spectrophotometric methods similar to those described in section 3.3, to obtain two-dimensional spatial distributions of the catalyst (oxidized form). An example of such a distribution, in the vicinity of the spiral core, is shown in fig. 14.

In another study [NTM] a similar experimental setup has been used to measure spiral wave characteristics, such as speed, wavelength and rotation period, for various initial concentrations of the BZ reagents. In addition, minimal and maximal values of the catalyst wave amplitude were measured and compared with the corresponding quantities of a solitary or large wavelength concentric wave. A conspicuous effect that comes out of the data is the increasing penetration depth of a spiral wave-front into the refractory wake ahead of it, as excitability is increased. This is reflected by a higher minimal amplitude value, an overall smaller wave amplitude and a shorter wavelength. Figure 15 shows wave profiles of spiral and concentric waves for a highly excitable medium; the amplitude of spiral waves is considerably smaller than that of concentric waves. This is in contrast to the case of low excitability where the two wave profiles are comparable in size.

Another effect implicit in [NMT] is the divergence of core size at sufficiently low excitability. For small enough values of $[H^+]$ and $[BrO_3^-]$, broken wavefronts were found to retract at the tips rather than curl into spiral waves. This suggests the existence of a critical concentration (of either species) at which the tip neither grows nor decays, and consequently, a limit where the core size diverges to infinity [PPM,DMZ]. This is one feature that distinguishes spiral waves in excitable media from their

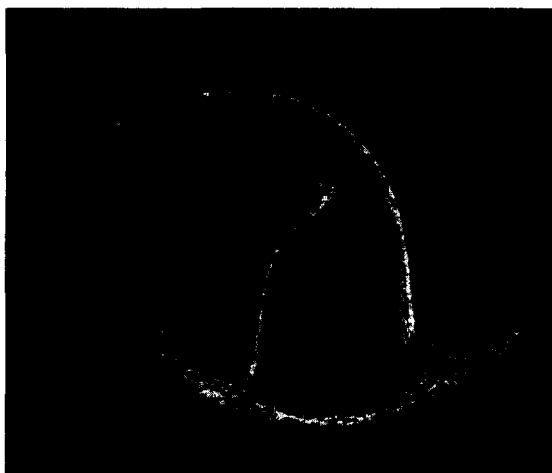


Fig. 14. Spatial distribution of ferric iron (Fe^{3+}), the oxidized form of the metal catalyst in the BZ reaction, in the vicinity of the core. (From Müller et al. [MPH1], reproduced with permission.).

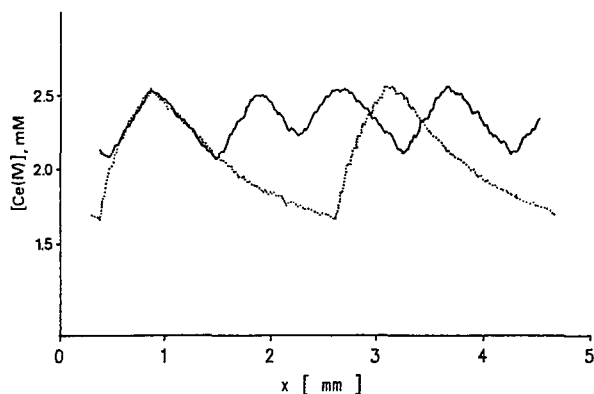


Fig. 15. Catalyst wave profiles of spiral (solid curve) and concentric waves (dotted curve) for a highly excitable BZ medium, indicating that any segment of the spiral front penetrates deeply into the wake of the preceding front. (From Nagi-Ungvarai et al. [NTM], reproduced with permission.)

counterparts in oscillating or convective patterns arising via supercritical bifurcations. Defects with large core sizes, however, may exist in patterns that have emerged through subcritical bifurcations [CGR].

Recently, a new experimental setup has been proposed which, like the annular reactor described in section 3.3, allows maintaining the reaction at a constant distance from thermal equilibrium. It consists of a reservoir to which reactants are delivered in a few separated feeds. The reservoir couples to a thin layer of polyacrylamide gel by means of a glass-capillary array and a filter membrane. The reactants diffuse through the capillary array and permeate the gel. The wave patterns that form within the thin gel layer are illuminated and viewed from above. To obtain homogeneous feed, the reactants in the reservoir are continuously stirred. The capillary array acts both as a feed to the gel that allows only perpendicular mass transport and as a hydrodynamic flow buffer; it prevents pattern formation within the feed and damps out convection from the stirring. The gel is introduced to prevent convection within the pattern layer. It is chemically inert and allows for unhindered molecular diffusion. Such an open reactor is particularly suitable for studying the long time scale dynamics associated with instability phenomena.

Steadily rotating spiral waves may become unstable by varying the excitability of the medium. Three studies [JSW,PMH,SKS] have recently demonstrated such an instability in the BZ medium.*¹ The resulting dynamics involves two frequencies and leads to flowery tip trajectories as shown in fig. 16. Such trajectories have been described in refs. [ZYK3,JSW,LUG,SKS,PMH] in terms of epicycloids whose forms can be written parametrically as

$$x(t) = R \cos(\Delta\omega t) + \rho_0 \cos(\omega t), \quad y(t) = R \sin(\Delta\omega t) + \rho_0 \sin(\omega t).$$

Here, ρ_0 is the radius of a circle whose center lies on another circle of radius R . The two circles rotate with frequencies ω and $\Delta\omega$, respectively. The coordinates $x(t)$ and $y(t)$ describe a point fixed on the circle of radius ρ_0 . A fit of an epicycloid to an experimental tip trajectory is shown in fig. 16. The radius

*¹ Nonsteady rotation has also been observed in ref. [APR] but attributed to nonuniform excitability along the vertical direction caused by exposing the top surface to oxygen.

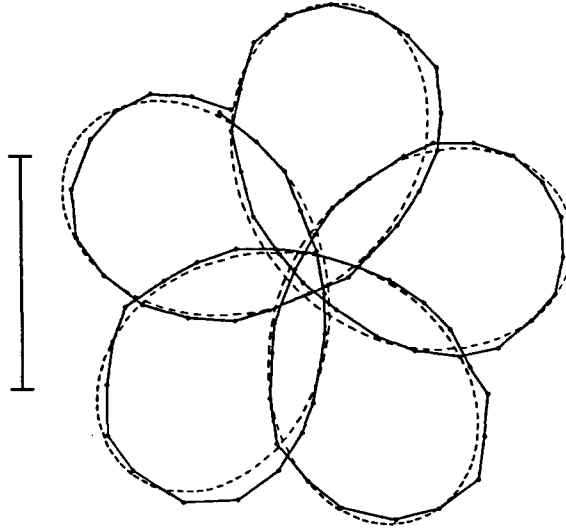


Fig. 16. Tip trajectory (solid curve) during compound rotation in the BZ medium and a fitted epicycloid (dashed curve). (From Skinner and Swinney [SKS], reproduced with permission.)

and frequency ρ_0 and ω pertain to the original, primary tip rotation. The frequency $\Delta\omega$ is just the difference between the primary frequency, ω , and the secondary frequency, ω_1 , that modulates the primary motion [JSW]. To see this let t_1 denote the instance of (say) largest departure from the center of rotation and t_2 the next such instance. From the parametric form above we find $(\Delta\omega - \omega)t_1 = (\Delta\omega - \omega)t_2 + 2\pi$, or $\Delta\omega = \omega - \omega_1$, where we have identified $2\pi/(t_2 - t_1)$ with ω_1 . Indeed, negative (positive) $\Delta\omega$ values give rise to outward (inward) petal flowers as we expect for modulational frequencies larger (smaller) than the primary frequency [WIN8] (see also next section). The relation of R to the primary and secondary frequencies is not obvious. It appears though that R must diverge as $\Delta\omega \rightarrow 0$, for then the modulation of the tip trajectory always occurs in the same direction thus yielding an averaged drift of the tip along a straight line.

Flowery tip dynamics is often referred to as “tip meander” [WIN3]. In the following we will use the term “compound rotation”, suggested in ref. [SKS], for strict two-frequency dynamics and use “meander” as a global name for nonsteady rotation. Tip meander is another property of spiral waves in excitable media that has no analog in smoothly oscillating systems or in defect dynamics.

In refs. [JSW,PMH] the transition to compound rotation was observed as excitability was decreased. In contrast, compound rotation in [SKS] was observed by increasing excitability. The main difference between the chemical compositions in these studies is that in ref. [SKS] the bromate-ion concentration was smaller by an order of magnitude than that in refs. [JSW,PHM]. This may suggest that the media in the latter studies were considerably more excitable than the medium in ref. [SKS]. Indeed, when $[\text{BrO}_3^-]$ in ref. [SKS] was sufficiently increased a transition back to steady rotation was observed. Unfortunately, this transition was accompanied by bulk oscillations in the reservoir (presumably because of the small bromide ion concentration used in that experiment). The picture that emerges from this comparison is that there is a finite range of excitability at which compound rotation is observed. At sufficiently high or low excitabilities steady rotation prevails.

The open reactor proposed in ref. [SKS] allowed a closer examination of the transition to compound

rotation. Approaching the transition point from below and from above indicated no hysteresis. The increase in relaxation time as the transition point was approached provided another indication for the supercritical nature of the transition; bromate-ion concentrations differing by 5% or more from the critical one led to relaxation times shorter than 5 hours, whereas concentrations deviating by no more than 1% gave relaxation times above 24 hours. Another question that could be investigated with that kind of reactor is whether compound rotation is frequency-locked. If this was the case, intervals of bromate-ion concentration could be found that correspond to a constant winding number ω_1/ω . Within the experimental resolution such intervals were not found, suggesting that the observed rotation is therefore quasiperiodic.

During compound rotation the wave-front curvature changes periodically in time. Figure 17 shows images of the spiral wave-front at two phases pertaining to minimal (top) and maximal (bottom) wave-front curvatures. The dramatic change in curvature is accompanied also by a change in the wave

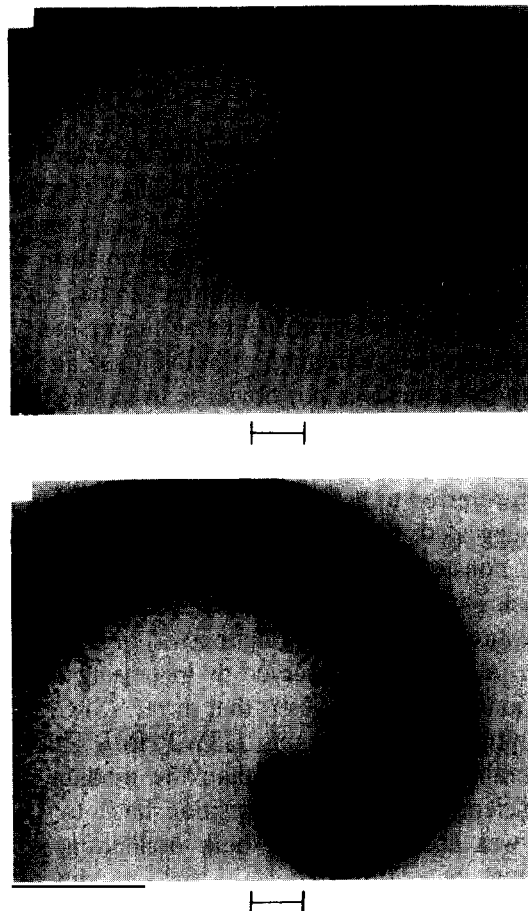


Fig. 17. Spiral wave-front in the BZ medium at two phases pertaining to minimal (top) and maximal (bottom) front curvatures. The bars represent 1 mm (From Skinner and Swinney [SKS], reproduced with permission.)

profile; while in the upper figure the profile is quite uniform along the wave-front, in the lower figure the excited domain near the tip becomes wider than it is further back from the tip. These variations in curvature and wave profile affect both normal wave-front velocity and tangential tip speed. The latter are also affected by the nonuniform refractory wake ahead of the propagating wave-front.

The creation of spiral waves in refs. [JSW,PMH,SKS] has been achieved by breaking propagating wave-fronts. In ref. [PMH], for example, a circular wave-front has been broken mechanically, by ejecting a gentle blast of air into a small section of the wave-front. In ref. [SKS] optical means have been used. Exposure of the system to UV light has the effect of reducing oxidation wave-fronts. Illumination of one part of a wave-front therefore annihilates that part and leads to the creation of a free end.

A different way of initiating spiral waves has been suggested in ref. [WIN4] and later in refs. [WIN3,WIN5] in the context of cardiac arrhythmias. It exploits a topological property of spiral waves, namely, that a line integral of the gradient of the local-dynamics phase over a closed loop that contains the spiral core, does not vanish. Imposing initial conditions that satisfy this topological constraint yields spiral waves. The heart muscle is an excitable medium that can support spiral waves [ABS1,ABS2]. Such waves induce fast heartbeat (tachycardia) which very often degrades into ventricular fibrillation. The onset of fibrillation has long been associated with the appearance of a premature electrical stimulus in the vulnerable phase^{*)} [MIN]. It has been pointed out in refs. [WIN3,WIN5] that the effect of applying a concentric stimulus at the wake of a propagating wave-front is to set the initial conditions needed for the creation of phase singularities or spiral waves. These singularities should occur at the intersection points of a circle of critical stimulus strength and a line of critical recovery phase. There should be, in general, two such intersection points giving rise to two counter-rotating spiral waves. These ideas were successfully tested in refs. [SCD,FWW] using multiple-electrode mapping techniques, and later in refs. [DKC,DKJ] using voltage-sensitive dyes and photodiode arrays to detect fluorescence patterns.

4.3.3. Numerical simulations

The dependence of the period of rotation, $T = 2\pi/\omega$, on ε has attracted considerable theoretical attention as we shall see later on, but only a limited amount of numerical effort [MIZ,WIN8]. It has a characteristic U-shape, the period diverging at relatively large ε values because of tip retraction, and in the limit $\varepsilon \rightarrow 0$, because of unbounded increase in the duration of excitation and recovery, T_+ and T_- , respectively.^{**)} A related significant observation [WIN8], made for a nondiffusive v variable, is that the levels v_f and v_b along the spiral arm (but not too close to the tip) approach the value v^* as ε is decreased. For ε sufficiently small the scaling form, $v^* - v_f \sim \varepsilon^{1/3}$, has been obtained.

Most numerical studies in recent years have focused on the problem of nonsteady rotation. Simulations on simple model systems (FitzHugh–Nagumo, Oregonator and others) are consistent with the experimental observation that compound rotation prevails within a finite range of excitability, and can be reached either by lowering the excitability of a highly excitable medium or by increasing the excitability of a barely excitable medium. Various quantities have been used as control (or bifurcation) parameters in these simulations, and in order to relate them to the somewhat loosely defined property of excitability (see section 3.3) we examine the manner in which they affect the speed of propagation. One parameter that has been widely used is the threshold of excitation [a in model (2.1a)], or the

^{*)} A period in the recovery phase during which a relatively small perturbation can trigger fibrillation.

^{**)} Other space and time scalings, however, may yield different shapes for the $T-\varepsilon$ curves.

related quantity Δ^{-1} where $\Delta = v^* - v_s$]. This parameter obviously affects the propagation speed as is evident from (3.7), (3.9) or (3.18); the higher the threshold, the smaller the speed. High threshold values can thus be associated with low excitability. In ref. [BKT] the onset of compound rotation was observed as the threshold was increased (or excitability decreased), whereas in ref. [KAR1] compound rotation was obtained by decreasing the threshold (or increasing excitability).

Another parameter that is commonly varied in numerical simulations is the time scale ratio ε . According to (3.18) increasing ε reduces speed and thus excitability. This raises the question to what extent ε and threshold variations are equivalent (as both quantities affect excitability). The clue to this question seems to lie in a significant distinction made in ref. [ZYK3] between two slow time scales, governing the time evolution of the slow variable v along the right and left branches, $u_+(v)$ and $u_-(v)$, respectively. Denoting the corresponding time scale ratios with respect to the fast variable by ε_+ and ε_- ,*) we replace $\varepsilon g(u, v)$ in (3.1a-c) by $\varepsilon_+ g(u, v)$ for $g > 0$ and $\varepsilon_- g(u, v)$ for $g < 0$. The speed of propagation is affected by ε_+ but is insensitive to ε_- . The latter affects the time the system spends on the left branch, or the duration of the refractory period. Thus, we may associate ε_+^{-1} with excitability, and in this sense regard it as equivalent to the inverse threshold, but we must consider ε_- as an independent parameter.

In refs. [ZYK3,LUG] a semiquantitative phase diagram for spiral wave dynamics in the $(\varepsilon_+, \varepsilon_-/\varepsilon_+)$ plane is evaluated. Transitions to compound rotation have been obtained either by decreasing ε_+ at constant ratio $\varepsilon_-/\varepsilon_+$, or by decreasing that ratio at constant ε_+ . The former transition is consistent with the experimental observations in ref. [SKS] of inducing compound rotation by increasing excitability. The latter transition cannot be directly related to the experimental observations. It amounts to obtaining compound rotation by increasing the refractory period (decreasing $\varepsilon_-/\varepsilon_+$) at constant speed (constant ε_+). Recently, two other numerical studies, exploring spiral wave dynamics in two-parameter planes, have appeared [JAW,WIN8]. The two parameters used are (original) ε and threshold of excitation (from the above discussion both can be regarded as independent). In that parameter space, compound rotation appears in a tongue-like domain surrounded by a domain of steady rotation, as shown in fig. 18. In a wide ε range, increasing threshold (decreasing excitability) at constant ε leads to a transition from steady to compound rotation, a reverse transition to steady rotation and finally to the disappearance of spiral waves (by tip retraction). This qualitative picture is consistent with the experimental observations. At smaller ε values the onset of compound rotation is followed by a transition to more complex forms of nonsteady rotations (see also ref. [ROK]). The exact nature of these nonsteady rotations has not been studied yet. At still smaller ε values nonsteady rotation prevails. In all these studies a crossover has been observed in the domain of compound rotation from outward-petal flowers to inward-petal flowers. The borderline is reached when the primary and modulational frequencies become equal, and is characterized by a drift of the spiral wave along a straight path.**)

The onset of compound rotation has been carefully examined in refs. [BKT,KAR1]. Decay rates slightly below the transition and amplitudes of the oscillatory modes slightly above the transition were calculated as functions of the control parameters (threshold of excitation). The oscillatory modes were found to grow from zero at the same critical parameter values where the decay rates cross the imaginary axis. The decay rates were linear in the deviations of the control parameters from their critical values, whereas the amplitudes followed square root laws. These findings indicate that compound rotation sets in via a supercritical Hopf bifurcation.

*) The parameters ε_+ and ε_- correspond to ε and εk_s , respectively, in ref. [ZYK3].

**) Similar behavior results when a steadily rotating spiral wave is subjected to an external periodic force [ADM].

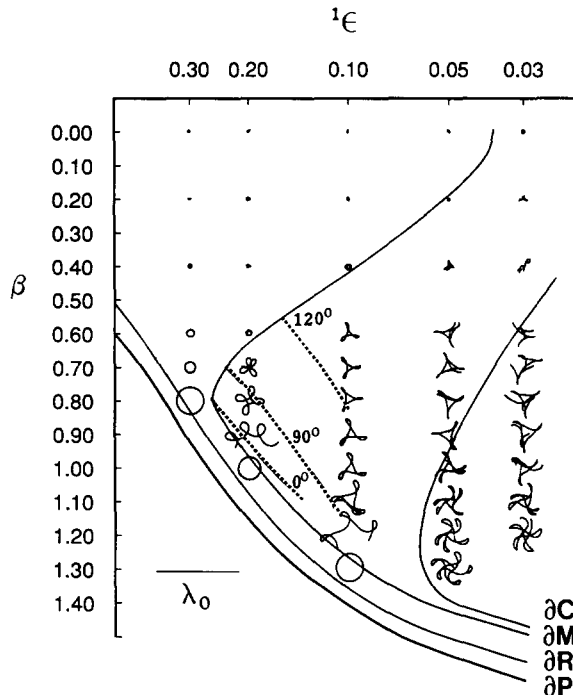


Fig. 18. Phase diagram for spiral wave behavior in a FitzHugh–Nagumo type model. The parameter β is a measure of the threshold of excitation whereas $\epsilon = \sqrt{\bar{\epsilon}}$ (note the logarithmic scale of ϵ). Shown are five regimes pertaining to failure of planar front propagation (below ∂P), failure of spiral wave propagation (between ∂P and ∂R), steady spiral wave rotation (between ∂R and ∂M), compound rotation (between ∂M and ∂C), and irregular rotation. The patterns shown describe typical tip trajectories in the relevant regimes. For more details the reader is referred to ref. [WIN8]. (From Winfree [WIN8], reproduced with permission.)

The spatial structure of the unstable eigenmode has been studied very recently in ref. [BAR1] for an instability that sets in as the threshold of excitation is increased. At the bifurcation point, this mode has been found to develop a maximum at the point of zero curvature on the spiral interface, and to follow a power-law decay away from this point. This suggests that the instability is not localized at the tip.

The experimental and numerical studies described so far pertain to spiral waves in media that recover monotonically after excitation. We have seen in section 3.2.3 that oscillatory recovery gives rise to a multitude of nonuniformly spaced stable wavetrains. What is the effect of oscillatory recovery on spiral wave dynamics? This question has been addressed recently in refs. [WIN6,WIN7] where numerical simulations on a FitzHugh–Nagumo type model were carried out. The interesting outcome of this study is the possible existence of a discrete family of stable spiral wave solutions differing from each other in rotation frequencies and core sizes.*) This is in sharp contrast to the case of monotonic recovery where unique frequency and core size are selected. We turn now to theoretical studies of spiral wave dynamics.

*) The same result appears implicitly in ref. [KAR1]. Parameter values that have been used in this study give rise to oscillatory recovery. It has been suggested in that work that the secondary mode that appears in compound rotation is closely related to a coexisting, longer wavelength, spiral wave solution. It should be stressed, however, that although cross effects of nonsteady rotation and multiplicity of spiral wave solutions may exist, the latter is not a prerequisite for the former.

4.3.4. Kinematical theories

4.3.4.1. *The geometrical approach.* The essence of the geometrical approach is to describe the spiral arm in terms of a one-dimensional curve with a free end, whose normal speed and tangential free-end speed are determined by the local curvature alone. The temporal evolution of the spiral arm follows then from a partial differential equation for the curvature. The first formulation of such an approach in the context of excitable media^{*)} was presented in ref. [ZYK4]. Many other studies have appeared since then [BDM,BDZ1,DMZ,MIK1,BKK,MEP,MIZ,ZYM]. We first outline the derivation of the curvature evolution equation using purely geometrical considerations. We then describe a phenomenological theory of spiral waves that has emerged from the earlier work [ZYK4] and the subsequent works [BDM,BDZ1,MIZ,ZYM].^{**)}

Consider a curve, $X(s, t)$, in the (x, y) plane with a free end at arclength $s = 0$ as illustrated in fig. 19. Let $\theta(s, t)$ be the angle between the tangent to the curve and a fixed direction, say, the x axis. The unit vectors along and normal to the curve are given by

$$\hat{s} = \cos \theta \hat{x} + \sin \theta \hat{y}, \quad \hat{r} = -\sin \theta \hat{x} + \cos \theta \hat{y}, \quad (4.35)$$

respectively. At any point $s > 0$ the curve propagates in the normal direction,

$$d\mathbf{X}(s, t)/dt = c_r(s, t)\hat{r}(s, t). \quad (4.36)$$

The normal propagation elongates or shortens the curve according to the sign of its curvature. As a result the arclength of the curve varies in time. Taking this into account we find from (4.36)

$$(\partial\mathbf{X}/\partial t)_s = c_r\hat{r} - (ds/dt)\hat{s}, \quad (4.37)$$

where the subscript s denotes partial derivative at fixed s and we used the identity $\partial\mathbf{X}/\partial s = \hat{s}$.

Consider now the total time derivative of \hat{s} . From (4.35) we find

$$d\hat{s}/dt = (d\theta/dt)\hat{r}. \quad (4.38)$$

On the other hand,

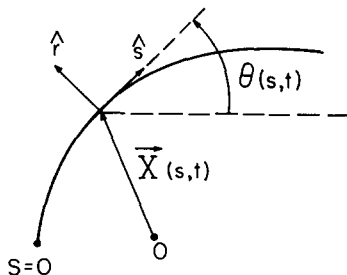


Fig. 19. Geometrical representation of a front, $X(s, t)$, with a free end (tip) at arclength $s = 0$. The unit vectors normal and tangent to the front are denoted by \hat{r} and \hat{s} , respectively. The angle that \hat{s} makes with a fixed direction is denoted by $\theta(s, t)$.

^{*)} A similar approach was used earlier in the study of spiral screw dislocations [BCF].

^{**)} The reader is also referred to a recent book by A.S. Mikhailov [MIK2] where this theory is reviewed.

$$d\hat{s}/dt = (d/dt) \partial X/\partial s = (\partial/\partial s)(\partial X/\partial t)_s - \kappa(ds/dt)\hat{r}, \quad (4.39)$$

where the curvature is given by $\kappa = -\partial\theta/\partial s$. Using (4.37) in (4.39) and comparing (4.39) with (4.38) we find

$$(\partial/\partial s) ds/dt = \kappa c_r, \quad d\theta/dt = \partial c_r/\partial s. \quad (4.40a, b)$$

Taking the partial derivative of (4.40b) with respect to s at constant t we find

$$\partial\kappa/\partial t = -(\kappa^2 + \partial^2/\partial s^2)c_r - (\partial\kappa/\partial s) ds/dt, \quad (4.41)$$

where according to (4.40a),

$$\frac{ds}{dt} = \int_0^s ds' \kappa c_r + c_t, \quad c_t = \left(\frac{ds}{dt}\right)_{s=0}. \quad (4.42)$$

The first term on the right-hand side of (4.42) represents the change in arclength due to normal expansion. The second term, c_t , represents the growth rate of the free end, or the tangential tip velocity [BDM,BDZ1,ZYM]. In general, both c_r and c_t are assumed to be functions of the curvature.

Equations (4.41) and (4.42) determine the curve $X(s, t)$ up to rotations and translations in the plane. To determine this curve completely we use (4.35) and the identities $\hat{s} = \partial_s X$ and $\kappa = -\partial_s \theta$ to write

$$X(s, t) = \int_0^s ds' \cos \theta(s', t) + X_0(t), \quad Y(s, t) = \int_0^s ds' \sin \theta(s', t) + Y_0(t), \quad (4.43)$$

$$\theta(s, t) = -\int_0^s ds' \kappa(s', t) + \theta_0(t). \quad (4.44)$$

The tip coordinates (X_0, Y_0) are obtained from (4.37) once we identify $\dot{X}_0 \equiv \partial_t X|_{s=0}$ and $\dot{Y}_0 \equiv \partial_t Y|_{s=0}$,

$$\dot{X}_0 = -c_{r0} \sin \theta_0 - c_t \cos \theta_0, \quad \dot{Y}_0 = c_{r0} \cos \theta_0 - c_t \sin \theta_0, \quad c_{r0} = c_r|_{s=0}. \quad (4.45)$$

The angle θ_0 is obtained from (4.40b),

$$\partial\theta_0/\partial t = (\partial c_r/\partial s)_{s=0} + \kappa_0 c_t. \quad (4.46)$$

Equations (4.41)–(4.46) provide a geometrical framework for studying spiral wave dynamics.

Two questions arise when we come to apply this framework. First, under what conditions is such an approach applicable, and second, what forms should we use for c_r and c_t in (4.41) and (4.42). For the geometrical approach to be valid, the dynamical effects due to nonuniform distribution of v along the spiral arm should be negligible. Such a situation is realized if the width of the spiral arm is much smaller than the spiral wavelength or pitch. Then, practically, any portion of the arm propagates through a medium at rest, for which $v = v_s$. One way to achieve this “thin arm” regime is to consider ε values

sufficiently large. We know from the discussion in section 4.1.4 that there exists a critical curvature, κ_c , beyond which forward propagation fails. We also know that the critical radius, κ_c^{-1} , increases as ε is increased [see (4.27) and (4.28)]. The radius of curvature at the tip is of the order of the width, λ_+ , of the excited domain. The latter decreases as ε increases [see (3.27a)]. Thus, upon increasing ε the radius of curvature at the tip decreases while the critical radius increases. Evidently there will be a critical value, ε_{c2} , at which the tip can no longer grow or sprout [PPM,DMZ,MIZ].*) Beyond that value the tip retracts. This phenomenon has been observed in experiments [NMT] and in numerical simulations [DMZ,KAR2,JAW] and is demonstrated in fig. 20. A broken wave will evolve into a spiral wave only if $\varepsilon < \varepsilon_{c2}$. Large-wavelength spiral waves are obtained for ε values slightly smaller than ε_{c2} . The width of the spiral arm depends on the size of the excited domain and on the decay rate, $\eta_e = \eta_- = |\varepsilon G'(v_s)/c_\infty|$, of the refractory tail. As ε increases the excited domain becomes smaller and the decay rate larger. The thin arm regime can therefore be obtained by increasing ε toward ε_{c2} .

The thin arm limit can also be obtained by increasing the threshold of excitation, or alternatively, the rest value v_s of the slow field v (keeping ε constant) [KAR2]. Again, there will be a critical value, $\Delta_c > 0$, of $\Delta = v^* - v_s$ for which the spiral tip neither sprouts nor retracts. At this critical value the spiral pitch diverges to infinity. As for the arm width, here it also decreases as the infinite pitch limit is approached; the excited domain, λ_+ , shrinks and the decay rate, η_e , increases since $c_\infty \approx \mu(v_s)$ becomes smaller the closer v_s and v^* are [recall that $\mu(v^*) = 0$]. We may conclude that the geometrical approach is applicable for values of ε or threshold sufficiently high, or for barely excitable media.

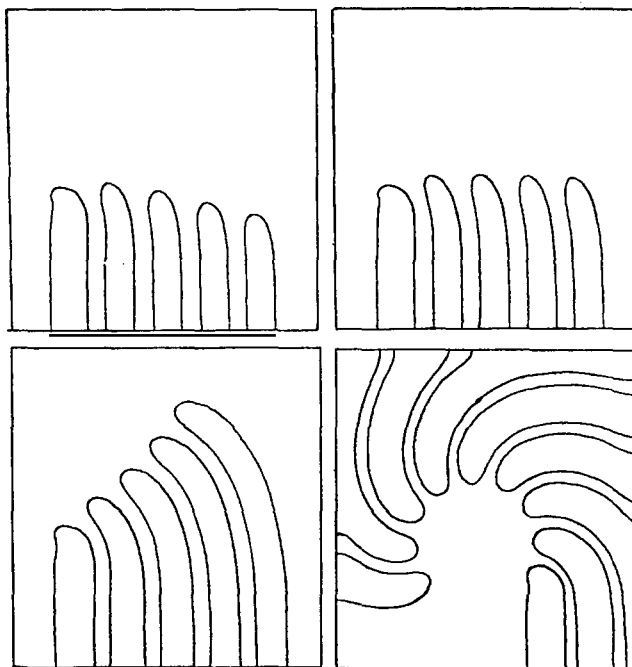


Fig. 20. Numerical simulation of spiral wave propagation in the limit of low excitability where ε is close to ε_{c2} . Tip retraction (top-left), steady, finger-like propagation (top-right), and spiral waves (bottom) are obtained with $\varepsilon > \varepsilon_{c2}$, $\varepsilon = \varepsilon_{c2}$ and $\varepsilon < \varepsilon_{c2}$, respectively. (From Mikhailov and Zykov [MIZ], reproduced with permission.)

*) The reader should not confuse ε_{c2} with ε_c , the critical ε value at which planar solitary waves fail to propagate (see section 3.1.3).

The second question concerns the forms of c_r and c_t to be used in (4.41) and (4.42). For ε values sufficiently small we can use for c_r the form (4.10). For higher ε values eqs. (4.21) or (4.26) should be used. The question of what form to use for c_t is more subtle. In refs. [BDM,BDZ1] it has been postulated that the tip velocity is determined by the curvature, $\kappa_0(t) \equiv \kappa(0, t)$ of the (infinitely thin) spiral arm at $s = 0$. More specifically, a linear relation

$$c_t = d(\kappa_{c_2} - \kappa_0), \quad (4.47)$$

has been assumed, where d is a positive constant and κ_{c_2} is a second critical curvature, defined as the curvature of the spiral arm at the tip for which the tip neither grows nor retracts. That c_t should somehow be related to κ_0 can be understood in the following way. In the thin arm regime, the tip velocity, c_t , is affected primarily by the width, λ_+ , of the excited domain near the tip, as this width determines the curvature of the tip [the reader should not confuse the curvature of the tip with κ_0 which is the curvature, $\kappa(s)$, of an infinitely thin spiral arm in the limit $s \rightarrow 0$]. This width, in turn, is affected by the normal velocity of the spiral arm near the tip, and thus by its curvature κ_0 , for according to (3.27) λ_+ is proportional to the speed. One may therefore expect c_t to increase as κ_0 decreases.

We are in a position now to apply (4.41)–(4.46) to spiral wave dynamics [BDM,MIZ]. Consider a steadily rotating spiral wave. Such a form of rotation is shown in fig. 13 (top). The spiral wave rotates as a whole with constant frequency denoted here by ω . During the rotation the tip traces a circular trajectory about a fixed core region. The curvature of the spiral arm is independent of time and the tip neither grows nor retracts (i.e., $c_t = 0$). Integrating (4.41) and (4.42) we find

$$\kappa \int_0^s ds' \kappa c_r + \frac{\partial c_r}{\partial s} = \omega, \quad (4.48)$$

where ω , the integration constant, is just the frequency of rotation. This is readily seen once we notice that $\omega = \partial_s c_r|_{s=0}$ and that according to (4.40b), $\partial_s c_r|_{s=0} = d\theta/dt|_{s=0}$. The curvature has to satisfy the boundary conditions

$$\lim_{s \rightarrow 0} \kappa(s) = \kappa_{c_2}, \quad \lim_{s \rightarrow \infty} \kappa(s) = 0. \quad (4.49)$$

These conditions make (4.48) a nonlinear eigenvalue problem for the frequency of rotation, ω . To determine ω it is convenient first to rescale quantities according to $\tilde{\kappa} = \kappa/\kappa_{c_2}$, $\tilde{s} = s\kappa_{c_2}$ and $\tilde{\omega} = \omega/c\kappa_{c_2}$. Equation (4.48) then transforms into

$$\kappa \int_0^s ds' \kappa(1 - \beta\kappa) = \beta \frac{\partial \kappa}{\partial s} + \omega, \quad \beta = \frac{\bar{D}\kappa_{c_2}}{c}, \quad (4.50)$$

where we dropped the tilde signs for simplicity of notation and used (4.26) for c_r with c independent of s . In the thin arm regime which is considered here, β is much smaller than unity, for $c/\bar{D} \sim O(\kappa_c)$ is roughly the curvature of the tip, while κ_{c_2} is the much smaller curvature of the spiral arm. We can therefore neglect the term proportional to β on the left-hand side of (4.50). The term on the right side multiplies the curvature derivative and cannot be neglected. Indeed, a boundary layer, involving large curvature variations, exists near the tip. To see this consider (4.50) away from the tip where $\beta \partial_s \kappa \ll \omega$

and the derivative term can be neglected. Then, (4.50) has the outer solution

$$\kappa = (\omega/2s)^{1/2}. \quad (4.51a)$$

Evidently, $\partial_s \kappa \sim s^{-3/2}$ grows unboundedly as the tip is approached. Thus, near the tip, the derivative term should be kept. In that region, however, s is small. Using the smallness of s we find, to leading order, the inner solution

$$\kappa = 1 - (\omega/\beta)s. \quad (4.51b)$$

The rotation frequency, ω , is determined by matching the outer and inner solutions. Continuity of the solutions and of their first derivatives at a point $s = s_0$ then leads to

$$\omega = \varpi\beta^{1/2}, \quad s_0 = (3\beta/8)^{1/2}, \quad \varpi = (2/3)^{3/2} = 0.544. \quad (4.52)$$

Direct numerical integration of (4.50) yields the value $\varpi = 0.685$. The dimensional frequency reads

$$\omega = \varpi(c\bar{D})^{1/2}\kappa_{c2}^{3/2}. \quad (4.53)$$

The core radius can be obtained using the relation $\omega\rho_0 = c_{r0}$. This gives $\rho_0 = c\omega^{-1} + O(\beta)$. The complete steadily rotating spiral solution is obtained by using (4.51) in (4.44) and evaluating (4.43), where $\theta_0(t) = \omega t + \phi$ with ϕ being a constant phase [see (4.46) and (4.48)], and $X_0 = -\rho_0 \cos(\omega t + \phi)$, $Y_0 = \rho_0 \sin(\omega t + \phi)$.

We discuss now the significance of these results. The outer solution (4.51a), or $\kappa = (\omega/2sc)^{1/2}$ in dimensional quantities, describes an involute of a circle of radius ρ_0 , a form that has already been used to describe spiral waves in excitable media [WIN1]. This form holds down to arclength $s_0 \sim \beta\rho_0 \ll \rho_0$ where deviations from the involute become significant. The (unique) frequency of rotation goes to zero and the core radius diverges as $\kappa_{c2} \rightarrow 0$ in accord with (4.47) and fig. 20.

To evaluate the rotation frequency as a function of ε one needs to know how κ_{c2} is related to ε . We describe now how this relation is obtained in ref. [MIZ]. At $\varepsilon = \varepsilon_{c2}$, the tip of a planar broken wave-front neither grows nor retracts. One is motivated then to assume the existence of a broken wave-front solution of

$$-c_c \partial_\chi u = f(u, v) + \partial_\chi^2 u + \partial_y^2 u, \quad -c_c \partial_\chi v = \varepsilon_{c2} g(u, v), \quad (4.54a, b)$$

where $\chi = x - c_c t$.*) Consider now ε values slightly smaller than ε_{c2} that allow for large-wavelength steadily rotating spiral waves. Transforming to polar coordinates, ρ and ϑ , (4.54a) becomes

$$-(c_\rho + \kappa_{c2}) \partial_\chi u = f(u, v) + \partial_\chi^2 u + \partial_y^2 u, \quad -c_\rho \partial_\chi v = \varepsilon g(u, v), \quad (4.55a, b)$$

where now $\chi = \rho - c_\rho t$ and $y = \vartheta/\kappa_{c2}$. In obtaining (4.55a) it has been assumed that curvature variations along the spiral arm are negligible, thus $\kappa = \kappa_{c2}$. Equations (4.55a, b) can be brought to the form of (4.54a, b) once the identification

*) We note that the existence of such a solution has not been proven yet.

$$\varepsilon_{c2} = \varepsilon(1 + \kappa_{c2}/c_\rho), \quad c_c = c_\rho + \kappa_{c2}, \quad (4.56)$$

is made. Eliminating c_ρ one finds

$$\kappa_{c2} = (c_c/\varepsilon_{c2})(\varepsilon_{c2} - \varepsilon), \quad (4.57)$$

or using (4.53)

$$\omega \sim (\varepsilon_{c2} - \varepsilon)^{3/2}. \quad (4.58)$$

Equations (4.53) and (4.57) have been tested in ref. [MIZ] by comparing the implied ω - ε dependence with direct numerical simulations on a particular reaction-diffusion model. Unfortunately, the numerical data was too poor to test the scaling law (4.58) conclusively. Deviations of the numerical data from the theoretical curve are reasonably small at large ε values but become large as ε is decreased, presumably due to refractory tail effects that become important as the spiral pitch decreases. Another possible source of error (even in the regime of large ε values) is the large curvature variations, $|\partial_s \kappa| = \omega \beta^{-1} \sim \beta^{-1/2} \gg 1$ (in dimensionless quantities), in the boundary layer near the tip. The extent to which such variations are compatible with the assumption of weak curvature dependence on arclength, used in deriving the curvature-speed relation, has yet to be estimated.

Linear stability analysis of steadily rotating spiral waves, within the framework of this theory, has not been performed yet. It is easy to see, however, that the growth of the tip according to (4.47) has a stabilizing effect. Linearizing the corresponding term in (4.41) and (4.42) about a steadily rotating spiral solution, $\kappa_\omega(s)$, yields a contribution of the form $d(d\kappa_\omega/ds)_{s=0}$ to the growth rate of a perturbation $\delta\kappa$ at $s=0$. Since $d\kappa/ds$ is always negative for steadily rotating spiral waves and $d>0$ this contribution is negative. We shall return to this question in section 4.3.4.3.

4.3.4.2. Refractory tail effects. When the excitability of the medium gets higher the rotation period decreases and the value v_t of v at the spiral wave-front is no longer the rest-state value, v_s ; repeated excitation occurs before complete recovery is achieved. In general, v_t will not be constant along the spiral arm, and this nonuniformity will affect the spiral wave dynamics. In the case of steady rotation we may expect $v_t(s)$ to be uniform, apart from a small neighborhood of the tip, for any excited site is visited again after the same period of time. Inside the core, on the other hand, the medium is never excited and therefore v assumes the (smaller) rest state value, v_s .

Refractory tail effects (incomplete recovery) in the case of steady rotation can be incorporated into the kinematical approach described in section 4.3.4.1 by letting c and κ_{c2} depend on the constant period of rotation, $T = 2\pi/\omega$. Phenomenological forms for these functions have been suggested in refs. [ZYK5,ZYM,MIK1,MIK2]. They take the forms

$$c(T) = c_\infty(1 - \Gamma_1/T), \quad \kappa_{c2}(T) = \kappa_{c2}(\infty)(1 - \Gamma_2/T), \quad (4.59a, b)$$

where Γ_1 and Γ_2 are phenomenological constants proportional to T_{\min} , the minimal wavetrain period below which propagation fails (see section 3.2.1). We note that the form (4.59a) for the dispersion relation $c = c(T)$ does not coincide at long periods with the asymptotic exponential form (3.48). In the case of nonsteady rotation, T becomes a field, $T(s, t)$, representing the time that has elapsed since the

last passage of the spiral wave-front through a point which is presently at arclength s . This field is constructed in refs. [ZYK5,ZYM] as

$$T = t - T^*(X(s, t), Y(s, t)), \quad (4.60)$$

where T^* , the last passage time at $(X(s, t), Y(s, t))$, is determined numerically during the integration of the kinematical equations.

Another kinematical approach, intended specifically to address refractory tail effects, has been proposed in refs. [MER1,MER2]. It is basically an extension of the one-dimensional kinematical approach of section 3.2.2 to two dimensions. To make the analogy to the one-dimensional case more apparent, a spiral coordinate system is introduced and split into parallel sections so as to map the problem into one consisting of an array of approximately planar wave-fronts, as described below.

The close similarity of spiral wave-fronts to involutes of circles (see section 4.3.2) motivated the choice of a coordinate system in the form of an involute of a circle of radius ρ_* and rotating at frequency ω ,

$$\mathbf{x} = X_{\text{in}}(\sigma, t) + r\hat{\mathbf{r}}_{\text{in}}(\sigma, t), \quad (4.61)$$

where $\hat{\mathbf{r}}_{\text{in}}$ is a unit vector normal to the involute spiral and

$$\begin{aligned} X_{\text{in}} &= \rho \cos[\vartheta_{\text{in}}(\rho) - \omega t], & Y_{\text{in}} &= \rho \sin[\vartheta_{\text{in}}(\rho) - \omega t], \\ \vartheta_{\text{in}}(\rho) &= \sigma - \arctan \sigma, & \sigma &= [(\rho/\rho_*)^2 - 1]^{1/2}. \end{aligned} \quad (4.62)$$

The range of the normal coordinate r is chosen to be $(-\lambda_{\text{in}}/2, \lambda_{\text{in}}/2)$ where $\lambda_{\text{in}} = 2\pi\rho_*$ is the pitch of the involute spiral. The range of σ is $\sigma_{\text{tip}} < \sigma < \infty$ where $\sigma_{\text{tip}} > 0$ to avoid the singularity in the involute curvature, $\kappa_{\text{in}} = (\rho_*\sigma)^{-1}$ at $\sigma = 0$.

We now decompose the range of σ into intervals, S_l , representing parallel portions of the involute spiral

$$S_l = [\sigma_{\text{tip}} + 2\pi(l-1), \sigma_{\text{tip}} + 2\pi l], \quad l = 1, 2, \dots,$$

and construct solitary wave-fronts that are peaked on these intervals

$$H_k(\sigma, r) \equiv H(r + n(\sigma)\lambda_{\text{in}} - k\lambda_{\text{in}}), \quad k = 1, 2, \dots; \quad n(\sigma) = l \quad \text{if } \sigma \in S_l. \quad (4.63)$$

Thus, $H_k(\sigma, r) = H(r)$ for $\sigma \in S_k$ and therefore assumes maximal values on the k th segment.

To describe the spiral wave-front (in the rotating frame) we introduce a displacement function $r = \zeta(\sigma, t)$. In the laboratory frame the spiral wave-front is given by

$$X_{\text{sp}} = X_{\text{in}}(\sigma, t) + \zeta\hat{\mathbf{r}}_{\text{in}}(\sigma, t). \quad (4.64)$$

In analogy to (3.36) we approximate a spiral wave solution by

$$U(\sigma, r, t) \approx \sum_k H_k(\sigma, r - \zeta_k), \quad \zeta_k \equiv \zeta(\sigma_k, t), \quad \sigma_k = \sigma + 2\pi[k - n(\sigma)]. \quad (4.65)$$

To understand better this form consider, for example, the first interval $\sigma \in S_1$. On this interval $n(\sigma) = 1$ and

$$U(\sigma, r, t) \approx H[r - \zeta(\sigma, t)] + H[r - \lambda_{\text{in}} - \zeta(\sigma + 2\pi, t)] + \cdots, \quad \sigma \in S_1.$$

Thus the main contribution comes from the wave-front that is peaked on S_1 . In addition, U contains contributions from the tails (or residual fields) of wave-fronts ahead of it.

In order to proceed as in section 3.2.2 we express the reaction–diffusion equations,

$$\partial_t U = LU + N(U) + D\nabla^2 U, \quad (4.66)$$

in the involute coordinate system and recast them in the form

$$LU + N(U) + D \partial_r^2 U + c_\infty \partial_r U = P, \quad (4.67a)$$

$$P = -D\kappa_1 \partial_r U + \partial_t U + \Omega_D \partial_\sigma U - D\kappa_1^2 \partial_\sigma^2 U, \quad (4.67b)$$

$$\kappa_1(\sigma, r) = \kappa_{\text{in}}/(1 + r\kappa_{\text{in}}), \quad \Omega_D(\sigma, r) = \omega + \rho_* D\kappa_1^3,$$

where $\kappa_{\text{in}}(\sigma) = (\rho_* \sigma)^{-1}$ is the involute curvature and we identified $\omega\rho_*$ with c_∞ , the speed of a planar solitary wave-front. Were P negligible, eq. (4.67a) would have reduced to the one-dimensional problem (3.35). The method of section 3.2.2 is still applicable for small P . For this to happen we have to exclude the immediate vicinity of the tip from the range of σ , because at the tip $\partial_\sigma U$ is of the same order as $\partial_r U$. Once this is done (see discussion below) $\partial_\sigma U$, $\partial_\sigma^2 U$ and $\partial_t U$ are small in comparison with $\partial_r U$, for the involute spiral provides a good zeroth order approximation. If in addition, $\kappa_{\text{in}}(\sigma_{\text{tip}}) \ll c_\infty$ [assuming δ is at most of $O(1)$], then P can be regarded as a perturbation.

Writing a spiral solution in the form

$$U(\sigma, r, t) = \sum_k H_k(\sigma, r - \zeta_k) + R(\sigma, r, t), \quad (4.68)$$

where R is a small correction term, and using this form in (4.67) we obtain the spiral evolution equation

$$\partial_t \zeta = -\bar{D}\kappa_1 - \bar{\Omega}_D \partial_\sigma \zeta + \bar{D}\kappa_1^2 \partial_\sigma^2 \zeta + q_\ell(\zeta^+ - \zeta + \lambda_{\text{in}}), \quad (4.69)$$

where $\kappa_1(\sigma, \zeta) = (\rho_* \sigma + \zeta)^{-1}$, $q_\ell(-x)$ is given by (3.46b), $\zeta^+ \equiv \zeta(\sigma + 2\pi, t)$, \bar{D} is given (4.26b) and $\bar{\Omega}_D = \omega + \rho_* \bar{D}\kappa_1^3$. In deriving (4.69) we assumed $\kappa_{\text{in}} \sim \gamma \ll c_\infty \sim O(1)$, where $\gamma = \exp(-\eta_\ell \lambda_{\text{in}})$. Equation (4.69) has been studied so far only numerically. One consequence, however, is immediately inferred; in the absence of refractory tail effects ($\gamma \ll \kappa_{\text{in}}$) (4.69) admits an involute solution ($\zeta = 0$) as $\sigma \rightarrow \infty$.

To relate the spiral evolution equation (4.69) to relations with which we are already familiar, let us express this equation in terms of the normal velocity,

$$c_r = \partial_r X_{\text{sp}} \cdot \hat{r}, \quad \hat{r} = [(Y_{\text{sp}})_\sigma \hat{x} - (X_{\text{sp}})_\sigma \hat{y}] N^{-1},$$

and curvature,

$$\kappa = [(X_{\text{sp}})_\sigma (Y_{\text{sp}})_{\sigma\sigma} - (Y_{\text{sp}})_\sigma (X_{\text{sp}})_{\sigma\sigma}] N^{-3}, \quad N = [(X_{\text{sp}})_\sigma^2 + (Y_{\text{sp}})_\sigma^2]^{1/2},$$

of the spiral front X_{sp} , where the subscript σ denotes partial derivative with respect to σ . Using (4.62) and (4.64) we find

$$c_r = c(\lambda) - \bar{D}\kappa; \quad c(\lambda) = c_\infty + q_\ell(\lambda), \quad \lambda = \zeta^+ - \zeta + \lambda_{\text{in}}. \quad (4.70a, b)$$

This is just the curvature–speed relation (4.26) where the planar wave speed c is given by the dispersion relation (3.48) evaluated at $\lambda = \zeta^+ - \zeta + \lambda_{\text{in}}$.

The kinematical approach described above avoids the consideration of the two-dimensional structure of the spiral tip and assumes constant wave width (the solitary wave width). A consequence of these simplifications is that the dynamics of the tip in the tangential direction cannot respond independently to variations in the recovery field nor to variations in wave width. The latter effect could be modeled as in (4.47) and (4.59b) with T replaced by $\lambda = \zeta^+ - \zeta + \lambda_{\text{in}}$. An extension of the theory along this line, however, has not been attempted. Despite these limitations interesting results can already be obtained with this simplified approach, as we shall see in the next section.

4.3.4.3. The onset of nonsteady rotation. The two kinematical approaches described in sections 4.3.4.1 and 4.3.4.2 allow the study of nonsteady rotation. Both approaches give in wide parameter ranges stable steady rotation and both exhibit a transition to meander. Integration of eqs. (4.41)–(4.46) using (4.59) and (4.60) yields a transition to meander as the values of Γ_1 and Γ_2 in (4.59), or T_{min} , are increased [ZYK5,ZYM,MIK1,MIK2]. The explanation given in these references as to why an increase in T_{min} should lead to meander is the following. Imagine that initially $T_{\text{min}}/T \ll 1$ so that steady rotation prevails, and $T_{\text{min}}/T \approx 0$ is rather uniform. As T_{min} is increased, a gradient of T_{min}/T develops at the tip, for inside the unexcited core $T = \infty$ and T_{min}/T remains zero. The tip that rests on such a gradient has a tendency to grow and penetrate into the unexcited core region, for as it grows the critical curvature κ_{c2} increases and consequently the tangential speed c_t increases as well [see (4.47)]. The forces that keep the tip from doing that prior to the onset of meander are not discussed in the above references.

Integration of equation (4.69) yielded a transition to compound rotation as the value of \bar{D} was increased [MER1]. In that reference a different explanation for the onset of meander has been given. As discussed in section 4.1.1 and illustrated in fig. 12, curvature acts to stabilize a propagating front against local or short-wavelength perturbations. It has been suggested in ref. [MER1] that this is true only away from the tip. Near the tip one may imagine local perturbations that will grow under the effect

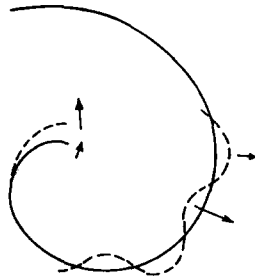


Fig. 21. The destabilizing effect of curvature near the tip. Perturbations (dashed curves) near the tip, like that depicted, may grow under the effect of curvature, in contrast to local perturbations away from the tip that disappear in the course of propagation.

of curvature as fig. 21 illustrates; upon straightening a small section of the spiral arm that includes the tip, curvature is reduced, normal velocity is enhanced, and further straightening is favored. This destabilizing effect is counterbalanced by the refractory repulsion that the accelerating wave-front experiences as it comes closer to the wave-front ahead of it. By increasing the parameter \bar{D} one strengthens the destabilizing curvature effect. At a critical value of this parameter, the gain in normal velocity because of reduced curvature just balances the loss due to refractory repulsion. Beyond that critical value one may expect the instability to set in. The tangential speed of the tip provides another stabilizing mechanism as we have already discussed at the end of section 4.3.4.1. This mechanism is expected to be dominant in the regime of long periods where refractory tail effects are negligible.

The onset of meander may occur either by increasing the excitability of a barely excitable medium, or by decreasing the excitability of a highly excitable medium (see sections 4.3.2 and 4.3.3). The explanation given in refs. [ZYK5,ZYM,MIK1,MIK2] emphasizes tangential tip growth and appears more applicable to the former transition. The explanation given in ref. [MER1] attributes an important role to dynamics in the normal direction and seems more suitable for the latter transition. Evidently both velocity components play active roles during meander.

The kinematical approach of section 4.3.4.2 has been used in ref. [MER1] to study the effect of oscillatory recovery on spiral wave dynamics. In a wide parameter range spiral cores have been found to expand in time. This behavior has been attributed to uniform normal-velocity profiles along the spirals that become feasible because of the oscillatory recovery; the increased excitability (beyond that of the rest state) at proper wave-front spacings may compensate for the reduction in normal velocity due to curvature and tip structure. We recall though that direct numerical simulations so far revealed a discrete family of steadily rotating spiral waves with increasing core sizes rather than expanding cores (see section 4.3.3). It remains to be seen whether parameter ranges can be found that sufficiently enhance the velocity compensation effect due to increased excitability.

4.3.5. Free boundary formulations

In the free boundary approach the spiral arm is conceived as consisting of a front and a back that meet at a distinct point, the tip. The compound interface interacts with a relaxation field, v , whose effect is most prominent near the tip. Such an approach was advanced for the first time in ref. [FIF1] and later in ref. [TYK1] (see also ref. [KEL3]). Both works pose free boundary problems but do not solve them. Recently, successful attempts to solve similarly posed problems have been reported [PES1,KEE3,KAR2]. Since they rely on earlier, time-independent geometrical theories of spiral waves [KEE2,KET2,ZYK1,TYK1], we describe the latter first (following primarily ref. [KEE2]).

Consider the wave-front of a steadily rotating spiral wave. The location of the wave-front can be described by

$$X = \rho \cos[\vartheta(\rho) - \omega t], \quad Y = \rho \sin[\vartheta(\rho) - \omega t], \quad (4.71)$$

where ρ is a radial coordinate with respect to the center of rotation, and ϑ is the polar angle describing the wave-front position. The curvature and normal velocity of the front are given by [KEE2]

$$\kappa = \psi' / (1 + \psi^2)^{3/2} + \psi / [\rho(1 + \psi^2)^{1/2}], \quad (4.72a)$$

$$c_r = \omega\rho / (1 + \psi^2)^{1/2}, \quad \psi = \rho\vartheta'(\rho). \quad (4.72b)$$

Far from the tip where curvature is negligible we can approximate $c_r \approx c$. This leads to a solution in the

form of an involute of a circle of radius c/ω . Using the full form (4.10) of the curvature–speed relation (for ε small enough) we obtain the shape equation

$$\rho \, d\psi/d\rho = (1 + \psi^2)[c\rho(1 + \psi^2)^{1/2} - \omega\rho^2 - \psi]. \quad (4.73)$$

For an infinite system one should require

$$\psi(\rho) \sim k\rho \quad \text{as } \rho \rightarrow \infty, \quad (4.74a)$$

as far from the core the spiral wave becomes an involute of a circle, which in turn, approaches the form of an Archimedian spiral. In addition, $\psi(\rho)$ should be specified at $\rho = \rho_0$, the radius of the spiral core. The latter boundary condition poses a difficulty because the wave-front speed $c = \mu(v_t)$ becomes a strong unknown function of ρ as the tip is approached. Only away from the tip, can c be regarded as independent of ρ (see section 4.3.4.2). To avoid this difficulty a spiral wave rotating around a hole of radius ρ_0 has been considered, with ρ_0 chosen to be large enough. At this boundary, the no-flux boundary condition

$$\psi(\rho_0) = 0, \quad (4.74b)$$

was employed.

Equations (4.73) and (4.74) constitute an eigenvalue problem for ω , thus leading to the so called “critical relation”,*)

$$\omega = \Omega(c, \rho_0). \quad (4.75a)$$

Some information about this relation can be obtained at once using the symmetry transformation, $\psi \rightarrow \psi$, $\rho \rightarrow A\rho$, $\omega \rightarrow \omega/A^2$ and $c \rightarrow c/A$, which leaves (4.73) invariant [KEE2]. Applying this transformation to (4.75) with $A = c$ we find

$$\omega = c^2\Omega(c\rho_0), \quad (4.75b)$$

where we dropped the first constant argument. An explicit form for $\Omega(x)$ has been evaluated in ref. [KEE2] for c values sufficiently large. It reads $\Omega(x) = \Omega_0 - \Omega_1 x^2$.

The critical relation expresses in a formal way the intuitive observation that there must be some relation among the three quantities ω , c and ρ_0 ; were curvature effects negligible, this relation would have simply been $c = \omega\rho_0$. In addition, ω and c should satisfy the dispersion relation, $c = c(2\pi/\omega)$ (expressed in terms of periods rather than wavelengths), for far away from the core the traveling waves that propagate at speed c have the spiral period of rotation. The intersection point of the critical curve (4.75) and the dispersion curve determines the rotation frequency as a function of ρ_0 . We can understand now why oscillatory recovery may give rise to a multiplicity of stable spiral solutions [WIN6,WIN7,KEE2]; the critical curve may intersect the nonmonotonic dispersion curve at several points. Intersection points occurring on positive slopes pertain to stable spiral solutions.

The theory just sketched has been tested by comparing the critical relation (4.75) with direct

*) In ref. [TYK1] this relation has been called the “curvature” relation.

numerical simulations [PEP]. Good agreement has been found [TYK1]. The theory has also been applied to the BZ medium [KET2], using the Oregonator model to evaluate the dispersion curve and an empirical value for ρ_0 . The agreement with experimental data was satisfactory. Notice that once ρ_0 is given, the critical relation (4.75) is known irrespective of the particular reaction kinetics. One should bear in mind though that (4.75) has been derived using the curvature–speed relation (4.10) which is valid for sufficiently small ε values. For higher ε values the relation (4.21), which does contain information about the particular reaction kinetics, has to be used instead. Applications of the theory to models describing the myocardium and slime mold aggregation have been reported in refs. [TYK2] and [TAM], respectively.

We turn now to the free boundary formulation presented in refs. [PES1,KEE3] for steadily rotating spiral waves. As we shall see, it resolves the frequency selection problem by determining uniquely the core radius, ρ_0 . We will follow here the more general presentation of ref. [KEE3]. The basic idea [TYK1] is to view a spiral pattern as excited and recovery domains separated by a compound interface consisting of a front and back, as illustrated in fig. 22. To determine the interface position one introduces the polar angles, $\vartheta_f(\rho)$ and $\vartheta_b(\rho)$, for the front and back, respectively, and use the curvature–speed relations

$$c_{rf} = c_f - \kappa_f, \quad c_f = \mu(v_f); \quad c_{rb} = c_b - \kappa_b, \quad c_b = -\mu(v_b), \quad (4.76)$$

to obtain the interface equations

$$\rho \, d\psi_j/d\rho = (1 + \psi_j^2)[c_j \rho(1 + \psi_j^2)^{1/2} - \omega \rho^2 - \psi_j], \quad j = f, b, \quad (4.77)$$

where, as before, $\psi_j = \rho \vartheta'_j$. Notice that the planar wave-back speed, c_b , has been chosen to have the same sign as the wave-front speed, c_f , for $v_f < v^* < v_b$. Also notice that both κ_f and κ_b are positive for the far spiral wave.

Continuity of the field v through the tip requires $v_f(\rho_0) = v_b(\rho_0)$, whereas away from the tip $v_f < v^*$ and $v_b > v^*$. Evidently v_f and v_b cannot remain constant near the tip. Since the interface equations depend on v_f and v_b through the planar speeds c_f and c_b , they must be coupled to the field equation of v . To simplify the problem a nondiffusive field has been assumed in refs. [PES1,KEE3]. Thus

$$\omega \, dv/d\vartheta = -\varepsilon G_{\pm}(v), \quad v = v(\vartheta - \omega t; \rho), \quad (4.78)$$

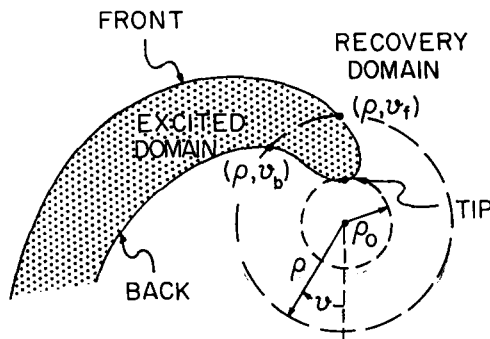


Fig. 22. The free-boundary-formulation view of the spiral tip. The front and back meet at the tip tangentially to a circle of radius ρ_0 . The compounded interface separate excited (dotted) and recovery regions.

where the \pm signs denote, as usual, the excited (+) and the recovery (-) regions. Integrating (4.78) along a circle of radius ρ (see fig. 22) we find

$$T_+(\rho) = \frac{\vartheta_f - \vartheta_b}{\omega} = \frac{1}{\varepsilon} \int_{v_f(\rho)}^{v_b(\rho)} \frac{dv}{G_+(v)}, \quad T_-(\rho) = T - T_+(\rho) = -\frac{1}{\varepsilon} \int_{v_f(\rho)}^{v_b(\rho)} \frac{dv}{G_-(v)}, \quad (4.79a, b)$$

where T_+ and T_- are the durations of excitation and recovery, respectively, and $T = 2\pi/\omega$ is the period of rotation. Equations (4.79) can be used to determine v_f and v_b as functions of T_+ and ω , and consequently c_f and c_b : $c_f = C_f(T_+, \omega)$, $c_b = C_b(T_+, \omega)$. Substituting these forms into (4.77) we obtain

$$\rho d\psi_j/d\rho = (1 + \psi_j^2)[C_j(T_+, \omega)\rho(1 + \psi_j^2)^{1/2} - \omega\rho^2 - \psi_j], \quad j = f, b. \quad (4.80)$$

In addition, using the definition (4.79) of T_+ we have

$$\omega\rho dT_+/d\rho = \psi_b - \psi_f. \quad (4.81)$$

Equations (4.80) and (4.81) form a closed system of ordinary differential equations that can be solved for the shape functions ψ_f and ψ_b once appropriate boundary conditions are specified. On the boundary of the system one may require either

$$\psi_f(\rho) = \psi_b(\rho) \sim k\rho \quad \text{as } \rho \rightarrow \infty, \quad (4.82a)$$

for very large systems, or the no-flux boundary conditions

$$\psi_f(\rho_L) = \psi_b(\rho_L) = 0, \quad (4.82b)$$

for smaller systems (of size ρ_L). At the tip the normal velocities of the front and back are zero as the tip moves along a circle of constant radius, ρ_0 [PES].*) Thus from (4.72b) one obtains

$$\psi_b(\rho_0) = -\psi_f(\rho_0) = \infty. \quad (4.83a)$$

In addition, since $\vartheta_f(\rho_0) = \vartheta_b(\rho_0)$, we have

$$T_+(\rho_0) = 0. \quad (4.83b)$$

Equations (4.80) and (4.81) subject to the boundary conditions (4.82) and (4.83) constitute an eigenvalue problem for *both* ω and ρ_0 . This eigenvalue problem was solved numerically in ref. [PES1] using a piecewise linear model. Rigorous arguments for the existence of isolated solutions were presented soon afterwards [KEE3]. We describe now some properties of the computed solutions.

Evaluation of the levels, v_f and v_b , of the field v along the spiral arm reveals that they remain almost

*) Notice that in this free boundary formulation zero normal velocity at the tip amounts to zero tangential velocity in the kinematical formulation of section 4.3.4. This stems from the different views of the spiral arm in the two approaches; in the former, it consists of two curves that meet at the tip, whereas in the latter it is conceived as a single curve that terminates at the core.

constant everywhere except for a small region near the tip where both quantities drop to the rest state value v_s . The planar wave speeds, $c_f = \mu(v_f)$ and $c_b = -\mu(v_b)$, behave accordingly; for most of the spiral arm $c_f \approx c_b$, but as v_b drops below v^* , c_b changes sign and reaches the value $-c_f = -\mu(v_s)$ at the tip. Similarly, away from the tip $\kappa_f \approx \kappa_b$, but as the tip is approached κ_b reverses its sign so that at the tip, $\kappa_b = -\kappa_f$. The frequency of rotation, ω , and the core radius, ρ_0 , were found [PES1] to diminish and to diverge, respectively, as ε approaches a critical value which we identify with ε_{c2} . This result is in qualitative agreement with the kinematical theory of section 4.3.4.1. The value ε_{c2} was found [PES1] to be a monotone decreasing function of the excitation threshold.

Under what conditions is the free boundary formulation presented above expected to be valid? The formulation is based on the curvature–speed relations (4.76). For these relations to be valid the radius of curvature should be much larger than the wave-front width, w_f (see section 4.1.2), in particular, at the point of highest curvature, the tip. Thus

$$R_{\text{tip}} \gg w_f \sim O(1), \quad R_{\text{tip}} = \kappa(\rho_0)^{-1}. \quad (4.84)$$

Large values of R_{tip} , in turn, can be obtained by decreasing ε , for then the width of the excited domain increases and consequently the radius of curvature. Thus, we expect (4.84) to hold for sufficiently small ε values. Another assumption that has been made in deriving the curvature–speed relations is that curvature variations along the interface are negligible. Near the tip curvature variations are obviously significant, but again we might expect them to become negligible for ε values sufficiently small.

But how small should ε be in order for (4.84) to hold, and is there any restriction on the threshold of excitation, the other significant control parameter in many numerical simulations? We address these questions following arguments that have been presented in refs. [FIF4,KAR2,KAR3]. At the tip, normal velocity is zero and $v_f = v_s$. Consequently, $c_f = c_\infty \sim R_{\text{tip}}^{-1}$. Since $R_{\text{tip}} \gg 1$, we find $c_\infty \ll 1$. The latter inequality can be satisfied only if

$$\Delta = v^* - v_s \ll 1, \quad \varepsilon \ll 1 \quad (4.85)$$

(see section 3.1.3). Thus we must consider small Δ values or high thresholds [KAR3]. High threshold media give rise to long rotation periods and consequently to v levels $v_f \approx v_s$ and planar wave speeds $c_f \approx c_\infty$ away from the tip as well. Since the radius of curvature at the tip is of the order of the width of the excited domain, λ_+ , evaluated at a distance of $O(R_{\text{tip}})$ or greater from the tip, we obtain $\lambda_+ \sim c_\infty T_+ \sim R_{\text{tip}} \sim c_\infty^{-1}$ or

$$c_\infty^2 \sim T_+^{-1}. \quad (4.86)$$

Using the smallness of $\Delta = v^* - v_s$ we find to leading order $c_\infty \sim \varepsilon T_+ \sim v^* - v_s$, which together with (4.86) yields the rather restrictive condition on ε ,

$$\Delta \sim \varepsilon^{1/3} \ll 1. \quad (4.87)$$

In addition we find

$$R_{\text{tip}} \sim \varepsilon^{-1/3}, \quad T_+ \sim \varepsilon^{-2/3}, \quad c_\infty \sim \varepsilon^{1/3}. \quad (4.88)$$

Thus, it is only for very small ε values, $\varepsilon^{1/3} \ll 1$, that $R_{\text{tip}} \sim \varepsilon^{-1/3}$ satisfies (4.84). Note that $c_f \sim c_\infty$ is much larger than $c_{\text{min}} \sim \varepsilon^{1/2}$, the minimal speed below which propagation fails. Scalings for space and time as in (4.88) were suggested for the first time in ref. [FIF1].

The scaling form (4.87) holds in particular for the critical value, $\Delta = \Delta_c(\varepsilon)$, at which the spiral core diverges to infinity, where ε is assumed to be sufficiently small. The exact form of this relation (i.e., including the prefactor) has been obtained in ref. [KAR2] by solving the free boundary problem in the limit of infinite core size. The calculated relation has then been compared with direct numerical simulations. Good agreement has been obtained for $\varepsilon = 10^{-3}$ corroborating the free boundary formulation in the range implied by (4.88).

The considerations presented above are based on the observations that at the core v assumes the rest state value v_s . This led to the conclusion that in order for (4.84) (and thus for the free boundary formulation) to hold, barely excitable media, satisfying (4.85), should be considered. In the other extreme of highly excitable media the level of v at the tip, $v_f(\rho_0)$, may no longer coincide with the rest state value, v_s . This is not surprising when diffusion of v is allowed, for in highly excitable media the core size becomes of $O(1)$ and diffusion from the surrounding recovering medium may significantly raise the level of v . Recent numerical studies [WIN8] suggest that this might be the case for a nondiffusive v variable as well. In any event, it is then the condition $v^* - v_f(\rho_0) \ll 1$ that must be satisfied for (4.84) to hold (for $\varepsilon \ll 1$), and if $v_f(\rho_0)$ deviates significantly from v_s , no constraint on excitability is imposed. In other words, the free boundary formulation may be applicable to highly excitable media as well, provided the inequality $v^* - v_f(\rho_0) \ll 1$ is satisfied.

Highly excitable media give rise to short-wavelength spiral waves for which repeated excitation occurs well before complete recovery is achieved, that is, at values v_f closer to v^* . This has been observed in numerical simulations (see for example ref. [WIN8]) and is also implied by the experimental findings displayed in fig. 15. It is therefore reasonable to assume that for sufficiently high excitability the inequality $v^* - v_f \ll 1$ holds everywhere along the spiral. These considerations motivated the hypothesis that $v^* - v_f$ scales *uniformly* with ε [FIF3,FIF4]. Using arguments similar to those presented for the case of barely excitable media one finds [FIF4]

$$v^* - v_f \sim \varepsilon^{1/3} \ll 1, \quad c_f \sim \varepsilon^{1/3} \ll 1. \quad (4.89)$$

These scaling forms are widely referred to as ‘Fife scaling’. The simulations reported in ref. [WIN8] indeed suggest such scaling behavior at ε values sufficiently small. A consequence of (4.89) is that at small ε values the frequency of rotation scales like $\omega \sim \varepsilon^{2/3}$ or $\omega' \sim \varepsilon^{-1/3}$ for the rescaled system (3.1d, e).

There is another important consideration that bears on the validity of the free boundary formulation. The formulation is based on the assumption that the singular perturbation approach holds everywhere along the spiral including the tip. Strictly speaking, this requirement cannot be satisfied, for within a radius of order unity around the tip the width of the excited domain, λ_+ , becomes comparable to the wave-front thickness, w_f , thus making the distinction between outer and inner regions meaningless. Since this neighborhood of the tip becomes comparatively smaller (with respect to other length scales of the spiral) as ε is decreased, we might expect the free boundary formulation to work considerably well for ε values sufficiently small, as the study of barely excitable media, reported in ref. [KAR2] indeed indicates. The case of highly excitable media is more intricate, for too small ε values may give rise to nonsteady rotation [WIN8]. In any event, better results are expected once the finite thickness of the interface is taken into account. An analysis along these lines has been presented in ref. [KEE3]. It

retains the basic structure of the original problem leaving eqs. (4.80) and (4.81) as they are but improves the evaluation of $c_f = C_f(T_+, \omega)$ and $c_b = C_b(T_+, \omega)$ as explained below.

Instead of using (4.78) to evaluate $v_f(\rho)$ and $v_b(\rho)$ one resorts to the original equation

$$\omega \, dv/d\vartheta = -\varepsilon g(u, v), \quad (4.90)$$

and use an approximation for u better than $u = u_{\pm}(v)$. The approximation used in ref. [KEE3] is the following. At each point (x, y) in the plane for which eq. (4.90) is to be solved, the value of v is assumed to be known and the one-dimensional interface equation

$$d^2u/dz^2 + c(v) \, du/dz + f(u, v) = 0, \quad (4.91)$$

is solved, where $u(z; v) \rightarrow u_+(z)$ as $z \rightarrow \infty$ and $u(0; v)$ has maximal slope. The coordinate $z(x, y)$ is interpreted as the shortest distance from the point (x, y) to the spiral wavefront and is taken to be positive (negative) if the point (x, y) lies in a recovery (excited) region. Once $u(z(x, y); v)$ is known it can be used in (4.90) to obtain $v_f(\rho) = v(\vartheta_f; \rho)$ and $v_b(\rho) = v(\vartheta_b; \rho)$ and consequently, $C_f = c_f(v_f)$ and $C_b = c_b(v_b)$. This modified problem has been solved in ref. [KEE3] for symmetric spirals^{*)} using a numerical iterative scheme. For moderately small ε values (0.05) the results are substantially improved as compared with those obtained with the original formulation, demonstrating the need for a more refined treatment of the spiral tip.

Progress in that direction has been made most recently in refs. [KAR4, KLR1] for the case of highly excitable media, having very sharp time scale separations ($\varepsilon^{1/3} \ll 1$) and giving rise to pointwise cores. The free boundary problem as presented above is regarded in these works as an outer problem whose solution should match a short scale core solution. The outer problem was simplified by assuming constant v levels along the front and back, and by exploiting the boundary condition (4.74b) with $\rho_0 = 0$ (pointwise core) for the interface shape equation [KAR4]. The inner core problem has been obtained from the full system (3.1a–c) by considering uniformly rotating solutions with frequency $\omega \sim \varepsilon^{2/3}$ and spatial scale $x \sim O(1)$ [KLR1]. It has been emphasized in refs. [KAR4, KLR1] that although the inner solution is needed to match smoothly the different v levels at the front and back away from the core, the rotation frequency is solely determined by the outer problem. We recall that for higher ε values significant error can result by considering the outer problem alone [KEE3].

We have considered so far free boundary formulations for a nondiffusive v field only. The analogous problem, with diffusion of v allowed, has been addressed very recently in refs. [BER, KEE5]. The problem consists of solving the interface equations (4.77) now coupled to a *diffusive* field equation,

$$\omega \, dv/d\vartheta = -\varepsilon G_{\pm}(v) + \delta \nabla^2 v. \quad (4.92)$$

Unlike the singly diffusive case ($\delta = 0$), this free boundary problem can still be valid at the tip region provided the diffusion length of v is large in comparison with the front width [BER]. In ref. [BER] slow diffusion of v has been considered which allowed neglecting diffusive effects far from the tip. Spiral solutions have been obtained by matching the core, where diffusion is significant, to the far field. In ref. [KEE5] an iterative numerical scheme has been proposed for symmetric spirals, that rapidly converges to spiral wave solutions.

Apart from information about spiral shapes and rotation frequencies, the free boundary formulations

^{*)} Symmetric spirals are obtained when the nonlinear functions $f(u, v)$ and $g(u, v)$ have a point of odd symmetry.

can be used to obtain stability boundaries for steady rotation in the small ε portion of the ε -threshold parameter space (see the boundary line ∂M in fig. 18). Stability analyses of steady rotation, for the case of a nondiffusive v field, have not yielded so far an instability [PES2,PES3]. In these studies the outer solution, that is, the solution of (4.77) and (4.78), has been used. These findings may indicate that the outer solution is inadequate to describe the destabilization of steady rotation in the case of singly diffusive media, even for $\varepsilon^{1/3} \ll 1$. Stability analysis of steady rotation in the case of slow v diffusion, on the other hand, has yielded an instability to compound rotation [KLR2].

5. Discussion

Two basic theoretical approaches have been described throughout this review; singular perturbation theory that makes a distinction between outer (excited and recovery) regions and inner (front and back) regions, and kinematical theories which view solitary waves as integral entities that propagate invariably in space. The two approaches have different ranges of validity; the singular perturbation theory exploits the smallness of ε , while the kinematical theories assume long-wavelength patterns. They also differ in the type of questions they can address. The singular perturbation approach is concerned primarily with static aspects (constant speed traveling waves, steadily rotating spiral waves, etc.) while the kinematical approach allows the study of dynamical aspects as well, such as relaxational propagation and nonsteady spiral wave rotation. On the other hand, the singular decomposition of the solitary wave structure allows for the study of dispersion relations at short wavelengths and the consideration of spiral tip structures. The two approaches therefore complement each other in many respects.

There exists also a regime where the two approaches overlap: long period, steady propagation in systems characterized by very sharp time scale separations (small ε). This regime allows for comparison. In one space dimension both approaches successfully describe wave propagation, and dispersion relations coincide when the proper limits are taken (see section 3.2.2). In the case of spiral patterns the regime of long period and small ε is attainable with high threshold values or small Δ . As Δ approaches the critical value Δ_c pertaining to an infinite spiral a power law of the form $\omega \sim (\Delta - \Delta_c)^p$ is expected. Both approaches account for frequency selection, but it is not yet clear whether both yield the same power law.

Comparative studies of the two theoretical approaches to rotating spiral waves are highly desired. The kinematical approach is simpler and thus more appealing, particularly as far as dynamical aspects are concerned. For relatively large ε values it is also the only approach currently available. However, it does not resolve the tip structure and, unlike the singular perturbation approach, cannot yield rigorous results. This holds in particular for the onset of meander which originates at the tip. The current intensive study of the tip structure (using the singular perturbation approach), will presumably lead to the resolution of this problem in the not too far future, at least for some limiting cases. This progress should then be used to re-examine, substantiate or modify certain assumptions that lie at the basis of the kinematical approach, especially those concerning the tangential tip dynamics.

The scope of this review has been limited to a few fundamental phenomena occurring in homogeneous, isotropic, unforced excitable media. As a consequence, many topics have been left aside. A few of them are briefly discussed below.

Considerable work has been devoted recently to developing cellular automaton type models that

allow fast simulations of wave propagation in excitable media [FEK,MAH,MKH,GST1,GST2]. These models and others are reviewed in ref. [RAY]. Many features characteristic of excitable media have been observed using such models and their advantage in reducing computation time is evident. The main concern with cellular automaton models is their degree of reliability. A thorough discussion of this aspect appears in ref. [GST1]. A different approach to reducing computation time has been presented in ref. [BAR2]. Starting from a particularly chosen reaction–diffusion equation, an algorithm is devised for simulating wave patterns at variable spatio-temporal resolutions. For coarse resolutions, computation times comparable with those of cellular automaton models are obtained, whereas for fine resolutions, accurate solutions of the underlying reaction–diffusion equations are reproduced.

In sections 3.2.2 and 3.2.3 we motivated the view of complex patterns in one space dimension as many-body systems of interacting impulses. In two dimensions the basic “building blocks” of complex patterns are spiral waves as fig. 1 suggests. How do spiral waves interact? When the two cores in a spiral pair are sufficiently apart, interactions are screened by the surrounding spiral wave-fronts. At distances of the order of the core size, however, bound spiral pairs may form. Such pairs have been observed numerically in ref. [EPS]; pairs of spiral waves rotating in the same direction precess about fixed points in space, while pairs of counter rotating waves drift in directions perpendicular to the axes that connect the cores. At yet smaller distances counter rotating spiral waves attract and annihilate. Similar behavior has been observed in numerical simulations on oscillating media [SAK,AKW]. The interaction between counter rotating spiral waves bears on the problem of ventricular fibrillation. The critical distance at which attractive interactions change into repulsive ones has been used in ref. [WIN9] to define a threshold for the onset of ventricular fibrillation. The theoretical derivation of spiral interactions in excitable media is a hard problem that has not been solved yet. Considerable progress has been made though on the analogous problem in oscillating media [ARR,RIT1,RIT2,ELM,AKW,PIN,WCK].

The emergence of complex or turbulent patterns in two-dimensional excitable media has been addressed primarily in the context of inhomogeneous media. Inhomogeneities can be introduced artificially [KSS,PAV,MAS1] or can be induced by coupling the reaction to convective flow [AKP,WAL,MMP]. The main effect of an inhomogeneity is to break a wave-front with the consequent outcome of producing a pair of spiral waves. Can spiral waves nucleate spontaneously in *homogeneous* excitable media? So far no direct observations have been reported in simple models or in controlled experiments. Spontaneous nucleation, however, has been observed [WIN11] in the Beeler–Reuter model [BRE] and in discrete models [GST3,ITG]. The interest in this question derives in part from recent observations of transitions to turbulence in smoothly oscillating media that are mediated by spontaneous nucleation of spiral waves [KUR,CGL1,CGL2,BPJ,WUK]. Similar transitions have been obtained in other pattern forming systems [RRS,TRG] and it will come as no surprise if the same kind of transition is observed in most excitable media away from the singular limit.

Other topics that have attracted considerable attention include wave propagation on curved surfaces [MAS2,DAZ,GOH], wave propagation in inhomogeneous [PEY,ZMH,MAS2,LIE] and anisotropic [KEE4,YAM] media, periodically forced media [ADM,BDZ2], and chemical media subjected to dc electric fields [FSO,SCO,SEM1,SEM2,SSM]. We also mention new reactor designs involving inhomogeneous feed of chemicals that have produced new types of patterns [TVS,TAS,OBR,OCB] and renewed the interest in Turing structures [TUR,ROV,CDB,BCD,OUS1,OUS2]. Further topics are covered in a recent volume of *Physica D* [SWK] devoted to pattern formation in chemical and biological media and in a recent proceedings of a workshop on nonlinear wave processes in excitable media [HMO].

Acknowledgements

I would like to thank Alexander Mikhailov, Pierre Pelcé and Art Winfree for many helpful discussions and much correspondence. Special thanks should go to Ed Spiegel who suggested the view of excitable systems as slowly deforming potential systems. Special thanks to Art Winfree as well for his help in clarifying the relation between the secondary frequency that appears in compound rotation and the two rotation frequencies of an epicycloid. And thanks to the anonymous referee who carefully corrected typographical and grammatical errors. The support of the Bantrell Career Development Fellowship for Scientific Research is gratefully acknowledged.

References

- [ABS1] M.A. Allesie, F.I.M. Bonke and F.J.G. Schopman, *Circ. Res.* 39 (1976) 168.
- [ABS2] M.A. Allesie, F.I.M. Bonke and F.J.G. Schopman, *Circ. Res.* 41 (1977) 9.
- [ACS] A. Arneodo, P.H. Coulet, E.A. Spiegel and C. Tresser, *Physica D* 14 (1985) 327.
- [ADM] K.I. Agladze, V.A. Davydov and A.S. Mikhailov, *Pis'ma Zh. Eksp. Teor. Fiz.* 45 (1987) 601 (English transl. in *JETP Lett.*).
- [AID] D.J. Aidley, *The Physiology of Excitable Cells* (Cambridge, New York, 1978).
- [AKP] K.I. Agladze, V.I. Krinsky and A.M. Pertsov, *Nature* 308 (1984) 834.
- [AKW] I.S. Aranson, L. Kramer and A. Weber, *Physica D* 53 (1991) 376.
- [ALM] F. Alcantara and M. Monk, *J. Gen. Microbiol.* 85 (1974) 321.
- [APR] K.I. Agladze, A.V. Panfilov and A.N. Rudenko, *Physica D* 29 (1988) 409.
- [ARR] I.S. Aranson and M.I. Rabinovich, *J. Phys. A* 23 (1990) 299.
- [BAR1] D. Barkley, *Phys. Rev. Lett.* 68 (1992) 2090.
- [BAR2] D. Barkley, *Physica D* 49 (1991) 61.
- [BCD] J. Boissonade, V. Castets, E. Dulos and P. De Kepper, *Int. Ser. Num. Math.* 97 (1991) 67.
- [BCF] W.K. Burton, N. Cabrera and F.C. Frank, *Philos. Trans. R. Soc. London* 243 (1951) 299.
- [BDM] P.K. Brazhnik, A.V. Davydov and A.S. Mikhailov, *Teor. Mat. Fiz.* 74 (1987) 440 (English transl. in *Theor. Math. Phys.*).
- [BDZ1] P.K. Brazhnik, V.A. Davydov, V.S. Zykov and A.S. Mikhailov, *Sov. Phys. - JETP* 66 (1987) 984.
- [BDZ2] P.K. Brazhnik, V.A. Davydov, V.S. Zykov and A.S. Mikhailov, *Izv. VUZ Radiofiz.* 31 (1988) 574 (English transl. in *Radiophys. Quantum Electron.*)
- [BEL] B.P. Belousov, in: *Collections of Abstracts on Radiation Medicine* (Medgiz, Moscow, 1958) p. 145.
- [BER] A.J. Bernoff, *Physica D* 53 (1991) 125.
- [BKK] R.C. Brower, D.A. Kessler, J. Koplik and H. Levine, *Phys. Rev. A* 29 (1984) 1335.
- [BKT] D. Barkley, M. Kness and L.S. Tuckerman, *Phys. Rev. A* 42 (1990) 2489.
- [BPJ] T. Bohr, A.W. Pedersen and M.H. Jensen, *Phys. Rev. A* 42 (1990) 3626.
- [BRE] G.W. Beeler and H. Reuter, *J. Physiol.* 268 (1977) 177.
- [CAR] G. Carpenter, *J. Differ. Equations* 23 (1977) 152.
- [CCL] R. Casten, H. Cohen and P. Lagerstrom, *Quart. Appl. Math.* 32 (1975) 365.
- [CDB] V. Castets, E. Dulos, J. Boissonade and P. De Kepper, *Phys. Rev. Lett.* 64 (1990) 2953.
- [CER] P. Coulet, C. Elphick and D. Repaux, *Phys. Rev. Lett.* 58 (1987) 431.
- [CGB] K.S. Cole, R. Guttman and F. Bezanilla, *Proc. Natl. Acad. Sci.* 65 (1970) 884.
- [CGL1] P. Coulet, L. Gil and J. Lega, *Phys. Rev. Lett.* 62 (1989) 1619.
- [CGL2] P. Coulet, L. Gil and J. Lega, *Physica D* 37 (1990) 91.
- [CGR] P. Coulet, L. Gil and D. Repaux, *Phys. Rev. Lett.* 62 (1989) 2957.
- [COE] P. Coulet and C. Elphick, *Phys. Lett. A* 121 (1987) 234.
- [CON] C. Conley, *Mathematical Research Center Technical Report 1492*, University of Wisconsin, Madison (1975).
- [CRN] M.C. Cross and A.C. Newell, *Physica D* 10 (1984) 299.
- [CVI] P. Cvitanović, *Phys. Rev. Lett.* 61 (1988) 2729.
- [DAZ] V.A. Davydov and V.S. Zykov, *Physica D* 49 (1991) 71.
- [DKC] J.M. Davidenko, P.F. Kent, D.R. Chialvo, D.C. Michaels and J. Jalife, *Proc. Natl. Acad. Sci.* 87 (1990) 8785.
- [DKJ] J.M. Davidenko, P. Kent and J. Jalife, *Physica D* 49 (1991) 182.
- [DKT] J.D. Dockery, J.P. Keener and J.J. Tyson, *Physica D* 30 (1988) 177.
- [DMZ] V.A. Davydov, A.S. Mihailov and V.S. Zykov, in: *Nonlinear Waves in Active Media*, ed. Y. Engelbrecht (Springer, Berlin, 1989).

- [DOK] J.D. Dockery and J.P. Keener, *SIAM J. Appl.* 49 (1989) 539.
- [EFF] J. Evans, N. Fenichel and J.A. Feroe, *SIAM J. Appl. Math.* 42 (1982) 219.
- [EHT] G.B. Ermentrout, S.P. Hastings and W.C. Troy, *SIAM J. Appl. Math.* 44 (1984) 1131.
- [ELM] C. Elphick and E. Meron, *Physica D.* 53 (1991) 385.
- [EMR] C. Elphick, E. Meron, J. Rinzel and E.A. Spiegel, *J. Theor. Biol.* 146 (1990) 249.
- [EMS1] C. Elphick, E. Meron and E.A. Spiegel, *Phys. Rev. Lett.* 61 (1988) 496.
- [EMS2] C. Elphick, E. Meron and E.A. Spiegel, *SIAM J. Appl. Math.* 50 (1990) 490.
- [EPS] E.A. Ermakova, A.M. Pertsov and E.E. Shnol, *Physica D* 40 (1989) 185.
- [FAT] S. Fauve and O. Thual, *Phys. Rev. Lett.* 64 (1990) 282.
- [FEK] V.G. Fast, I.R. Efimov and V.I. Krinsky, *Phys. Lett. A* 151 (1990) 157.
- [FER] J.A. Feroe, *SIAM J. Appl. Math.* 46 (1986) 1079.
- [FIB] R.J. Field and M. Burger, *Oscillations and Traveling Waves in Chemical Systems* (Wiley, New York, 1985).
- [FIE] R.J. Field, in: *Oscillations and Traveling Waves in Chemical Systems*, eds R.J. Field and M. Burger (Wiley, New York, 1985).
- [FIF1] P.C. Fife, in: *Non-Equilibrium Dynamics in Chemical Systems*, eds C. Vidal and A. Pacault (Springer, New York, 1984).
- [FIF2] P.C. Fife, in: *Proc. AMS-SIAM Symp. on Asymptotic Methods and Singular Perturbations* (New York, 1976).
- [FIF3] P.C. Fife, *J. Stat. Phys.* 39 (1985) 687.
- [FIF4] P.C. Fife, *CBMS-NSF Reg. Conf. Series in Appl. Math.* 53 (1988) 1.
- [FIN1] R.J. Field and R.M. Noyes, *J. Chem. Phys.* 60 (1974) 1877.
- [FIN2] R.J. Field and R.M. Noyes, *J. Am. Chem. Soc.* 96 (1974) 2001.
- [FIT1] R. FitzHugh, in: *Biological Engineering*, ed. H.P. Schwan (McGraw-Hill, New York, 1969).
- [FIT2] R. FitzHugh, *J. Gen. Physiol.* 43 (1960) 867; *Biophys. J.* 1 (1961) 445.
- [FKN] R.J. Field, E. Koros and R.M. Noyes, *J. Am. Chem. Soc.* 94 (1972) 8649.
- [FMH] P. Foerster, S. Müller and B. Hess, *Science* 241 (1988) 685.
- [FOW] A.C. Fowler, *Stud. Appl. Math.* 83 (1990) 329.
- [FRS] M.L. Frankel and G.I. Sivashinsky, *J. Physique* 48 (1987) 25.
- [FSO] R. Feeney, S.L. Schmidt and P. Ortoleva, *Physica D* 2 (1981) 536.
- [FWW] D.W. Frazier, P.D. Wolf, J.M. Wharton, A.S.L. Tabg, W.M. Smith and R.E. Ideker, *J. Clin. Invest.* 83 (1989) 1039.
- [GAS] P. Gaspard, *Phys. Lett. A* 97 (1983) 1.
- [GER] G. Gerisch, *Wilhelm Roux' Archiv. Entwickl. Org.* 156 (1965) 127.
- [GLE] P. Glendinning, *Phys. Lett. A* 121 (1987) 411.
- [GLS] P. Glendinning and C. Sparrow, *J. Stat. Phys.* 35 (1984) 645.
- [GOH] J. Gomatam and D.A. Hodson, *Physica D* 49 (1991) 82.
- [GPT] J.D. Cross, M.J. Peacey and D.J. Trevan, *J. Cell Sci.* 22 (1976) 645.
- [GRE] J.M. Greenberg, *SIAM, J. Appl. Math.* 30 (1976) 199.
- [GST1] M. Gerhardt, H. Schuster and J.J. Tyson, *Physica D* 46 (1990) 392.
- [GST2] M. Gerhardt, H. Schuster and J.J. Tyson, *Physica D* 46 (1990) 416.
- [GST3] M. Gerhardt, H. Schuster and J.J. Tyson, *Science* 247 (1990) 1563.
- [GUH] J. Guckenheimer and P. Holmes, *Nonlinear Oscillations, Dynamical Systems and Bifurcations of Vector Fields* (Springer, New York, 1983).
- [HAG] P.S. Hagan, *SIAM, J. Appl. Math.* 42 (1982) 762.
- [HAM] S.P. Hastings and J.D. Murray, *SIAM J. Appl. Math.* 28 (1975) 678.
- [HAS] S.P. Hastings, *SIAM J. Appl. Math.* 42 (1982) 247.
- [HMO] A.V. Holden, M. Markus and H.G. Othmer, *Nonlinear Wave Processes in Excitable Media* (Plenum, London, 1991).
- [HOH] A.L. Hodgkin and A.F. Huxley, *J. Physiol.* 117 (1952) 500.
- [HOK] L.N. Howard and N. Kopell, *Stud. Appl. Math.* 56 (1977) 95.
- [ITG] H. Ito and L. Glass, *Phys. Rev. Lett.* 66 (1991) 671.
- [JAW] W. Jahnke and A.T. Winfree, *Int. J. Bifurc. Chaos* 1 (1991) 455.
- [JFC] R.W. Joyner and F.J.L. van Capelle, *Biophys. J.* 50 (1986) 1157.
- [JKL] C. Jones, N. Kopell and R. Langer, in: *Patterns and Dynamics in Reactive Media*, eds R. Aris, D.G. Aronson and H.L. Swinney (Springer, New York, 1991).
- [JSW] W. Jahnke, W.E. Skaggs and A.T. Winfree, *J. Phys. Chem.* 93 (1989) 740.
- [KAK] H.R. Karfunkel and C. Kahlert, *J. Math. Biol.* 4 (1977) 183.
- [KAR1] A. Karma, *Phys. Rev. Lett.* 65 (1990) 2824.
- [KAR2] A. Karma, *Phys. Rev. Lett.* 66 (1991) 2274.
- [KAR3] A. Karma, in: *Nonlinear Phenomena Related to Growth and Form*, eds M. Ben-Amar, P. Pelcé and P. Tabeling (Plenum, New York) in press.
- [KAR4] A. Karma, *Phys. Rev. Lett.* 68 (1992) 397.
- [KAS] E.R. Kandel and J.H. Schwartz, *Principles of Neural Science* (North Holland, Amsterdam, 1981):

- [KEE1] J.P. Keener, *SIAM J. Appl. Math.* 39 (1980) 528.
- [KEE2] J.P. Keener, *SIAM J. Appl. Math.* 46 (1986) 1039.
- [KEE3] J.P. Keener, The core of the spiral, *SIAM J. Appl. Math.* (1992), to appear.
- [KEE4] J.P. Keener, *J. Math. Biol.* 26 (1988) 41.
- [KEE5] J.P. Keener, Symmetric spirals in excitable media, preprint (1991).
- [KEL1] D.A. Kessler and H. Levine, *Physica D* 39 (1989) 1.
- [KEL2] D.A. Kessler and H. Levine, *Phys. Rev. A* 41 (1990) 5418.
- [KEL3] D.A. Kessler and H. Levine, *Physica D* 49 (1991) 90.
- [KET1] J.P. Keener and J.J. Tyson, The dynamics of scroll waves in excitable media, *SIAM Rev.* 34 (1992) 1.
- [KET2] J.P. Keener and J.J. Tyson, *Physica D* 21 (1986) 307.
- [KHR] R.N. Khramov, *Biofizika* 23 (1978) 871.
- [KKP] L. Kuhnert, H.-J. Krug and L. Pohlman, *J. Phys. Chem.* 89 (1985) 2022.
- [KLR1] D.A. Kessler, H. Levine and W.N. Reynolds, *Phys. Rev. Lett.* 68 (1992) 401.
- [KLR2] D.A. Kessler, H. Levine and W.N. Reynolds, Spiral core meandering in excitable media, preprint (1992).
- [KOK] S. Koga and Y. Kuramoto, *Prog. Theor. Phys.* 63 (1980) 106.
- [KRI] V.I. Krinsky, in: *Biologic and Biochemical Oscillators*, eds B. Chance, E.K. Pye, A.K. Ghosh and B. Hess (Academic Press, New York, 1973).
- [KSS] D.T. Kaplan, J.M. Smith, B.E.H. Saxberg and R.J. Cohen, *Math. Biosci.* 90 (1988) 19.
- [KUK] L. Kuhnert and H.-J. Krug, *J. Phys. Chem.* 91 (1987) 730.
- [KUR] Y. Kuramoto, *Chemical Oscillations, Waves and Turbulence* (Springer, Berlin, 1984).
- [LAN] J.S. Langer, *Rev. Mod. Phys.* 52 (1980) 1.
- [LEG] J. Lega, *J. Physique* 50 (1989) C3-193.
- [LER] H. Levine and W. Reynolds, *Phys. Rev. Lett.* 66 (1991) 2400.
- [LIE] H. Linde and H. Engel, *Physica D* 49 (1991) 13.
- [LIP] E.M. Lifshitz and L.P. Pitaevskii, *Physical Kinetics* (Pergamon, New York, 1981).
- [LUG] E. Lugosi, *Physica D* 40 (1989) 331.
- [MAG1] K. Maginu, *J. Math. Biol.* 6 (1978) 49.
- [MAG2] K. Maginu, *J. Math. Biol.* 10 (1980) 133.
- [MAG3] K. Maginu, *SIAM J. Appl. Math.* 45 (1985) 750.
- [MAH] M. Markus and B. Hess, *Nature* 347 (1990) 56.
- [MAR] G.H. Markstein, *J. Aero. Sci.* 18 (1951) 199.
- [MAS1] J. Maselko and K. Showalter, *Physica D* 49 (1991) 21.
- [MAS2] J. Maselko and K. Showalter, *Nature* 339 (1989) 609.
- [MBK] H. Müller-Krumbhaar, T.W. Burkhardt and D.M. Kroll, *J. Cryst. Growth* 38 (1977) 13.
- [MEI] H. Meinhardt, *Models of Biological Pattern Formation* (Academic Press, London, 1982).
- [MEP] E. Meron and Pierre Pelcé, *Phys. Rev. Lett.* 60 (1988) 1880.
- [MER1] E. Meron, *Physica D* 49 (1991) 98.
- [MER2] E. Meron, *Phys. Rev. Lett.* 63 (1989) 684.
- [MGO] J.L. Martiel and A. Goldbeter, *Biophys. J.* 52 (1987) 807.
- [MIK1] A.S. Mikhailov, in: *Nonlinear Wave Processes in Excitable Media*, eds A.V. Holden, M. Markus and H.G. Othmer (Plenum, London, 1991).
- [MIK2] A.S. Mikhailov, *Foundation of Synergetics I. Distributed Active Systems* (Springer, Berlin, 1990).
- [MIN] G.R. Mines, *Trans. R. Soc. Can.* 4 (1914) 43.
- [MIR] R.N. Müller and J. Rinzel, *Biophys. J.* 34 (1981) 227.
- [MIZ] A.S. Mikhailov and V.S. Zykov, *Physica D* 52 (1991) 379.
- [MKH] M. Markus, M. Krafczyk and B. Hess, in: *Nonlinear Wave Processes in Excitable Media*, eds A.V. Holden, M. Markus and H.G. Othmer (Plenum, London, 1991).
- [MKR] A.S. Mikhailov and V.I. Krinskii, *Physica D* 9 (1983) 346.
- [MMP] M. Markus, S.C. Müller, Th. Plesser and B. Hess, *Biol. Cybern.* 57 (1987) 187.
- [MNS] W.D. McCormick, Z. Noszticzius and H.L. Swinney, *J. Chem. Phys.* 94 (1991) 2159.
- [MPH1] C. Müller, T. Plesser and B. Hess, *Physica D* 24 (1987) 71.
- [MPH2] C. Müller, T. Plesser and B. Hess, *Physica D* 24 (1987) 87.
- [MSP] C.J. Marzec and E.A. Spiegel, *SIAM J. Appl. Math.* 38 (1980) 403.
- [MUR] J.D. Murray, *Mathematical Biology* (Springer, New York, 1989).
- [NAY] J.S. Nagumo, S. Arimoto and S. Yoshizawa, *Proc. IREE Aust.* 50 (1962) 2061.
- [NHM] Z. Noszticzius, W. Horsthemke, W.D. McCormick, H.L. Swinney and W.Y. Tam, *Nature* 329 (1987) 619.
- [NIM] Y. Nishiura and M. Mimura, *SIAM J. Appl. Math.* 49 (1989) 481.
- [NMT] Zs. Nagy-Ungvarai, S.C. Müller and J.J. Tyson, *J. Phys. Chem.* 93 (1989) 2760.

- [NTH] Zs. Nagy-Ungvarai, J.J. Tyson and B. Hess, *J. Phys. Chem.* 93 (1989) 707.
- [NTM] Zs. Nagy-Ungvarai, J.J. Tyson, S.C. Müller, L.T. Watson and B. Hess, *J. Phys. Chem.* 94 (1990) 8677.
- [OBR] Q. Ouyang, J. Boissonade, J.C. Roux and P. De Kepper, *Phys. Lett. A* 134 (1989) 282.
- [OCB] Q. Ouyang, V. Castets, J. Boissonade, J.C. Roux and P. De Kepper, Sustained patterns in chlorite-iodide reactions in a one-dimensional reactor, preprint.
- [OHM] T. Ohta and M. Mimura, in: *Formation, Dynamics and Statistics of Patterns I*, eds K. Kawasaki, M. Suzuki and A. Onuki (World Scientific, New York, 1990).
- [OIT] T. Ohta, A. Ito and A. Tetsuka, *Phys. Rev. A* 42 (1990) 3225.
- [OMK] T. Ohta, M. Mimura and R. Kobayashi, *Physica D* 34 (1989) 115.
- [ORR] P. Ortoleva and J. Ross, *J. Chem. Phys.* 63 (1975) 3398.
- [OUS1] Q. Ouyang and H.L. Swinney, *Nature* 352 (1991) 610.
- [OUS2] Q. Ouyang, H.L. Swinney, *Chaos* 1 (1991) 411.
- [PAV] A.V. Panfilov and B.N. Vasiev, *Physica D* 49 (1991) 107.
- [PEP] A.M. Pertsov, E.A. Ermakova and A.V. Panfilov, *Physica D* 14 (1984) 117.
- [PES1] P. Pelcé and J. Sun, *Physica D* 48 (1991) 353.
- [PES2] P. Pelcé and J. Sun, *Phys. Rev. A* 44 (1992) R7906.
- [PES3] P. Pelcé and J. Sun, On the stability of steadily rotating waves in excitable media, preprint (1991).
- [PEY] A.M. Pertsov and Y.A. Yermakova, *Biophysics* 33 (1988) 364.
- [PIN] L.M. Pismen and A.A. Nepomnyashchy, *Physica D* 54 (1992) 283.
- [PMH] T. Plesser, S.C. Müller and B. Hess, *J. Phys. Chem.* 94 (1990) 7501.
- [PMT] A.V. Panfilov, O.A. Mornev, M.A. Tsyganov and V.I. Krinskii, *Biophysics* 27 (1982) 1116.
- [PPM] A.M. Pertsov, A.V. Panfilov and F.U. Medvedeva, *Biophysics* 28 (1983) 103.
- [PRO] I. Procaccia, *Nature* 333 (1988) 618.
- [RAY] R. Kapral, *J. Math. Chem.* 6 (1991) 113.
- [RIE] J. Rinzel and G.B. Ermentrout, in: *Methods in Neural Modeling*, eds C. Koch and I. Segev (MIT Press, London, 1989).
- [RIK] J. Rinzel and J. Keller, *Biophys. J.* 13 (1973) 1313.
- [RIM] J. Rinzel and K. Maginu, in: *Non-Equilibrium Dynamics in Chemical Systems*, eds C. Vidal and A. Pacault (Springer, New York, 1984).
- [RIN1] J. Rinzel, in: *Nonlinear Phenomena in Physics and Biology*, eds R.H. Enns, B.L. Jones, R.M. Miura and S.S. Rangnekar (Plenum, New York, 1981).
- [RIN2] J. Rinzel, in: *Mathematical Approaches to Cardiac Arrhythmias*, ed. J. Jalife, *Ann. NY Acad. Sci.* 591 (1990) 51.
- [RIT1] S. Rica and E. Tirapegui, *Phys. Rev. Lett.* 64 (1990) 878.
- [RIT2] S. Rica and E. Tirapegui, *Physica D* 48 (1991) 396.
- [ROK] O. Rössler and C. Kahlert, *Z. Naturforsch.* 34 (1979) 564.
- [ROV] A.B. Rovinsky, *J. Phys. Chem.* 91 (1987) 4606.
- [RRS] I. Rehberg, S. Rasenat and V. Steinberg, *Phys. Rev. Lett.* 62 (1989) 756.
- [SAK] H. Sakaguchi, *Prog. Theor. Phys.* 82 (1989) 7.
- [SCD] N. Shibata, P. Chen, E.G. Dixon, P.D. Wolf, N.D. Danieleley, W.M. Smith and R.E. Idekar, *Am. J. Physiol.* 255 (1988) H891.
- [SCO] S. Schmidt and P. Ortoleva, *J. Chem. Phys.* 67 (1977) 3771.
- [SEM1] H. Sevcikova and M. Marek, *Physica D* 9D (1983) 140.
- [SEM2] H. Sevcikova and M. Marek, *Physica D* 21 D (1986) 61.
- [SHI] L.P. Shil'nikov, *Sov. Math.* 6 (1965) 163.
- [SHO] K. Showalter, *J. Phys. Chem.* 85 (1981) 440.
- [SIZ] E.D. Siggia and A. Zippelius, *Phys. Rev. A* 24 (1981) 1036.
- [SKS] G.S. Skinner and H.L. Swinney, *Physica D* 48 (1991) 1.
- [SKW] H.A. Swadlow, J.D. Kocsis and S.G. Waxman, *Ann. Rev. Biophys. Bioeng.* 9 (1980) 143.
- [SSM] O. Steinbock, J. Schütze, and S.C. Müller, *Phys. Rev. Lett.* 68 (1992) 248.
- [SUO] R. Sultan and P. Ortoleva, *J. Chem. Phys.* 85 (1986) 5068.
- [SWK] H.L. Swinney and V.I. Krinsky, *Waves and Patterns in Chemical and Biological Media*, *Physica D* 49 (1991) Nos. 1 and 2.
- [TAM] J.J. Tyson, K.A. Alexander, V.S. Manoranjan and J.D. Murray, *Physica D* 34 (1989) 193.
- [TAS] W.Y. Tam and H.L. Swinney, *Physica D* 46 (1990) 10.
- [TRE] C. Tresser, *Ann. Inst. Henri Poincaré* 40 (1984) 441.
- [TRF] W.C. Troy and R.J. Field, *SIAM J. Appl. Math.* 37 (1977) 561.
- [TRG] N.B. Tuffillaro, R. Ramshankar and J.P. Gollub, *Phys. Rev. Lett.* 62 (1989) 422.
- [TRO] W.C. Troy, in: *Theoretical Chemistry*, Vol. 4, eds H. Eyring and D. Henderson (Academic Press, New York, 1978).
- [TUR] A.M. Turing, *Philos. Trans. R. Soc. London B* 327 (1952) 37.
- [TVS] W.Y. Tam, J.A. Vastano, H.L. Swinney and W. Horsthemke, *Phys. Rev. Lett.* 61 (1988) 2163.
- [TYF] J.J. Tyson and P.C. Fife, *J. Chem. Phys.* 73 (1980) 2224.
- [TYK1] J.J. Tyson and J.P. Keener, *Physica D* 32 (1988) 327.

- [TYK2] J.J. Tyson and J.P. Keener, *Physica D* 29 (1987) 215.
- [TYS1] J.J. Tyson, in: *Oscillations and Traveling Waves in Chemical Systems*, eds R.J. Field and M. Burger (Wiley, New York, 1985).
- [TYS2] J.J. Tyson, *Lecture Notes on Biomathematics*, Vol. 10 (Springer, New York, 1976).
- [VCD] F.J. van Capelle and D. Durrer, *Circ. Res.* 47 (1980) 454.
- [WAL] D. Walgraef, in: *Non-Equilibrium Dynamics in Chemical Systems*, eds C. Vidal and A. Pacault (Springer, New York, 1984).
- [WCK] X.-G. Wu, M.-N. Chee and R. Kapral, *Chaos* 1 (1991) 421.
- [WIN1] A.T. Winfree, *Science* 175 (1972) 634.
- [WIN2] A.T. Winfree, in: *Lecture Notes on Biomathematics*, Vol. 2, eds S. Levin and P. van den Driessche (Springer, New York, 1974).
- [WIN3] A.T. Winfree, *When Time Breaks Down* (Princeton Univ. Press, Princeton, 1987).
- [WIN4] A.T. Winfree, *J. Theor. Biol.* 138 (1989) 353.
- [WIN5] A.T. Winfree, *Sci. Am.* 230 (1974) 82.
- [WIN6] A.T. Winfree, *Phys. Lett. A* 149 (1990) 203.
- [WIN7] A.T. Winfree, *Physica D* 49 (1991) 125.
- [WIN8] A.T. Winfree, *Chaos* 1 (1991) 303.
- [WIN9] A.T. Winfree, *J. Cardiovasc. Electrophysiol.* 1 (1990) 393.
- [WIN10] A.T. Winfree, in: *Theoretical Chemistry*, Vol. 4, eds H. Eyring and D. Henderson (Academic Press, New York, 1978).
- [WIN11] A.T. Winfree, private communication.
- [WOR] P.M. Woods and J. Ross, *J. Chem. Phys.* 82 (1985) 1924.
- [WUK] X.-G. Wu and R. Kapral, *Chemical turbulence and phase resetting dynamics*, *J. Chem. Phys.*, in press.
- [YAM] T. Yamaguchi and S.C. Müller, *Physica D* 49 (1991) 40.
- [YKP] Y.A. Yermakova, V.I. Krinskii, A.V. Panfilov and A.M. Pertsov, *Biophysics* 31 (1986) 348.
- [YOA] J.A. Yorke and K.T. Alligood, *Commun. Math. Phys.* 101 (1985) 305.
- [ZAZ1] A.N. Zaikin and A.M. Zhabotinsky, *Nature* 225 (1970) 535.
- [ZAZ2] A.N. Zaikin and A.M. Zhabotinsky, in: *Oscillatory Processes in Biological and Chemical Systems*, ed. E.E. Sel'kov (Pushkino, Moscow, 1971) (in Russian).
- [ZHA] A.M. Zhabotinsky, *Biophysics* 9 (1964) 329.
- [ZMH] A.M. Zhabotinsky, S.C. Müller and B. Hess, *Physica D* 49 (1991) 47.
- [ZYK1] V.S. Zykov, *Simulation of Wave Processes in Excitable Media* (Manchester Univ. Press, New York, 1987).
- [ZYK2] V.S. Zykov, *Biophysics* 25 (1980) 906.
- [ZYK3] V.S. Zykov, *Biophysics* 31 (1986) 940.
- [ZYK4] V.S. Zykov, in: *Control of Complex Systems*, ed. Z. Tsytkin (Nauka, Moscow, 1975).
- [ZYK5] V.S. Zykov, *Biophysics* 32 (1987) 365.
- [ZYM] V.S. Zykov and O.L. Morozova, *J. Nonlinear Biology* 1 (1991) 127.